ผลกระทบของแร่องค์ประกอบและสมบัติความยืดหยุ่น
ต่อตัวประกอบการขยายของตัวอย่างดินจากจังหวัดสมุทรปราการ

อิสราภรณ์ เศรษฐ์ธนันท์

ธรณีวิทยา

2558

ผลกระทบของแร่องค์ประกอบและสมบัติความยืดหยุ่น
ต่อตัวประกอบการขยายของตัวอย่างดินจากจังหวัดสมุทรปราการ

นางสาวอิสราภรณ์ เศรษฐ์ธนันท์

วิทยานิพนธ์นี้เป็นส่วนหนึ่งของการศึกษาตามหลักสูตรปริญญาวิทยาศาสตรบัณฑิต
ภาควิชาธรณีวิทยา คณะวิทยาศาสตร์ จุฬาลงกรณ์มหาวิทยาลัย
ปีการศึกษา 2558

EFFECTS OF MINERAL COMPOSITION AND ELASTIC PROPERTIES ON AMPLIFICATION FACTOR OF SOIL SAMPLES FROM CHANGWAT SAMUT PRAKAN

Miss Israporn Sethanant

A Thesis Submitted in Partial Fulfillment of the Requirements
for the Degree of Bachelor of Science Program in Geology
Department of Geology
Faculty of Science
Chulalongkorn University
Academic Year 2015

Thesis Title	EFFECTS OF MINERAL COMPOSITION AND ELASTIC PROPERTIES ON AMPLIFICATION FACTOR OF SOIL SAMPLES FROM CHANGWAT SAMUT PRAKAN
By	Miss Israporn Sethanant
Department	Geology
Thesis Advisor	Dr. Waruntorn Kanitpanyacharoen
Thesis Co-advisor	Assistant Professor Dr. Santi Pailoplee

Accepted by the Department of Geology, Faculty of Science, Chulalongkorn University in Partial Fulfillment of the Requirements for the Bachelor's Degree

THESIS COMMITTEE

..... Thesis Advisor
(Dr. Waruntorn Kanitpanyacharoen)

..... Thesis Co-advisor
(Assistant Professor Dr. Santi Pailoplee)

อิสราภรณ์ เศรษฐ์ธนันท์: ผลกระทบของแร่องค์ประกอบและสมบัติความยืดหยุ่นต่อตัวประกอบการขยายของตัวอย่างดินจากจังหวัดสมุทรปราการ. (EFFECTS OF MINERAL COMPOSITION AND ELASTIC PROPERTIES ON AMPLIFICATION FACTOR OF SOIL SAMPLES FROM CHANGWAT SAMUT PRAKAN) อาจารย์ที่ปรึกษา: อาจารย์ ดร. วรัญทร คณิตปัญญาเจริญ, อาจารย์ที่ปรึกษาร่วม: ผู้ช่วยศาสตราจารย์ ดร. สันติ ภัยหลบลี้, 62 หน้า.

เมื่อเกิดเหตุการณ์แผ่นดินไหว ชั้นดินเหนียวอ่อนและตะกอนสามารถก่อให้เกิดการขยายอัตราเร่งของคลื่นไหวสะเทือนที่ผิวดิน และหากสิ่งปลูกสร้างที่ตั้งอยู่บนชั้นดินเหนียวอ่อนเหล่านั้นตอบสนองต่อแรงสั่นสะเทือน ก็จะก่อให้เกิดความเสียหายในทรัพย์สินหรือความสูญเสียต่อชีวิตได้ ดังนั้นค่าตัวประกอบการขยายของอัตราเร่ง จึงถูกนำมาใช้เพื่อประเมินการสั่นสะเทือนของผิวดินก่อนการก่อสร้างอาคารเพื่อลดอันตรายจากภัยพิบัติดังกล่าว งานวิจัยนี้จึงมีจุดประสงค์เพื่อสร้างแบบจำลองการขยายอัตราเร่งโดยการคำนวณความเร็วคลื่นเฉือนโดยใช้ปริมาณแร่องค์ประกอบและสมบัติความยืดหยุ่นของตัวอย่างดินจากอำเภอบางพลี และอำเภอบางเสาธงในจังหวัดสมุทรปราการ ในขั้นแรกการจัดเรียงตัวจำเพาะของแร่และปริมาณแร่องค์ประกอบของตัวอย่างดิน จะถูกวิเคราะห์ด้วยวิธีดิฟแฟรกชันด้วยรังสีเอ็กซ์จากเครื่องซินโครตอน ผลจากการวิเคราะห์พบว่าตัวอย่างดินประกอบไปด้วยแร่ดินปริมาณสูงถึง 60-80 เปอร์เซ็นต์โดยปริมาตร ประกอบไปด้วยแร่อิลไลต์-ไมกา แร่มอนต์มอริลโลไนต์ และแร่ดิกไคต์ ข้อมูลเชิงปริมาณที่ได้จะถูกนำไปคำนวณหาความเร็วคลื่นเฉือนจากสมการคณิตศาสตร์ในโปรแกรม BEARTEX ร่วมกับค่าคงตัวยืดหยุ่นของแร่องค์ประกอบและความหนาแน่นของดิน นอกจากนี้ยังมีการประมาณความพรุนของดินเท่ากับ 21.5 เปอร์เซ็นต์ ผลจากการคำนวณแสดงให้เห็นว่าตัวอย่างดินจากบริเวณอำเภอบางพลีและอำเภอบางเสาธงในระดับความลึกไม่เกิน 20 เมตร มีค่าความเร็วคลื่นเฉือนประมาณ 90-150 เมตร/วินาที และ 70-130 เมตร/วินาที ตามลำดับ จากนั้นได้จำลองค่าอัตราเร่งสูงสุดของพื้นดินด้วยโปรแกรม DEEPSOIL ซึ่งพิจารณาความเร็วคลื่นเฉือนจากการคำนวณข้างต้น ข้อมูลชั้นดิน และคลื่นแผ่นดินไหวเป็นปัจจัยหลักสำหรับการสร้างแบบจำลอง แผ่นดินไหวสามเหตุการณ์ถูกเลือกจากแหล่งกำเนิดแผ่นดินไหวที่เป็นรอยเลื่อนมีพลัง ได้แก่ รอยเลื่อนพะเยา รอยเลื่อนเจดีย์สามองค์ และรอยเลื่อนสะกาย เพื่อเป็นตัวแทนเหตุการณ์ที่มีศักยภาพในการส่งผลกระทบต่อจังหวัดสมุทรปราการ ในการจำลองการตอบสนองบนผิวดิน คลื่นแผ่นดินไหวทั้งสามถูกขยายให้มีค่าอัตราเร่งสูงสุดของพื้นดินเท่ากับ 0.1 g ตัวประกอบการขยายจากการคำนวณในขั้นตอนสุดท้ายมีค่าระหว่าง 1.7 ถึง 2.1 สำหรับชั้นดินในอำเภอบางพลี และ 1.2 ถึง 1.5 สำหรับชั้นดินในอำเภอบางเสาธง ผลจากการศึกษานี้สรุปได้ว่าตัวประกอบการขยายของอัตราเร่งสามารถประเมินได้อย่างมีประสิทธิภาพจากความเร็วคลื่นเฉือนที่คำนวณจากแร่องค์ประกอบและสมบัติความยืดหยุ่นของดิน และบ่งชี้ว่าชั้นดินในพื้นที่ศึกษามีความสามารถในการการขยายอัตราเร่งเมื่อมีการตอบสนองเนื่องจากกระทำแผ่นดินไหว

ลายมือชื่อนิสิต.....

ภาควิชา ธรณีวิทยา ลายมือชื่อ อาจารย์ที่ปรึกษา.....

ปีการศึกษา 2558 ลายมือชื่อ อาจารย์ที่ปรึกษาร่วม.....

##5532746723: MAJOR GEOLOGY
KEYWORDS: SYNCHROTRON X-RAY DIFFRACTION/CLAY MINERALS/ ELASTIC PROPERTIES/AMPLIFICATION FACTOR

ISRAPORN SETHANANT: EFFECTS OF MINERAL COMPOSITION AND ELASTIC PROPERTIES ON AMPLIFICATION FACTOR OF SOIL SAMPLES FROM CHANGWAT SAMUT PRAKAN. THESIS ADVISOR: DR. WARUNTORN KANITPANYACHAROEN, THESIS CO-ADVISOR: ASSISTANT PROFESSOR DR. SANTI PAILOPLEE, 62 pp.

Soft sediments underlying Samut Prakan has long been postulated to cause ground motion amplification during earthquake events. To remediate the potential hazard, the amplification factor must be considered for ground motion assessment in earthquake-prone areas. This study thus focuses on modeling the amplification factor by calculating shear wave velocity from mineral composition and elastic properties of soil samples from Bang Phli (BP) and Bang Sao Thong (BS) districts. The composition, volume fractions, and crystallographic preferred orientation of minerals in the soil samples were quantified from synchrotron x-ray diffraction method. Soil samples generally contain high clay content, approximately 60-80 vol%, including illite-mica, montmorillonite, and dickite. The quantitative results were incorporated with elastic constants of constituent minerals and density of soil samples to calculate shear wave velocities, using mathematical averaging approaches in BEARTEX software. A total porosity of 21.5% was further used in shear wave approximation, suggesting that shear wave velocities within 20 m depth in BP and BS areas are approximately 90-150 m/s and 70-130 m/s, respectively. Calculated shear wave velocities, soil profiles, and earthquake waveforms were then incorporated in a 1D amplification model using DEEPSOIL program, to estimate the peak ground acceleration at the surface of the study areas. To represent potential earthquake sources that may cause damage to Samut Prakan, three different seismic events were chosen from active fault zones, which are Phayao Fault, Three Pagoda Fault Zone, and Sagaing Fault Zone. The earthquake records were scaled to peak acceleration of 0.1 g. The amplification factors range from 1.7 to 2.1 for BP and 1.2 to 1.5 for BS. In conclusion, amplification factor can be effectively estimated from shear wave velocity obtained from soil composition and elastic properties. Our results further suggest that soft sediments in the study areas have the ability to substantially amplify earthquake ground motions.

Student's signature .....
Department Geology Advisor's signature .....
Academic Year 2015 Co-advisor's signature .....

ACKNOWLEDGEMENTS

First of all, I would like to express my deepest gratitude to my advisor, Dr. Waruntorn Kanitpanyacharoen, whose expertise, understanding, and support on the senior project made it possible for me to work on a topic that was of great increase to me. I would like to thank her for every advice and encouragement throughout the research. She has taught me to be a problem solver and has inspired me to pursue my own passion of being a good researcher in the future. I am also grateful to my co-advisor, Assitant Professor Dr. Santi Pailoplee, who has given me insightful guidelines about earthquake geology and seismic hazard analysis. My sincere thanks also goes to the Mineral and Rock Physics group. I thank them for teaching all processes in MAUD software, for the great discussions, and the cheering up throughout work.

I owe a debt of gratitude to Associate Professor Suttisak Soralump, Head of Geotechnical Engineering Research and Development Center, Department of Civil Engineering, Kasetsart University. His immense knowledge has widen my perspective in the application of geology towards engineering. I would like to thank for his continuous guidance and support even though he is abroad. I could not have imagined having a better advisor for my study.

I would also like to thank Khun Jitrakon Prasomsri from the Dam and Earthquake Research Unit of the Geotechnical Engineering Research and Development Center (Department of Civil Engineering, Kasetsart University) for the DEEPSOIL program tutoring and explanations about dynamic soil properties. Our great discussions have solved various obstacles during the amplification modeling. I thank him for his patience and all useful suggestions. Moreover, I would like to acknowledge Khun Kanokwan Sornsoongnoen, Laboratory supervisor at Krungthep Geotechnique co., ltd, and Khun Monapat Sasingha (Master's student at the Department of Civil Engineering, Kasetsart University) for the support of soil samples.

I take this opportunity to gratefully thank Khun Santawat Sukrungsri, Seismologist at the Seismological Bureau (Thai Meteorological Department) for the support of earthquake waveforms in this study. Much appreciation for the help in SeisGram2K software and advice about the characteristics of the seismic records. His great guidance also influence the success of my project.

In addition, thank you to Khun Jiraprapa Niampan, Khun Sopit Pumpuang, and Khun Banjong Puangthong, staffs of the Department of Geology, Faculty of Science, Chulalongkorn University for the XRD guidelines and sample preparations. I would also like to acknowledge the Advance Light Source, California (USA) for the synchrotron x-ray diffraction experiments.

I would like to thank my Geo'56 friends for the support and encouragement in the past few years. Last but not least, I thank you my heartwarming family especially my brother, Pongpawan Sethanant, for the motivation and advice from his intense research experience. Thank you for being such an amazing brother!

CONTENTS

LIST OF TABLES

Page

LIST OF FIGURES

Page

CHAPTER I
INTRODUCTION

1.1 RATIONALE

Samut Prakan is a province neighboring Bangkok in the Lower Central Plain of Thailand. Although it is located far from seismic sources e.g. Sumatra-Andaman Subduction Zone or Sagaing Fault Zone, it can be affected by large earthquakes due to ground motion amplification. When an earthquake is generated, seismic waves propagate away from the source and reach the boundaries between rocks and soft, unconsolidated sediment layers. Velocity of shallower materials, i.e., soft sediment or soil, is typically lower than the material beneath them with greater stiffness. To conserve energy while the velocity is decreased, the amplitudes of seismic waves in soft sediments are generally increased or amplified. The amplification of ground motion occurs and may cause intense ground shaking. If the frequency of ground motion matches the natural frequency of a building, resonances can occur and the building may fail, leading to potential loss of lives. To avoid such a disaster, the characteristics of ground motion must be taken into account when constructing buildings in seismicity areas.

The geologic conditions differ from place to place. Seismic waves such as compressional, shear, surface waves travel through different materials at different speeds. Shear wave causes shearing deformations and creates most of the damages. It is the main contributor to ground shaking and influenced by various physical properties of the materials e.g. composition, density, porosity, and elastic constants. The mineral composition and elastic properties of soft sediments in the Lower Central Plain should have different patterns of ground motion in different areas. Therefore, to gain a better understanding of the ground motion characteristics in Samut Prakan, the amplification factor is resolved from the shear wave velocity calculated based on mineral volume fractions and elastic properties of soil samples from the study areas. Our study presents an alternative approach to understand response behaviors of the ground affected by significant tremors.

1.2 SEISMICITY OF SAMUT PRAKAN

Ornthammarath *et al*. (2011) conducted a seismic hazard map which shows that Samut Prakan has a peak ground acceleration of 2-4% g and 5-10% g, for 10% and 2% probabilities of exceedance in 50 years, respectively. This suggests that there are probabilities that earthquakes may cause ground shaking in Samut Prakan although it is far from earthquake epicenters. A similar devastation in Mexico City was caused by the 1985 Michoacan earthquake with an epicenter over 350 kilometers away, approximately the same distance from Samut Prakan to the Andaman Sea. The 2005

Nias–Simeulue earthquake in Myanmar that occurred on March 28, 2005 is one example of distant earthquake effects on Central Thailand. It had a Mw 8.6 and occurred just 3 months after the Indian Ocean earthquake (December 26, 2004). The generating source was the Sagaing Fault Zones which the Thai Meteorological Department (TMD) recorded a Mercalli intensity scale of IV in Bangkok region. The shake were felt particularly in high buildings.

Due to seismic wave attenuation or the loss of earthquake energy as they propagate through the Earth, the seismogenic zones that have the potential to cause damage to Samut Prakan should have high magnitude, releasing a significant amount of energy enough to reach the city. Ornthammarath *et al*. (2011) suggested that earthquakes from both near and far sources contribute to the seismic hazard in Bangkok area. Pailoplee and Choowong (2012) also defined 13 earthquake source zones within the Mainland Southeast Asia (Figure 1.1), based on the geologic, tectonic, and seismicity data. The concept of frequency–magnitude distribution is applied in order to evaluate the most probable largest magnitude, the mean return period, and the probability of earthquake of different magnitudes in different time spans. The estimated return period of different magnitudes are summarized in Table 1.1. Based on the previous studies, three potential earthquake sources for Samut Prakarn are chosen: Mae Chan Fault and Sagaing Fault Zone, representing teleseismic sources, and Three Pagoda Fault Zone representing local seismic sources. These sources are likely to generate serious earthquakes within decades.

1.2.1 Mae Chan Fault (zone J)

The Mae Chan Fault is a sinistral strike-slip fault located near Phayao Fault in the northern part of Thailand. The fault extends for about 140 km from Nam Mae Chan valley in northernmost Thailand near the border with Myanmar, across the Mekong River and into Laos (Fenton *et al*., 2003). It is characterized by shallow focal depth and the seismic productivity is not so high when compared to the other zones. However, on December 22, 1925, this area experienced an earthquake up to body wave magnitude (mb) 6.5. The recurrence interval of great earthquakes (earthquakes of magnitude 8 or more) is about 100 years.

1.2.2 Sagaing Fault Zone (zone C)

Sagaing fault is one of the major continental fault zones in Southeast Asia. This 1400-km long fault is active with a dextral strike-slip motion and strikes a N–S direction passing through the central part of Myanmar. The fault connects southwards into the back-arc spreading center in the Andaman Sea and splays northwards into several branches around the eastern Himalayas (Pailoplee, 2013). The next Mw 7.2–7.5 earthquake at the Sagaing Fault Zone may generate within the next two decades and should be aware of the prospective Mw 8.0 earthquake because the largest recorded earthquake, Mw 8.0, had already occurred on May 23, 1912.

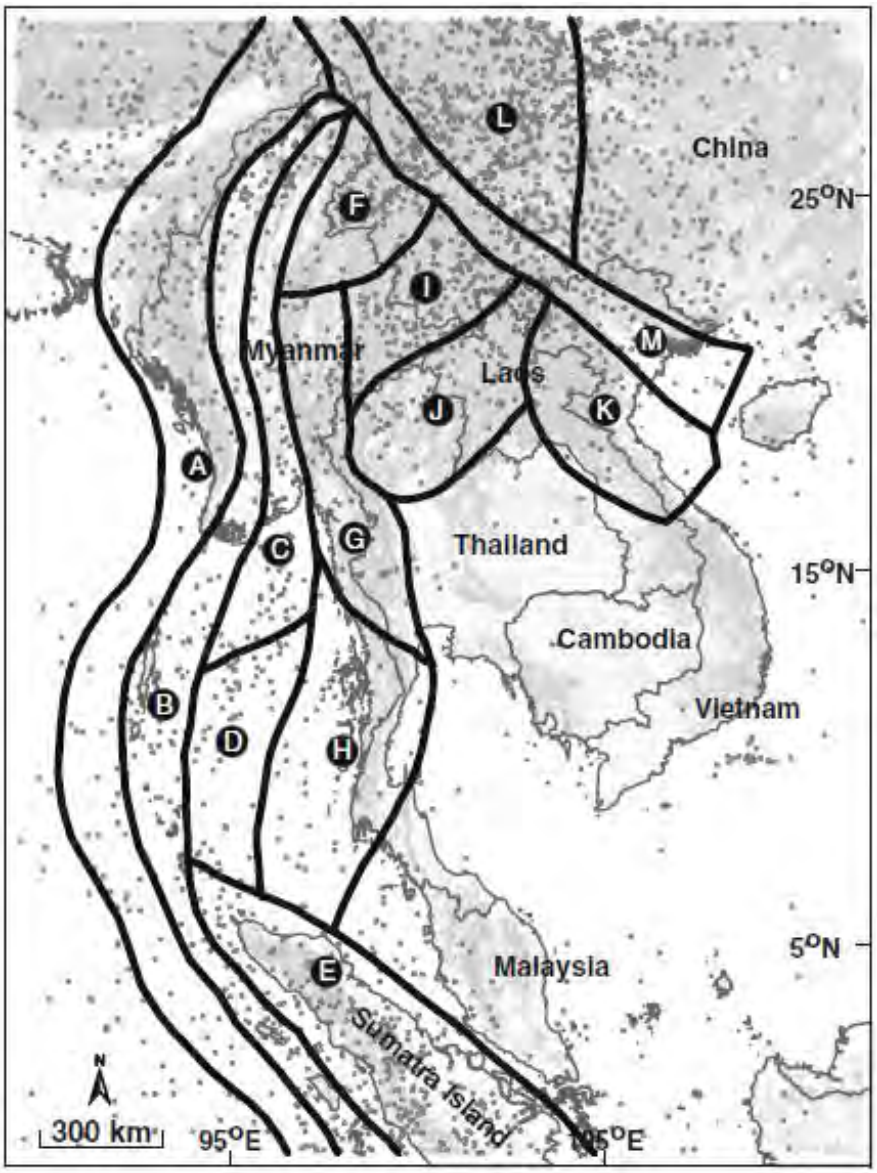

Figure 1.1 Map of the MSEA region showing the 13 earthquake source zones, bounded by the black line. The gray circles illustrate the earthquake epicentral distribution recorded during the period 1964 to 2010 for all magnitude ranges after declustering with the algorithm according to Gardner and Knopoff (1974). (Pailoplee and Choowong, 2012)

Table 1.1 Estimated return period in each of the 13 zones (dys days, yrs years; zone A: Sumatra-Andaman Interplate; zone B: Sumatra-Andaman Intraslab; zone C: Sagaing Fault Zone; zone D: Andaman Basin; zone E: Sumatra Fault Zone; zone F: Hsenwi-Nanting Fault Zone; zone G: Western Thailand; zone H: Southern Thailand; zone I: Jinghong-Mengxing Fault Zones; zone J: Northern Thailand-Dein Bein Fhu; zone K: Song Da-Song Ma Fault Zones Zone; and Zone M: Red River Fault Zone) (Pailoplee and Choowong, 2012).

Mw	Zone A	Zone B	Zone C	Zone D	Zone E	Zone F	Zone G	Zone H	Zone I	Zone J	Zone K	Zone L	Zone M
3	2.5 dys	3.9 dys	4.8 dys	86.2 dys	3.6 dys	12.4 dys	25.9 dys	26.7 dys	12.9 dys	4.3 dys	19.4 dys	6.4 dys	5.8 dys
3.5	5.1 dys	8.6 dys	10.9 dys	135.1 dys	8.4 dys	27.7 dys	49.7 dys	56.9 dys	25.9 dys	10.7 dys	45.2 dys	12.8 dys	15.3 dys
4	10.5 dys	18.7 dys	25.1dys	212.Odys	20.Odys	62.Odys	96 6 dys	120.9 dys	52.3 dys	26.7 dys	105.3 dys	25.7 dys	40.4 dys
45	21.7 dys	41.Odys	57.7 dys	332.5 dys	47.2 dys	138.5 dys	183.6 dys	256.9 dys	1O5.4 dys	66.7 dys	245.4 dys	51.7 dys	106.4 dys
5	449 dys	89.6 dys	132.5 dys	1.4 yrs	I11.5 dys	310.7 dys	1.Oyrs	1.5 yrs	212.5 dys	166.8 dys	1.6 yrs	104.1 dys	280.1 dys
5.5	92.7 dys	196.Odys	304.3 dys	2.2 yrs	263.5 dys	1.9 yrs	1.9 yrs	3.2 yrs	1.2 yrs	1.lyzs	3.7 yrs	209.3 dys	2.Oyrs
6	191.6 dys	1.2 yrs	1.9 yrs	35 yrs	1.7 yrs	43 yrs	3.6 yrs	6.8 yrs	2.4 yrs	2.9 yrs	5.5 yrs	1.2 yrs	5.3 yrs
65	l.lyrs	2.6 yrs	4.4 yrs	5.5 yrs	4.Oyrs	9.5 yrs	6.8 yrs	14.4 yrs	4.8 yrs	7.1yrs	19.8 yrs	2.3 yrs	l4.Oyrs
7	2.2 yrs	5.6 yrs	10.1 yrs	5.6 yrs	9.5 yrs	21.4 yrc	13.2 yrs	30.5 yrs	9.6 yrs	17.9 yrs	46.2 yrs	4.7 yrs	36.9 yrs
7.5	4.6 yrs	12.3 yrs	23lyrs	13.6 yrs	22.5 yrs	47.9 yrs	25.3 yrs	64.9 yrs	19.4 yrs	44.7 yrs	107.8 yrs	9.4 yrs	97.2 yrs
8	9.5 yrs	26.9 yrs	53.2 yrs	21.3 yrs	53.2 yrs	107.2 yrs	48.5 yrs	138.Oyrs	39.1yrs	ll17yrs	251.2 yrs	18.9 yrs	255.9 yrs
8.5	19.7 yrs	58.9 yrs	122.2 yrs	33.4 yrs	125.7 yrs	239.9 yrs	93.2 yrs	293.4 yrs	78.5 yrs	279.3 yrs	585.5 yrs	38.Oyrs	673.5 yrs
9	40.7 yrs	128.8 yrs	280.5 yrs	52.4 yrs	297.2 yrs	537.Oyrs	179.lyrs	623.7 yrs	158.9 yrs	698.2 yrs	1364.6 yrs	76.4 yrs	l774.2 yrs

1.2.3 Three Pagoda Fault Zone (zone G)

The NW-trending and dextral strike-slip fault is 350 km long, 25 km wide. It extends from just south of Moulmein, Myanmar, across the Three Pagodas Pass, along the Mae Nam Khwae Noi/Mae Nam Khwae Yai (River Kwai) drainage basin, and towards the Gulf of Thailand (Fenton *et al*., 2003). Many significant earthquakes also occurred in the Three Pagoda Fault Zone. For example, an earthquake of mb 5.6 occurred on February 17, 1975 and mb 5.9 on April 22, 1983. This fault zone should be considered of upcoming hazards because the recurrence interval of great earthquakes is only about 50 years onwards.

Many earthquake records from TMD revealed that remote areas can feel the shaking of earthquakes from the following fault zones. For instance, a Mw 6.9 earthquake caused by the Sagaing Fault Zone on March 24, 2011 was felt in high buildings in Bangkok with a III on the Mercalli intensity scale. The vibration are felt especially in high constructions in Bangkok and nearby provinces with soft clay beneath the city. Samut Prakan is also underlain by "Bangkok clay", a sequence of marine clay mainly composed of silty clay particles and very fine to fine sand grains. To determine the seismic hazard in this region, many studies of Bangkok clay response have been conducted for these sediments cover the capital city of Thailand, center of commerce, and city of dense population.

1.3 SHEAR WAVE VELOCITY & AMPLIFICATION OF BANGKOK CLAY

Shear wave velocity is an important contributor to ground shaking and is also considered as the main input for the amplification profile modeling. The numerous methods to achieve shear wave velocities include Crosshole seismic test, Downhole seismic test, Seismic Cone Penetration Test (SCPT), Spectral Analysis of Surface Waves Test (SASW), and Multichannel Analysis of Surface Wave Method (MASWM). These approaches are field tests which measure the in-place shear wave velocity profile of soil or rock. Thus, shear wave velocities can also be estimated from empirical correlations with soil properties, e.g. maximum shear modulus (G_{max}), Standard Penetration Test (SPT) N-values, and undrained shear strength (S_u). The N-values are measured from SPT and is used to estimate the approximate shear strength properties of the soil, including S_u. Ashford *et al*. (1997) propose an empirical correlation between shear wave velocity (V_S) in m/s and S_u in kPa for Bangkok soft clay as:

$$V_S = 23 S_u^{0.475}$$

which the velocity was further used for the amplification study of earthquake ground motions in Bangkok. For the best V_S estimation, Ashford *et al*. (1997) also reviewed several empirical correlations based on available field and laboratory measurements, then, confirmed by a limited number of in situ tests by downhole method. The ground motion was studied by earthquake records that were scaled to peak ground acceleration (PGA) value of 0.1 g. Amplification factors of Bangkok from the model range from 2.6

to 3.9. They suggest that the amount of amplification and the shape of the response spectra will vary with the input motion used. It was concluded that the soils underlying Bangkok has the ability to amplify earthquake ground motion, both in peak ground acceleration and spectral acceleration.

Another study of the response of Bangkok clay induced by earthquake forces by Yanuviriyakul and Soralump (2009) obtain V_S for the amplification modeling by MASWM and empirical equations converted from G_{max} expressed by the following equation:

$$G_{max} = \gamma \cdot g \cdot V_S$$

where γ is the total unit weight (t/m^3) and g is the acceleration due to gravity. Yanuviriyakul and Soralump (2009) conclude that soft clay thickness is the major factor influencing amplification factors. The amplification factor decreases with the increasing soft clay thickness (Figure 1.2). The PGA of the earthquake events were modified to 0.1 g before generating the 1D amplification profile of the soil layer. Results show that the amplification factor of soft Bangkok clay range from 1.5 to 2.0 (Figure 1.3), which also certifies the previous study by Ashford *et al*. (1997) that the surficial deposits in Bangkok can amplify ground motion induced by temblors.

Despite the dynamic soil properties that affect shear wave velocity, geologic characteristics of the soils, e.g. porosity, mineralogy, elastic properties, can also be influential. Therefore, the aim of this research is to understand the effect on amplification factor by obtaining shear wave velocity from mineral composition and elastic properties of soil samples. The shear wave velocity will be further used to model the amplification of the study areas in Samut Prakan. The modeling in our study will consider earthquake sources that have the potential to generate such an earthquake that can cause strong ground motion due to soil amplification in the Lower Central Plain of Thailand. The amplification profile and the amplification factor will simulate different ground motion responded from past earthquake events.

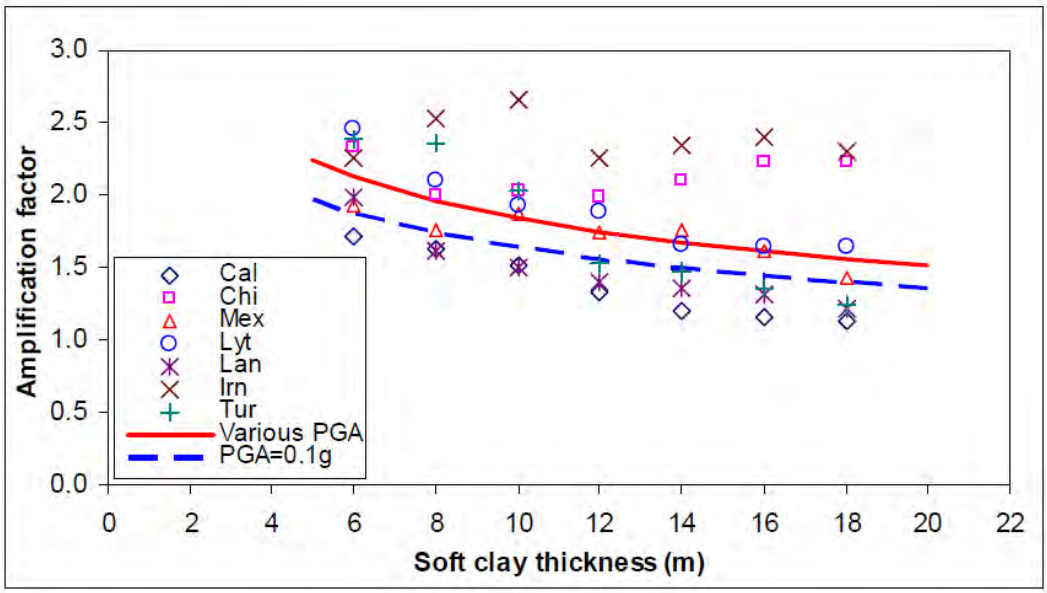

Figure 1.2 Changing of the amplification factor versus soft clay thickness (Yanuviriyakul and Soralump, 2009)

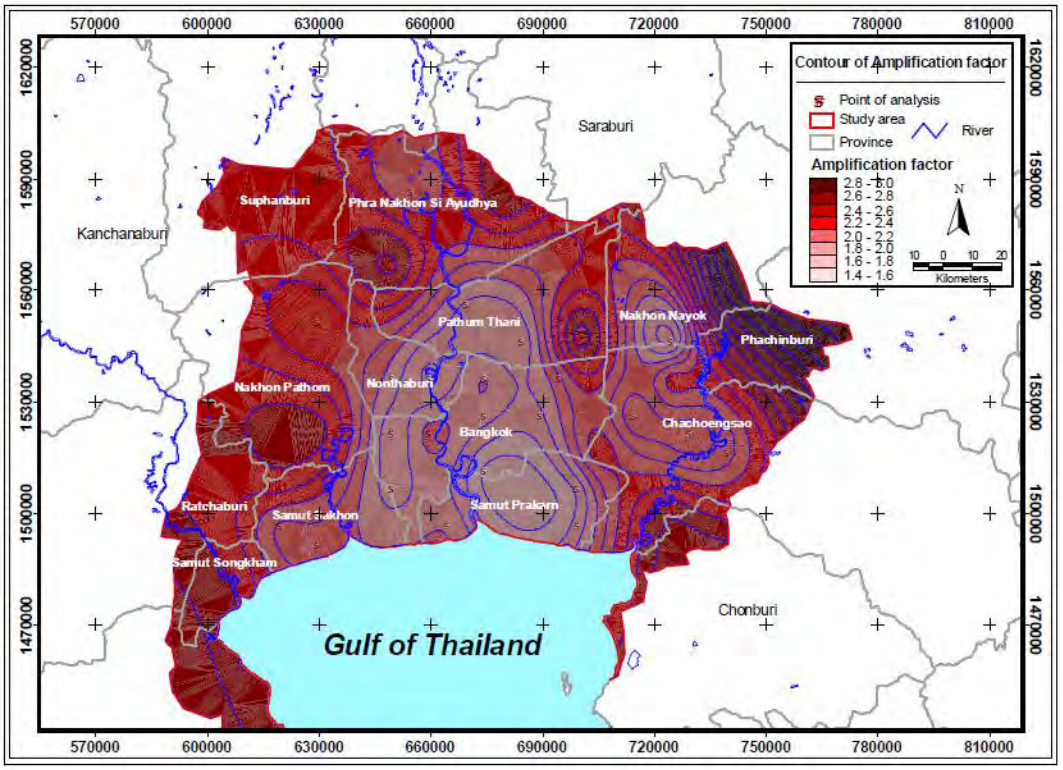

Figure 1.3 Amplification factor of soft Bangkok Clay (Yanuviriyakul and Soralump, 2009)

CHAPTER II
STUDY AREA AND METHODOLOGY

Ground motion amplification makes Samut Prakan a risk area that can be affected by earthquake forces although it is not a seismically active area. The characteristics of the chosen study area are explained in detail in this chapter. The procedure of understanding the site's amplification is completed by the brief following steps: synchrotron x-ray diffraction analyses, shear wave velocity calculation, and amplification modeling. The shear wave velocity in this study is based on mineral composition and elastic properties of soil samples. The samples are collected from Bang Phli and Bang Sao Thong districts in Samut Prakan province which is located in the Lower Central Plain of Thailand or the Chao Phraya Basin. Large sedimentary basins are sites where seismic amplification can occur. They are best targets to study ground shaking caused by seismic amplification.

2.1 STUDY AREA

The study area, Samut Prakan, is located in the southern part of the Lower Central Plain of Thailand which has Bangkok Clay as the uppermost sequence of the plain. The sequence thickness is up to about 15 m (Choowong, 2011) and some sites may thicken up to about 20 m (Tanabe *et al*., 2003). Bangkok clay, a term proposed by the Groundwater Division of the Department of Mineral Resources Thailand. This term defines the marine clay that is deposited due to the Holocene transgression and regression in the region of the Lower Central Plain. It is mainly green to greenish gray beds of soft silty clay intercalated with fine to very fine-grained sand (Choowong, 2011).

The soft clay is underlain by sand and bedrock of higher velocities due to greater bulk modulus and other rock properties. For that reason, when seismic waves travel from solid bedrock and reach the soft sediment, the waves are amplified and the ground may shake at a greater amplitude. Moreover, major minerals in Bangkok Clay are kaolinite, illite, and montmorillonite (Holmberg, 1977; Shibuya and Tamrakar, 2003; Tan, 2003) which were deposited in a marine deltaic environment. These clay minerals have anisotropic properties and different texture strengths affecting the difference of wave velocities in each of the directions. To give an accurate assessment of the ground motion, the shear wave velocities in different directions are calculated in this study based on the geologic characteristics of the soil, i.e., mineral composition and elastic properties of the samples.

2.2 METHODOLOGY

2.2.1. Data Collection and Soil Sampling

Soil samples are collected from two study areas. The first location, BP (13°40'32"N, 100°44'21"E), is a 42 m-borehole collected on October 15, 2015 near Suvarnabhumi Airport in Bang Phli district. The second study area, BS (13°40'15"N, 100°47'58"E), is a 30.5 m-borehole collected on October 23, 2015 at Wat Si Waree Noi School in Bang Sao Thong district (Figure 2.1). Samples from BP and BS are 23.00 m and 17.50 m deep, respectively. The undisturbed core samples are collected at a range of 50 cm and samples from some depths are missing due to the obstacles while drilling. Consequently, only an approximate of 15 to 20 cm can be extracted and preserved from each range. The valid ranges of the core samples are shown in Table 2.1.

The BP and BS soil samples are sampled with an interval of 1.5 m and 2.0 m, respectively. However, some are sampled with an interval less than 1.5 m or more than 2.0 m to average the samples from the missing depths. Table 2.1 shows the depth of the sampled soil from both boreholes.

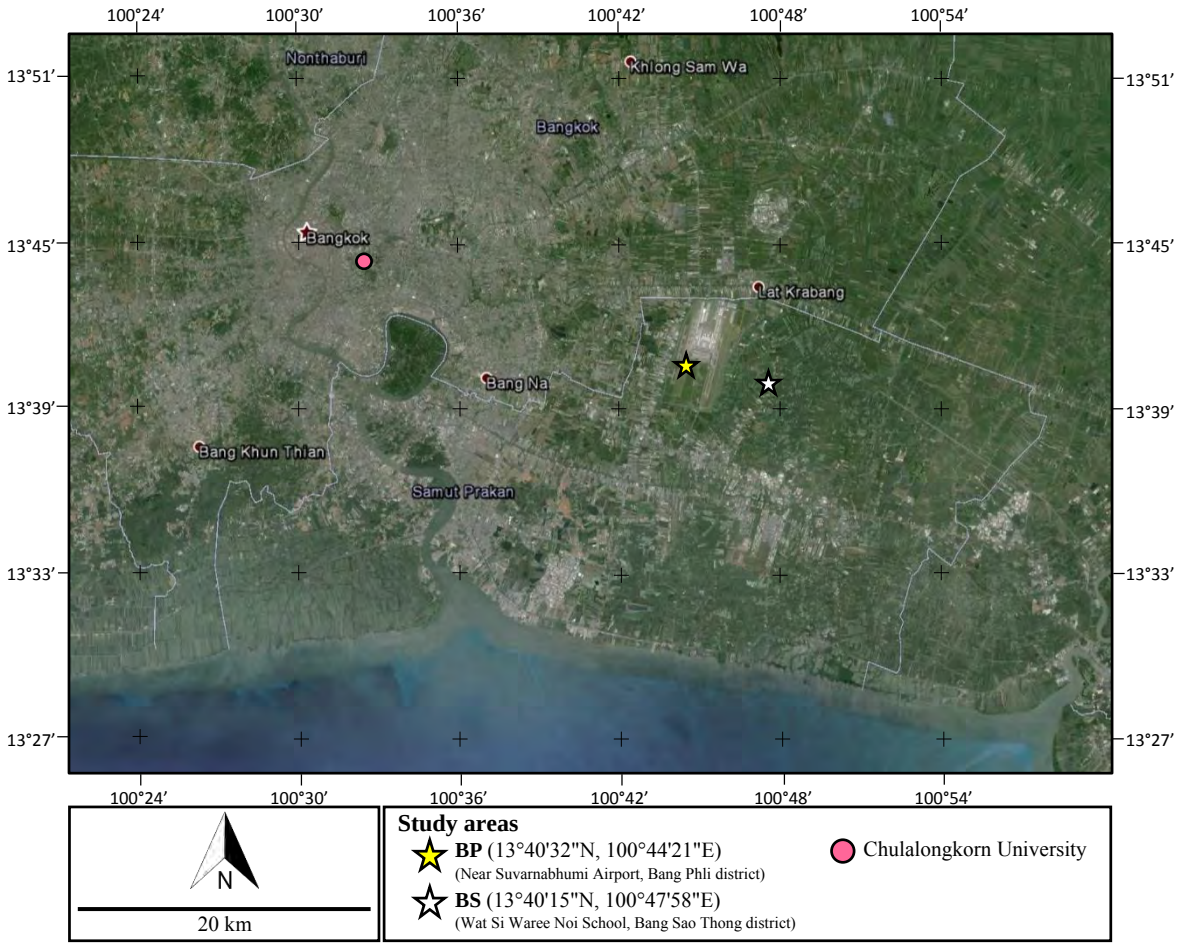

Figure 2.1 Locations of the study areas in Samut Prakan which are at Bang Phli (BP) and Bang Sao Thong (BS) districts. Chulalongkorn University is positioned as a reference.

Table 2.1 Depth of core samples from boreholes at the study areas and the sampled depth for x-ray diffraction analyses. The sampled depth in bold are further analyzed by synchrotron x-ray diffraction.

Amphoe Bang Phli (BP)		Amphoe Bang Sao Thong (BS)	
Core sample depth range (m)	**Sampled depth (m)**	**Core sample depth range (m)**	**Sampled depth (m)**
3.00-3.50	3.25	3.00-3.50	3.00
4.50-5.00	**4.75**	4.50-5.00	5.00
6.00-6.50	6.25	7.50-8.00	7.50
7.50-8.00	7.75	9.00-9.50	**9.00**
9.00-9.50	**9.25**	10.50-11.00	**11.00**
12.00-12.50	12.25	12.00-12.50	12.50
13.50-14.00	**13.75**	13.50-14.00	-
15.00-15.50	15.25	15.00-15.50	15.00
16.50-17.00	16.75	16.50-17.00	17.00
17.00-17.50	**17.25**	18.00-18.50	-
		19.00-19.50	19.00
		21.00-21.50	**21.00**
		22.50-23.00	**23.00**

2.2.2. Data Analyses

2.2.2.1 Synchrontron X-ray Diffraction

Synchrotron x-ray diffraction is a method using x-ray beams from synchrotron light source. It is the electromagnetic radiation emitted when accelerated electrons are forced to change direction under the action of a magnetic field. Synchrotron marks some particular differences from the x-ray diffraction practised in the laboratory (at the Department of Geology, Chulalongkorn University) by its greater intensity and brilliance. The x-ray beam generated from synchrotron light is also highly collimated and polarised.

Both x-ray diffraction at the department and synchrotron x-ray diffraction at the Advance Light Source (California, USA) were applied to the soil samples. At first, all samples were analyzed by XRD at the department to obtain the preliminary result of the mineral composition at each depth. The soil samples were heated at 80°C, according to the laboratory oven limitations, for twelve hours to dry out the samples. Our study predicts that there are montmorillonite comprising in the soil. This clay mineral is categorized in the smectite group, containing water molecules in

its structure. The final destruction of montmorillonite lattice begins at about 600°C, immediately following the loss of (OH) lattice water, and is essentially complete at 800°C to 850°C (Grim and Bradley, 1940). So, note that montmorillonite will not lose water from its structure by heating the sample at 80°C. The samples were then crushed into silt size grains and the x-ray diffraction was applied to all samples with an x-ray wavelength of 1.54 Å. The diffraction started from 5° to 50° with an increment of 0.01°.

To get a better resolution of the composing clay minerals, eight soil samples with high clay contents from the XRD results were further analyzed by synchrotron x-ray diffraction method. The x-ray beams from synchrotron light source interact with the samples at very low angle and the detector of the diffracted beam has a very large area. As a result, clay minerals that can be detected at very small angles are observed by this technique. Another set of samples were prepared from each chosen depth by cutting the soil into a 1 cm^3 cubic shape, and embedded in epoxy. The epoxy was polished until approximately 2 mm thick and until the soil surface was exposed. A monochromatic x-ray beam with a wavelength of 0.117418 Å was applied to the samples. The samples were rotated around the horizontal axis from -45° to 45° in 15° increments to improve the pole figure coverage for texture analysis, and seven diffraction images were recorded at the silicon detector situated about 2253 mm away. For the Rietveld refinement, MAUD (Material Analysis Using Diffraction) program was used to identify the mineral composition, volume fractions, and also computing the preferred orientation distributions (or texture). The quantitative texture analysis was analyzed in MAUD by the EWIMV algorithm using 10° resolution for the orientation distribution functions (ODFs). Then the ODFs were exported from MAUD and smoothed in BEARTEX software to calculate pole figures (Wenk *et al*., 1998).

2.2.2.2 Shear Wave Velocity Calculation

Velocities and elastic constants are related to each other. BEARTEX software contains various functions to determine the elastic constants of the soil, which are further used for shear wave velocity calculation. CSEC function was applied to impose symmetries of each ODFs of the minerals, reducing the elastic tensor from twenty-one to five independent components in standard two-index Voigt notation, i.e., $C_{11} = C_{22}$, $C_{12} = C_{11}–2C_{66}$, $C_{13} = C_{23}$, C_{33}, and $C_{44} = C_{55}$, and all others are equal to zero (Vasin *et al*., 2013). The ODFs of each mineral and the single-crystal stiffness tensors were incorporated to determine the polycrystal tensor properties using TENS. Then, the volume fraction of the constituent minerals were taken into account to calculate soil's elastic stiffness coefficient, C_{ij}, using TENX. VELO calculates longitudinal and transverse wavespeed surfaces from stiffness tensors (Wenk *et al*., 1998) of the soil. The relationship of the velocity and elastic constants can be explained by means of the following equations (Dewhurst and Siggins, 2006):

$$V_{Pv} = (C_{33}/\rho)^{½},$$
$$V_{Ph} = (C_{11}/\rho)^{½},$$
$$V_{Sv} = (C_{44}/\rho)^{½},$$
$$V_{Sh} = (C_{66}/\rho)^{½},$$

and

$$C_{13}=(-C_{44}+[4\rho^2qV^4_{P45}-2\rho qV^2_{P45}(C_{11}+C_{33}+2C_{44})+(C_{11}+C_{44})(C_{33}+C_{44})]^{1/2})$$

where V_{Pv} is the P-wave velocity along the axis of rotational symmetry (the bedding normal), V_{Ph} is the P-wave velocity parallel to the bedding, V_{Sv} is the S-wave velocity normal to the bedding with polarization parallel to bedding, V_{Sh} is the S-wave velocity parallel to the bedding with polarization parallel to the bedding, qV_{P45} is the quasi P-wave phase velocity 45° to the bedding and ρ is the bulk density. Here, our study consider shear wave velocity which the elastic coefficients associated with S-wave propagations are C_{44} and C_{66}.

2.2.3 Amplification Profile Modeling

One dimensional site response analysis of the study area was modeled by DEEPSOIL software. To begin with a simple modeling, this study focuses on the equivalent linear frequency domain and non-linear dynamic properties formulations. The equivalent linear method approximates nonlinear behavior of soil by incorporating a shear strain dependent shear modulus and damping soil curves (Park and Hashash, 2004). Figure 2.2 illustrates the idealized soil stratigraphy used for frequency domain solution which could solve the propagating wave through a multi-layered soil column. In brief, there are three main concerns to function in DEEPSOIL: soil profile and dynamic properties of soils, shear wave velocity, and input motion or earthquake waveform.

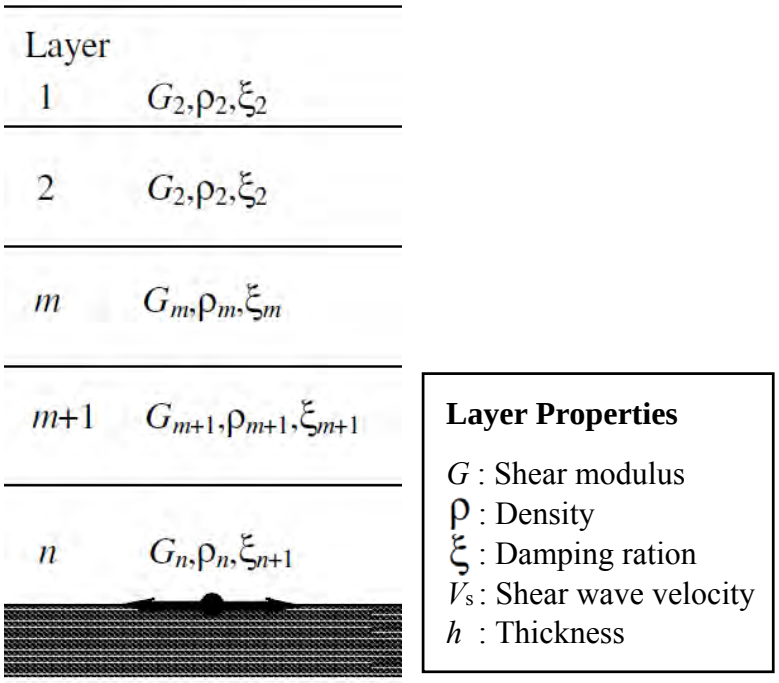

Figure 2.2 Layered soil column and properties used for frequency domain solution (Park and Hashash, 2004).

2.2.3.1 Soil Profile and Dynamic Soil Properties

The soil profile were modeled to 40 m deep for the amplification simulation. The input motions are ought to be released at the bottom of the deepest layer in BP and BS. For this reason, if the earthquake waveforms are collected exactly beneath BP and BS, the modeling results will be realistic. However, there are no accelerometer stations at BP and BS. The earthquake waveforms used in this study are provided from the Thai Meteorological Department (TMD). The accelerometer of TMD in Bangkok (Bang Na district), TMDA station, is located at 13°40'6"N 100°36'24"E, around 14 and 20 km to the west from BP and BS, respectively. It is placed in a borehole at approximately 47 m deep. According to the depth of the accelerometer, the soil profiles in our study are required to the depth of 40 m for DEEPSOIL modeling, assuming that the soil properties at 40 m are similar between TMDA and the study areas, and so the earthquake waveforms have less differences between these two locations.

For the purposes of seismic site response analyses, the depth to bedrock itself is not as important as the depth to rock-like material that behaved essentially as bedrock (Lysmer *et al.*, 1970), i.e., material having a shear wave velocity on the order of 800 to 1200 m/s or 2000 m/s (Duangsano, 2014). In fact, Lysmer *et al.* (1970) found that the response at the ground surface was relatively independent of the shear wave velocity of the assumed rock-like material. Some effect was observed, however, on the assumed depth to rock-like material, and whether or not an intermediate rock-like layer was modeled between the bottom of the soil profile and the surface of the bedrock. This effect was mainly on the frequency content of the motion at the ground surface; the peak ground acceleration was relatively unaffected. Lysmer *et al.* (1970) concluded that effect of depth to rock-like material can have a significant effect on the computed response, especially the shape of the response spectra, and that the effect on the analyses of the assumed bedrock conditions should be considered. Nevertheless, modeling with assumed rock-like material would likely have little effect on the predicted levels of peak ground acceleration. Moreover, the average shear wave velocity of the top 30 m of the Earth is a widely used parameter for classifying sites to predict their potential to amplify seismic shaking (Boore, 2004). According to previous studies and the available soil log data of BP and BS reaching only to the depth of approximately 40 m, this study simulated the amplification profile starting from the surface to 40 m deep, excluding the depth to rock-like layer.

The soil log data of BP and BS provide information of their soil type, i.e., soft clay, stiff clay, and sand. It also gives information on some dynamic soil properties which is the unit weight of soil. However, the input data for DEEPSOIL modeling require other dynamic soil properties such as damping ratio, reference stress, and reference strain, which can be measured in laboratory tests. Therefore, the missing dynamic soil properties in our study are mainly based on the study by Duangsano (2014). The Bangkok soft clay samples from three different sites, Chulalongkorn University (CU), AIT, and Ban Tumru in Samut Prakan were tested. The experiments

resulted in a normalized shear modulus reduction curve and material damping curve, which the dynamic properties of soils can be extracted from these curves. Among the three sites, BP and BS use the soil data and dynamic soil properties of CU site because they are all located on the same sediment distribution, i.e., delta plain (Figure 2.3). CU site is approximately 20-30 km to the west from BP and BS. The soil profile at CU can be a good representative for Bangkok clay in the delta plain.

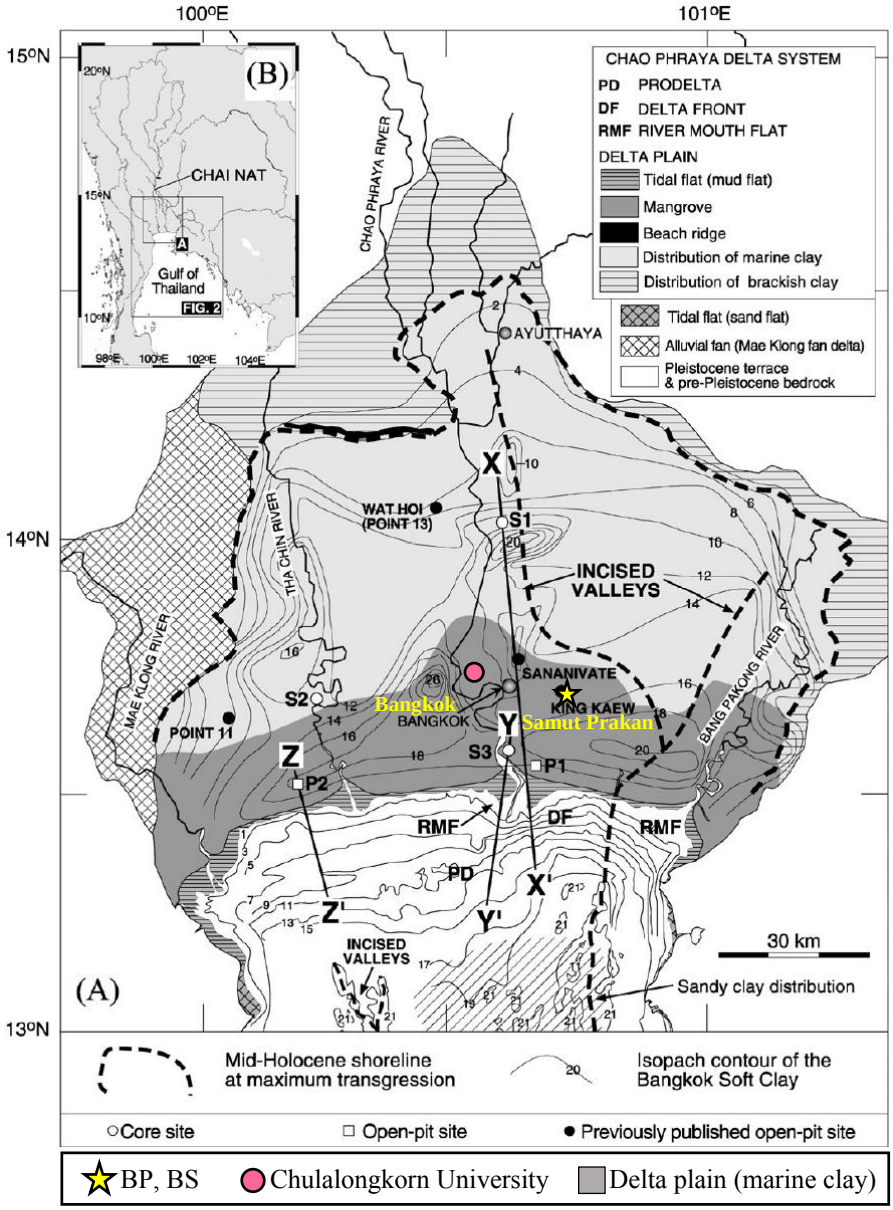

Figure 2.3 Geomorphology and sediment distribution of the Chao Phraya delta plain and the adjacent region (Modified from Tanabe *et al*., 2003). Sediment distributions on the delta plain and in the Gulf of Thailand are based on Somboon (1988). CU, BP, and BS are located on the same sediment distribution which is the delta plain region.

BP's soil log data are provided up to 42 m deep and the soil types are defined to all depths (Figure 2.4). The missing data, the dynamic soil properties, are based on CU site. On the other hand, the borehole at BS was drilled to 30.5 m deep. The soil types are identified to the depths with the soil log data (Figure 2.4), but the soil types below 30.5 m and the missing dynamic soil properties are based on the soil data of CU site as well.

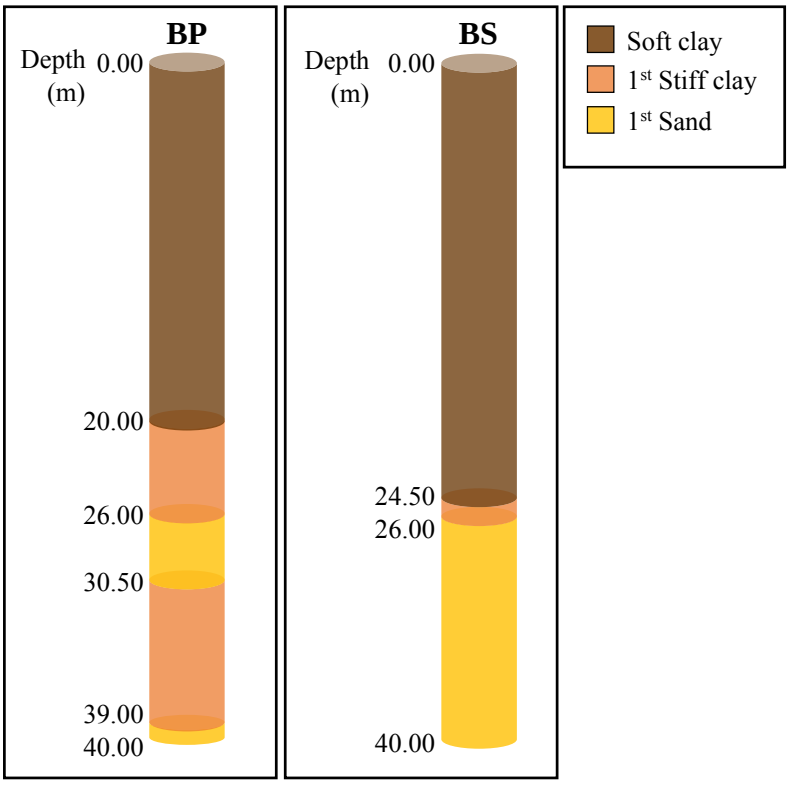

Figure 2.4 Soil type according to depth at BP and BS. BP's soil types are determined based on soil log data. For BS, the soil types until 30.5 m are defined based on the available soil log data but values below 30.5 m use CU soil profile data from the study by Duangsano (2014).

2.2.3.2 Shear Wave Velocity for DEEPSOIL Modeling

Shear wave velocities accomplished by the previous step in BEARTEX software are based on the available soil samples. The soil types of the samples are defined as soft clay. The depths with V_S values from BP soil samples are 4.75, 9.25, 13.75, 17.25 m, and for BS soil samples are 5.00, 9.00, 11.00, and 23.00 m. BP and BS have velocity values only until the depth of 17.25 m and 23.00 m, respectively. Accordingly, shear wave velocities below those elevations are based on shear wave velocities of CU soil profile from the study by Duangsano (2014). Soil below the samples are classified as stiff clay and sand which the shear wave velocities assigned to 1st stiff clay and 1st sand of CU site are 170 and 250 m/s, respectively.

2.2.3.3 Earthquake Waveforms

Earthquake waveforms from three seismic sources, Phayao Fault, Three Pagoda Fault Zone, and Sagaing Fault Zone, were used for the response analysis. The earthquake events are chosen based on three main reasons. First, the events have high magnitude, having enough energy and the potential to reach Central Thailand. Second, the seismic sources that caused the events, excluding Phayao Fault, have records of affecting tall buildings in Bangkok and neighboring provinces. Third, the chosen events are caused by far and near earthquake sources, giving waveforms of different accelerating patterns (Figure 2.5). Note that the earthquake record from Phayao Fault is used to estimate the probable earthquake generated from Mae Chan Fault. Due to lack of recent records from TMD, the responses from Mae Lao Earthquake (Phayao Fault) are assumed to concurrently represent the ground motion from Mae Chan Fault, the worrying active fault in north Thailand.

Responses from different seismic events simulate different ground shaking behaviors. The teleseismic sources are represented by Sagaing Fault Zone and Phayao Fault, and Three Pagoda Fault Zone express the local seismic source. The earthquake records are provided by the Seismological Bureau of TMD. Only events after year 2007 are valid. The seismic waves at the TMDA station were recorded in three oscillation movements: N-S, E-W, and Z-axis perpendicular to the Earth's surface. Mae Lao Earthquake and Thabeikkyin Earthquake use the oscillation in N-S direction, and Sangkhlaburi Earthquake uses the E-W axis for the amplification modeling. Table 2.2 displays details of the earthquake events.

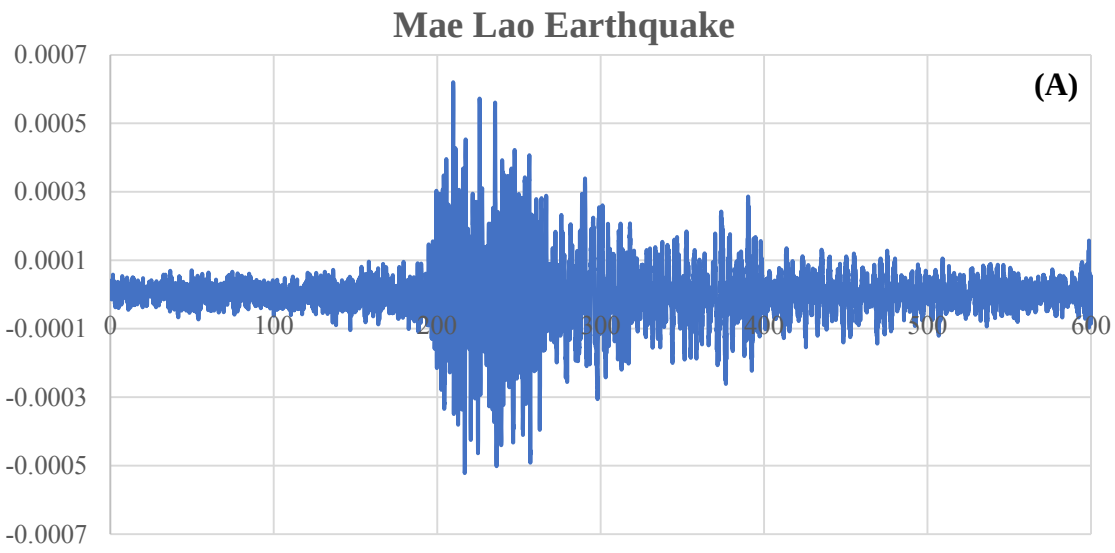

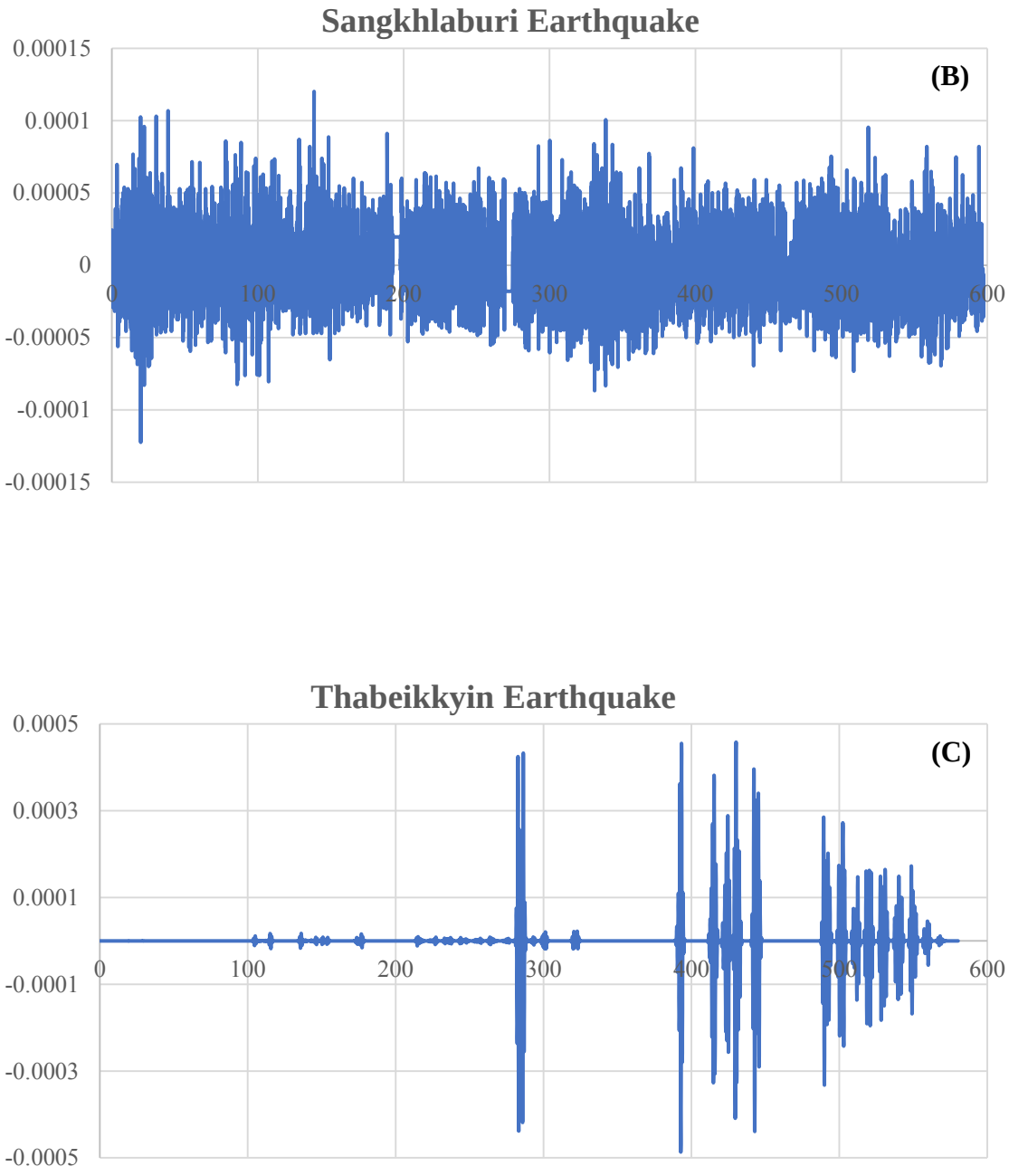

Figure 2.5 Wave patterns of different earthquake records, (A) Mae Lao, (B) Sangkhlaburi, and (C) Thabeikkyin Earthquake (Myanmar). The peak ground acceleration at TMDA for each event are 0.00062 g, 0.00012 g, and 0.00049 g, respectively.

Table 2.2 Earthquake events for 1D amplification modelling in DEEPSOIL.

Date	Event	Moment Magnitude (Mw)	Source
May 5, 2014	Mae Lao Earthquake	6.3	Phayao Fault
July 14, 2015	Sangkhlaburi Earthquake	4.8	Three Pagoda Fault Zone
November 11, 2012	Thabeikkyin Earthquake	6.8	Sagaing Fault Zone

SeisGram2K software was used to export the wave records into numerical data. The obtained data were in time versus count unit. Counts were converted to m/s^2 by dividing with 213909.5, a constant of the TMDA's accelerometer, and converted again to standard gravity, g. The timing of the recorded acceleration had a 0.01 s increment. The amplification profile were modeled using 0.05 s increment to decrease the excessive data, but remark that this may have deducted some amplitude peaks of the waves.

Ornthammarath *et al.* (2011) proposed a set of probabilistic seismic hazard maps for Thailand to present expected ground motions in terms of peak ground acceleration (PGA) and spectral acceleration (SA). Samut Prakan is situated in the region of PGA ranging from 0.02-0.04 g and 0.05-1.0 g, corresponding to a probability of exceedance of 10% and 2% in 50 years (475 and 2,475 years), respectively. Consequently, the PGA of the waveforms in this study are scaled to 0.1 g to best represent the strong ground motion positively to occur. The waveforms were input into DEEPSOIL, incorporating with the soil profiles, dynamic soil properties, and shear wave velocities. The amplification profiles were modeled from the software, displaying the PGA responded from the earthquakes at each soil layer. Finally, the amplification factors are calculated from the following equation:

$$\mathrm{AF} = \frac{PGA_{surface}}{PGA_{rock\ site}}$$

whereas our study exclude the rock site layer, the amplification factor is defined from the PGA at the surface to the PGA at the top of the bottommost soil layer where the waveforms were released in the model.

CHAPTER III
RESULTS

This chapter presents results from synchrotron x-ray diffraction experiments and the Rietveld analyses in MAUD software for mineral composition of soil samples, volume fractions, and crystallographic preferred orientation (CPO). The CPO and mineral volume fractions are used to further calculate elastic properties and shear wave velocities of soil samples in BEARTEX software. The resultant velocities are key parameters for predicting amplification factors. By incorporating shear wave velocities with soil profile, dynamic soil properties, and earthquake waveforms in DEEPSOIL software, the ground motion response from earthquake records can be obtained.

3.1 MINERAL COMPOSITION

BP samples with high clay contents are chosen from depths of 4.75, 9.25, 13.75, and 17.25 m. Likewise, the depths of high clay contents for BS are 5.00, 9.00, 11.00, and 23.00 m. The total eight samples were examined by synchrotron x-ray diffraction and examples of diffraction images from the experiment are shown in Figure 3.1. Intensity variations along the Debye rings reveal some CPO of the composing minerals. The soil samples at BP 17.25 m and BS 9.00 m display the strongest CPO among the samples from other depths.

The calculated spectra analysis in MAUD software are shown in Figure 3.2 which indicates a close similarity in analyzed intensities and position of diffraction peaks of mineral phases, compared to the experimental spectra. The mineralogy of the soil samples are dominated by phyllosilicates approximately 60-80 vol%, i.e., illite-mica, montmorillonite, and dickite. The sheet silicates show degrees of preferred orientation. The other major component is quartz which occupy about 20-35 vol% and other minerals are presented in relatively minor amounts which includes calcite, pyrite, halite, gypsum, and magnesite. Table 3.1 summarizes the composition and volume fractions of each samples.

3.2 CRYSTALLOGRAPHIC PREFERRED ORIENTATION

Textures for illite-mica, montmorillonite, and dickite are strong in (001), parallel to the bedding plane. Figure 3.3 shows 2D map plots of the samples at the tilting angle with the strongest texture, i.e., 0° for BP 1725 and -45° for BS 900. The images represent stacks of the 36 diffraction images. The observations are at the bottom while the calculated refinements are at the top, and the comparison fits suitably which suggests that the refinements are reliable. The textures can also be described by pole figures which is displayed in Figure 3.4. Pole densities are normalized so that the integral over a pole figure is 1.0 and densities are expressed in multiples of random

distribution (m.r.d.). The pole figures for the sheet silicates are displayed in (001) plane and their densities on the projections are reported in Table 3.2. The maximum possible CPO of the clay minerals range from m.r.d. of 1.2 to 4.1. Illite-mica display strongest texture in BP (4.12 m.r.d.) and is strongest for dickite in BS (2.56 m.r.d.). Quantitative results from Rietveld refinement, i.e., crystallographic preferred orientation distribution functions (ODFs) of the clay minerals are further used for the elastic properties and shear wave velocity calculations.

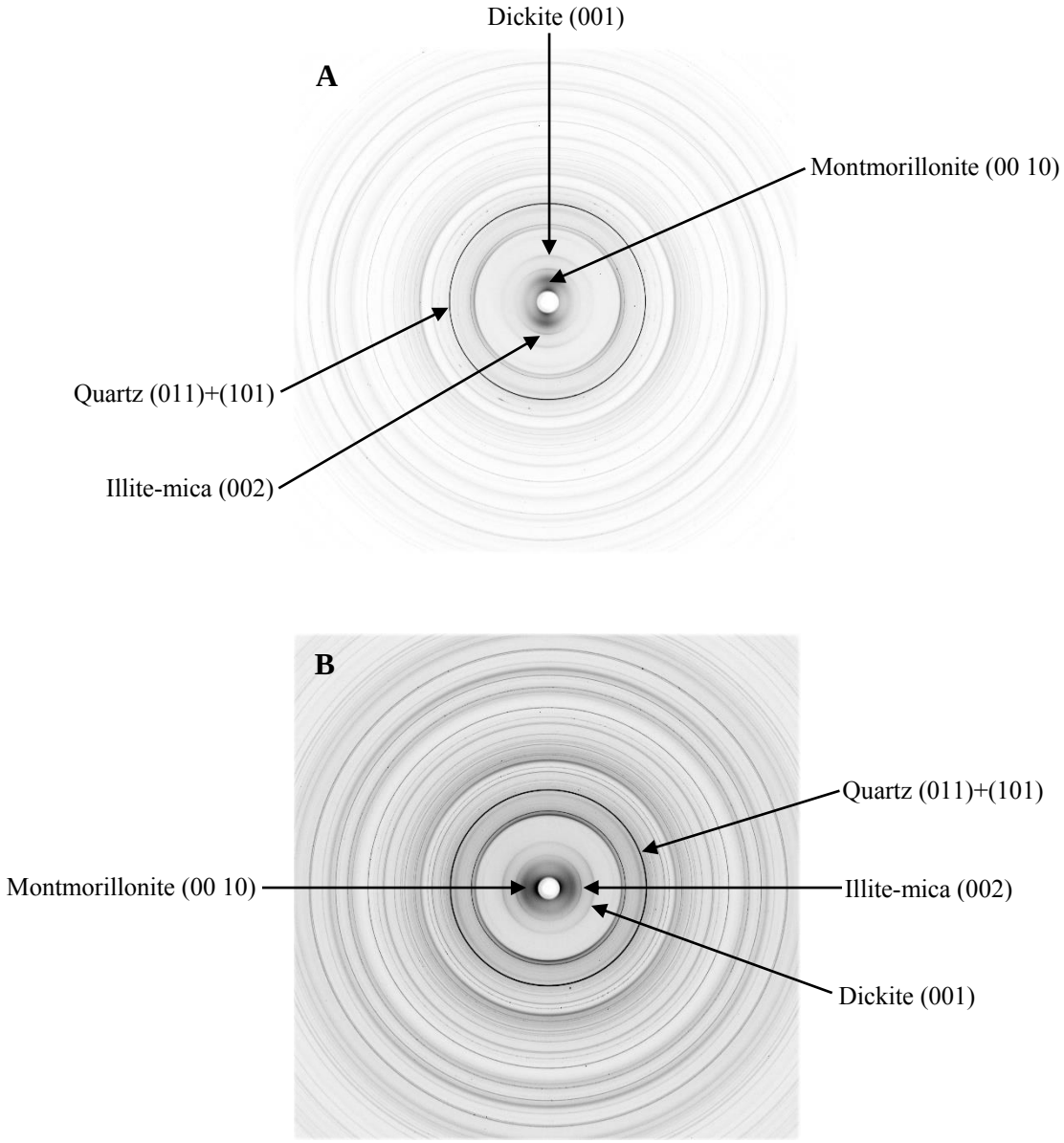

Figure 3.1 Diffraction images of (A) BP 1725 and (B) BS 900. Intensity variations along Debye rings are indicative of texture, particularly the inner rings with high *d*-spacings.

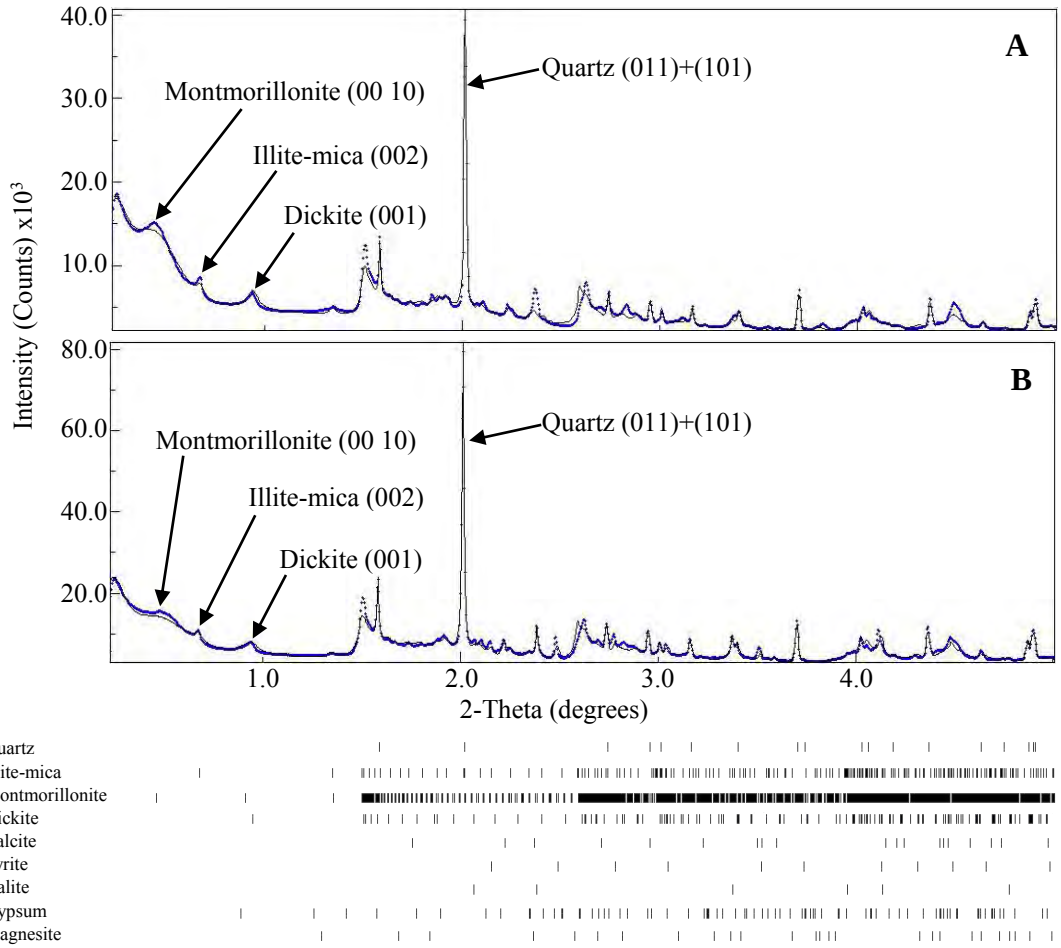

Figure 3.2 X-ray diffraction patterns of (A) BP 1725 and (B) BS 900 soil samples. Dots are experimental data and solid lines indicate the Rietveld fit. Scale is 2-Theta (degrees) and the location of diffraction peaks for individual phases are indicated at the bottom.

Table 3.1 Mineral composition and volume fractions of soil samples analyzed in this study.

	BP 475	**BP 925**	**BP 1375**	**BP 1725**	**BS 500**	**BS 900**	**BS 1100**	**BS 2300**
Quartz	28.61	24.54	29.13	16.42	21.86	17.31	34.08	22.14
Illite-mica	19.29	25.91	21.53	26.80	26.83	28.22	22.14	25.73
Montmorillonite	27.28	26.25	26.18	35.27	21.46	25.42	20.46	23.72
Dickite	19.98	19.02	21.19	20.49	22.85	24.69	18.49	21.71
Calcite	3.84	3.23	0.84	0.57		1.02	2.10	
Pyrite	1.00	0.78	1.13		3.85	1.14	0.15	3.41
Halite		0.29			1.18	1.62	1.69	1.37
Gypsum					1.96	0.59	0.88	1.93
Magnesite				0.46				

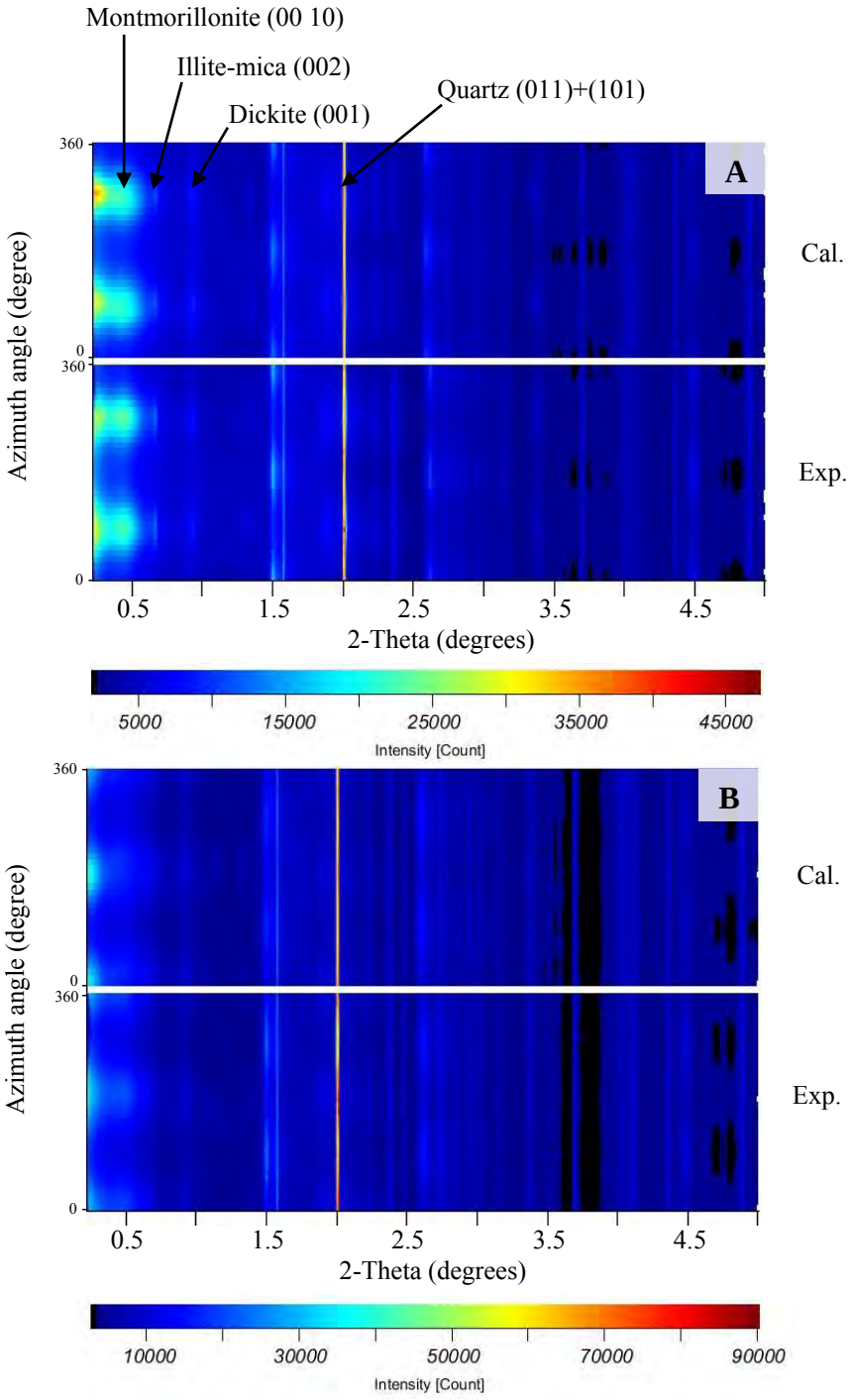

Figure 3.3 Two dimensional (2D) map plots of (A) BP 1725 and (B) BS 900 showing the stacking of diffraction patterns, comparing experimental data (bottom) with calculated spectra (top). The images represent stacks of 36 diffraction spectra averaged over 10° azimuthal intervals, and displays the strongest texture among images of seven tilting angles. Scale is 2-Theta (degrees).

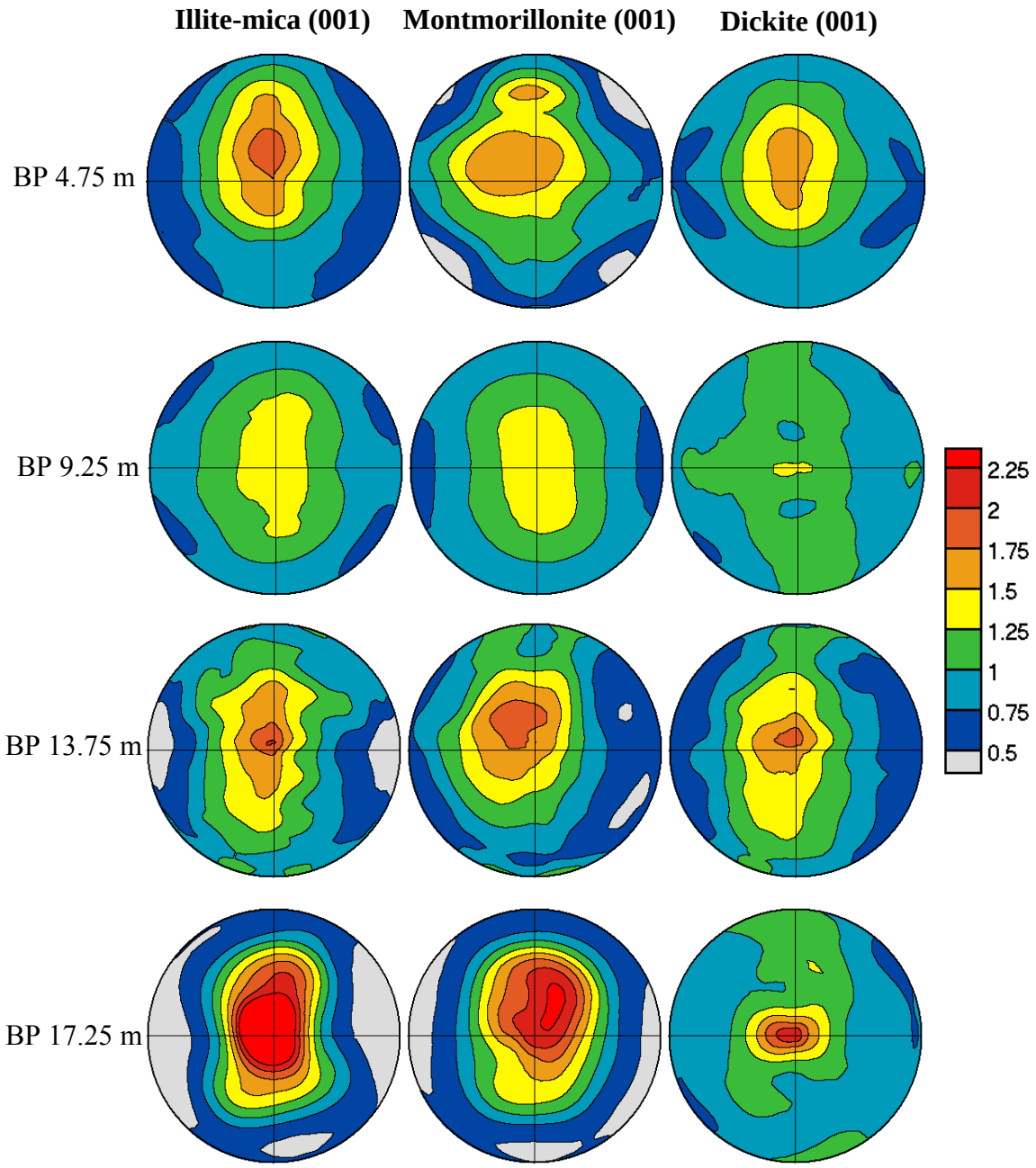
Illite-mica (001)
Montmorillonite (001)
Dickite (001)
BP 4.75 m
BP 9.25 m
BP 13.75 m
BP 17.25 m
2.25
2
1.75
1.5
1.25
1
0.75
0.5

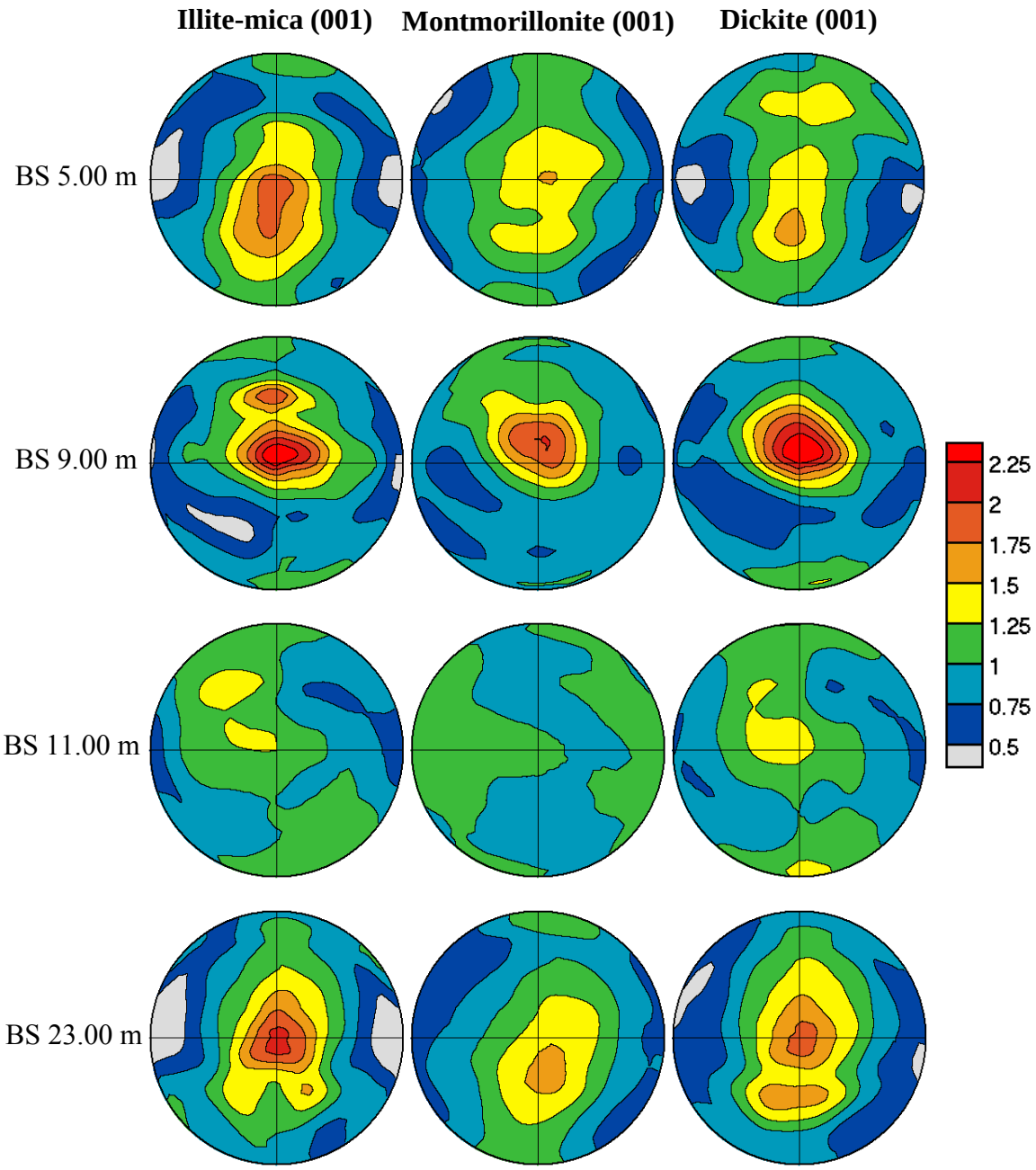

Figure 3.4 Pole figures of illite-mica, montmorillonite, and dickite at the sampled depths of BP and BS. Equal area projections on bedding plane, linear contour intervals, and values are in multiples of random distribution (m.r.d.). For texture strength, see also Table 3.2.

Table 3.2 Minimum (top) and maximum (bottom) values on pole figure (001) of phyllosilicates comprising the soil (in m.r.d.).

	BP 475	**BP 925**	**BP 1375**	**BP 1725**	**BS 500**	**BS 900**	**BS 1100**	**BS 2300**
Illite-mica	0.56 1.95	0.69 1.46	0.34 2.03	0.26 4.12	0.36 1.94	0.43 2.50	0.59 1.47	0.25 2.12
Montmorillonite	0.38 1.72	0.69 1.44	0.4 1.92	0.39 2.31	0.47 1.52	0.66 2.01	0.79 1.21	0.55 1.58
Dickite	0.63 1.65	0.71 1.32	0.53 1.88	0.6 2.23	0.41 1.74	0.58 2.56	0.65 1.43	0.3 1.87

3.3 SHEAR WAVE VELOCITY

Shear wave velocities are obtained from averaging mathematical algorithms in BEARTEX software. Minerals' stiffness tensors at 0 K (Table 3.3) are incorporated with ODFs exported from MAUD, to calculate elastic stiffness coefficient for the mineral phases using TENS function. The previous geometric mean stiffness tensors of each mineral from TENS are incorporated with the volume fraction of the composing minerals. TENX function is applied to calculate the multiphase stiffness tensor of the soil (Table 3.4). However, the minor minerals (i.e., calcite, pyrite, halite, gypsum, magnesite) are not considered for the calculation. These minerals do not have preferred orientations similar to quartz. Their amount of approximately 1-7 vol% are added into quartz in the TENX calculation. The elastic constants of the soil, C_{44} and C_{66}, are then used to calculate shear wave velocity, both V_{Sv} and V_{Sh}, at the observed depth (Table 3.5) by the following equations (Dewhurst and Siggins, 2006):

$$V_{Sv} = (C_{44}/\rho)^{½}$$

and

$$V_{Sh} = (C_{66}/\rho)^{½}$$

where C_{44} and C_{66} values derived from the calculations in BEARTEX and the bulk density of the soil (ρ) is 1.72 g/cm^3, obtained from the soil log data.

Results show that shear wave velocities of both soil profiles are approximately 4000 m/s. The velocities are overestimated due to several conditions in BEARTEX. For one reason, the program assumes that the material is densely packed with quartz, illite-mica, montmorillonite, and dickite, and the soil porosities are not considered in the calculation. Therefore, a porosity estimation has been assigned to the soil samples. An assumption of 200 m/s decrease in shear wave velocity in the horizontal plane at every 1% decrease in porosity (Vasin *et al*., 2013) is used to approximate the shear wave velocity in this study. Soil samples from the study areas are classified as silty or sandy clay (based on the Unified Soil Classification System, USCS) which porosity range from 20-64% (Hough, 1969). Consequently, a 21.5% porosity (including water content) is assigned to all samples to realistically average and reduce the calculated shear wave velocity. The reduced values are shown as V_{Sv}* and V_{Sh}* in Table 3.4. The shear wave

velocities at BP are approximately 200-380 m/s and 90-150 m/s in the vertical and horizontal plane, respectively. Note that the minus value of V_{Sv}* at 17.25 m is excluded for the amplification modeling. For BS, the shear wave velocities are approximately 110-410 m/s and 70-130 m/s in the vertical and horizontal plane, respectively.

Table 3.3 Stiffness tensors at 0 K of the composing minerals.

	C_{11}	C_{12}	C_{13}	C_{22}	C_{23}	C_{33}	C_{44}	C_{55}	C_{66}	
Quartz	87.3	6.6	12.0	87.3	12.0	105.8	57.2	57.2	40.4	e
Illite-mica	60.3	27.2	23.5	180.9	53.4	170.0	70.5	18.4	23.8	b
Montmorillonite	27.2	13.2	5.2	153.9	25.1	188.5	55.4	10.4	2.8	b
Dickite	169.1	66.1	15.4	179.7	10.2	81.1	17.0	26.6	57.6	b
Calcite	144	53.9	51.1	144	51.1	84.0	33.5	33.5	45.1	a, d, f
Pyrite	361	33.6	33.6	361	33.6	361	105.2	105.2	105.2	a, c, d
Halite	49.1	12.8	12.8	49.1	12.8	49.1	12.8	12.8	12.8	a, d, f
Gypsum	94.5	38	28.0	65.2	32.0	50.2	8.6	32.0	11	a, d, f
Magnesite	259	75.6	58.8	259	58.8	156	54.8	54.8	91.7	d, f

Note: (a) Mavko *et al.* (2009); (b) Militzer *et al.* (2011); (c) Simmons and Birch (1963); (d) Bass (1995); (e) Heylinger *et al.* (2003); (f) Hearmon (1979)

Table 3.4 Soil's stiffness tensors of (A) BP and (B) BS at each depth calculated from TENX function by BEARTEX software. The elastic constant used for shear wave velocity calculation are C_{44} and C_{66}.

(A)

Depth (m)	C_{11}	C_{12}	C_{13}	C_{22}	C_{23}	C_{33}	C_{44}	C_{55}	C_{66}
BP 4.75	89.565	23.300	25.522	89.565	25.522	87.479	34.985	34.985	33.146
BP 9.25	93.893	25.802	26.964	93.893	26.964	93.339	37.642	37.642	34.060
BP 13.75	90.692	24.159	26.038	90.692	26.038	88.500	34.785	34.785	33.279
BP 17.25	94.601	27.877	28.155	94.601	28.155	76.578	29.568	29.568	33.369

(B)

Depth (m)	C_{11}	C_{12}	C_{13}	C_{22}	C_{23}	C_{33}	C_{44}	C_{55}	C_{66}
BS 5.00	92.878	25.276	26.982	92.877	26.982	92.429	35.743	35.743	33.813
BS 9.00	92.842	27.222	28.183	92.842	28.183	91.196	33.503	33.503	32.819
BS 11.00	89.088	22.390	24.642	89.088	24.642	96.157	38.178	38.178	33.365
BS 23.00	91.806	25.182	26.755	91.806	26.755	91.111	35.219	35.219	33.324

Table 3.5 V_{Sv} and V_{Sh} of the soil samples from (A) BP and (B) BS, at the observed depth.

(A)

Depth (m)	V_{Sv} (m/s)	V_{Sh} (m/s)	V_{Sv}* (m/s)	V_{Sh}* (m/s)
BP 4.75	4510.00	4389.87	210.00	89.87
BP 9.25	4678.13	4449.98	378.13	149.98
BP 13.75	4497.09	4398.67	197.09	98.67
BP 17.25	4146.17	4404.61	-153.83	104.61

(B)

Depth (m)	V_{Sv} (m/s)	V_{Sh} (m/s)	V_{Sv}* (m/s)	V_{Sh}* (m/s)
BS 5.00	4558.60	4433.82	258.60	133.82
BS 9.00	4413.44	4368.16	113.44	68.16
BS 11.00	4711.32	4404.35	411.32	104.35
BS 23.00	4525.06	4401.64	225.06	101.64

*Approximation of 21.5% porosity

Due to the significant amount of clay minerals in the soil samples, our study consider shear wave velocity of seismic waves travelling parallel to the horizontal plane (V_{Sh}). Likewise, the seismic waves propagate parallel to the bedding plane of the sheet silicates. V_{Sh} are used for the amplification modeling which are 90-150 m/s and 70-130 m/s for BP and BS, respectively. The profile of the estimated V_{Sh} are shown in Figure 3.5.

3.4 1D Amplification Profile and Amplification Factor

The one dimensional amplification profile of the study areas were modeled in DEEPSOIL program. The input motions of three seismic events are scaled to peak ground acceleration (PGA) of 0.1 g at the bottom of the soil profile. Figure 3.6 shows the amplification profiles responded from different earthquake records. The graphs are plotted between the soil profile in meters and PGA in g. Note that the data at the bottom most of the soil profile is the first PGA value responded from the 0.1 g-input motion. Following that, the PGA values at the top and bottom of the soil profile are acquired to calculate the amplification factor. Table 3.6 displays the calculated amplification factors of BP and BS. In Samut Prakan, the ground shaking are accelerated approximately 1.7 to 2.1 and 1.2 to 1.5 times at BP and BS, respectively.

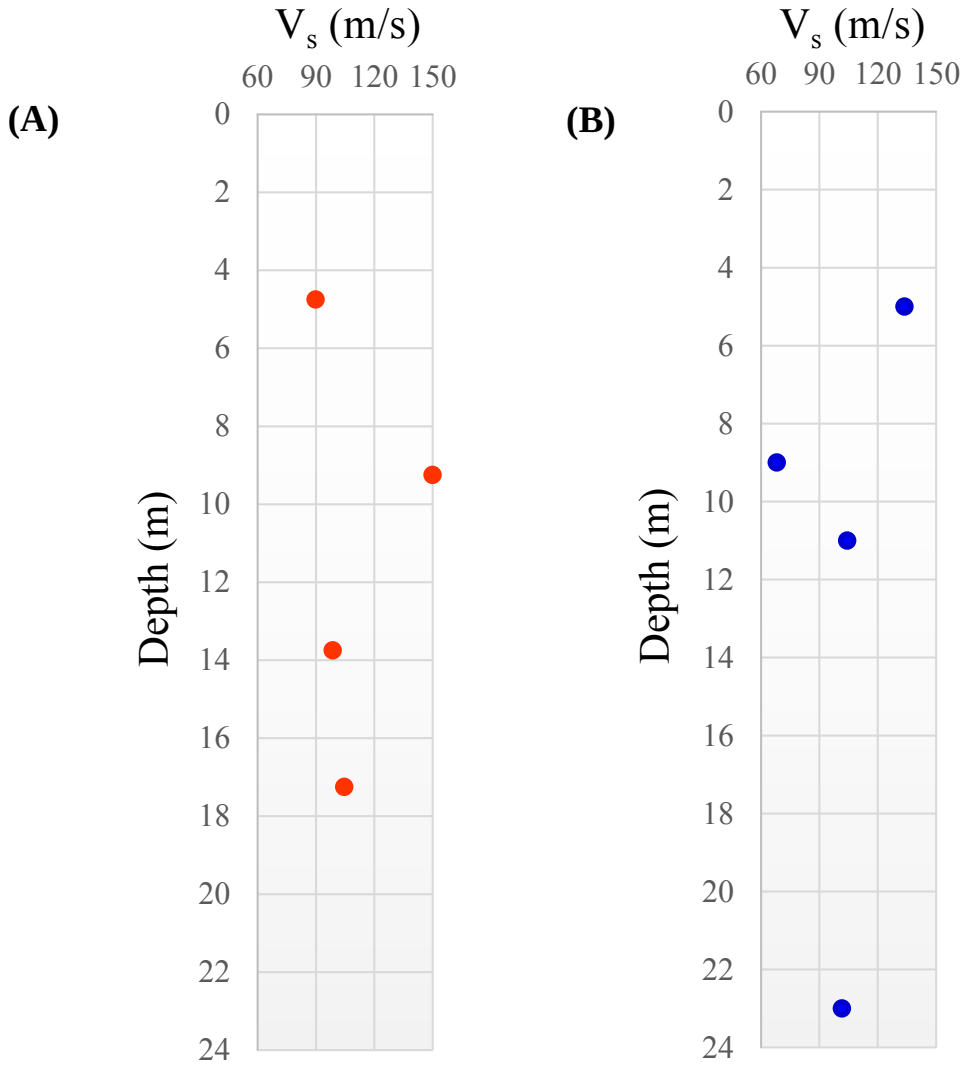

Figure 3.5 V_{Sh} profile of (A) BP and (B) BS. The figure is plotted between shear wave velocities in the horizontal plane in m/s versus depth in meters. The shear wave velocities are calculated from BEARTEX, obtained by soil's elastic properties and volume fraction of the composing minerals. A 21.5% porosity is used to approximate the overestimated values.

(A) Mae Lao Earthquake

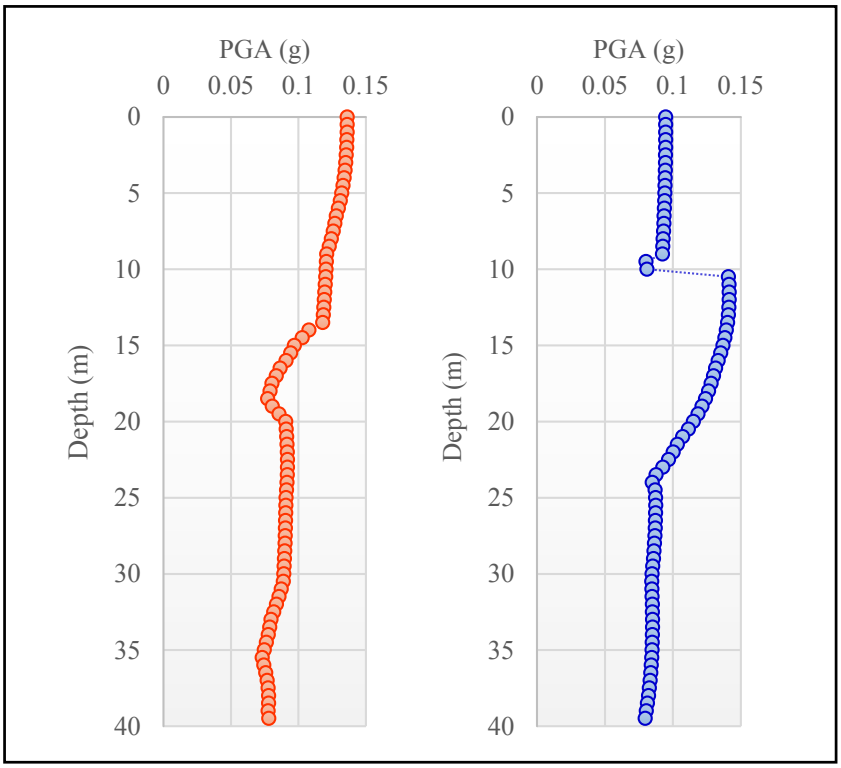

(B) Sangkhlaburi Earthquake

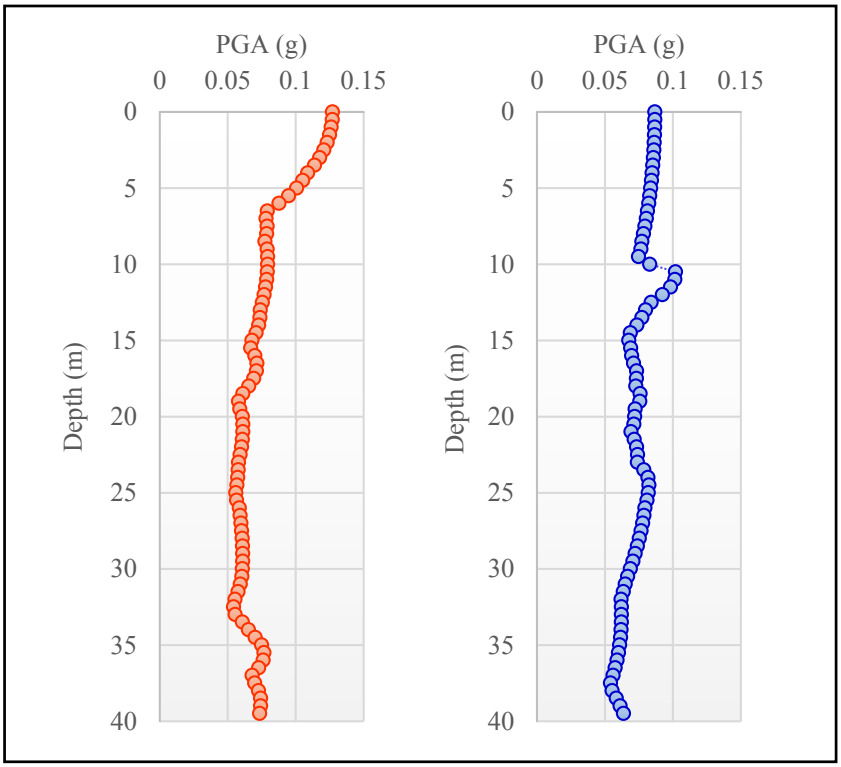

(C) Thabeikkyin Earthquake

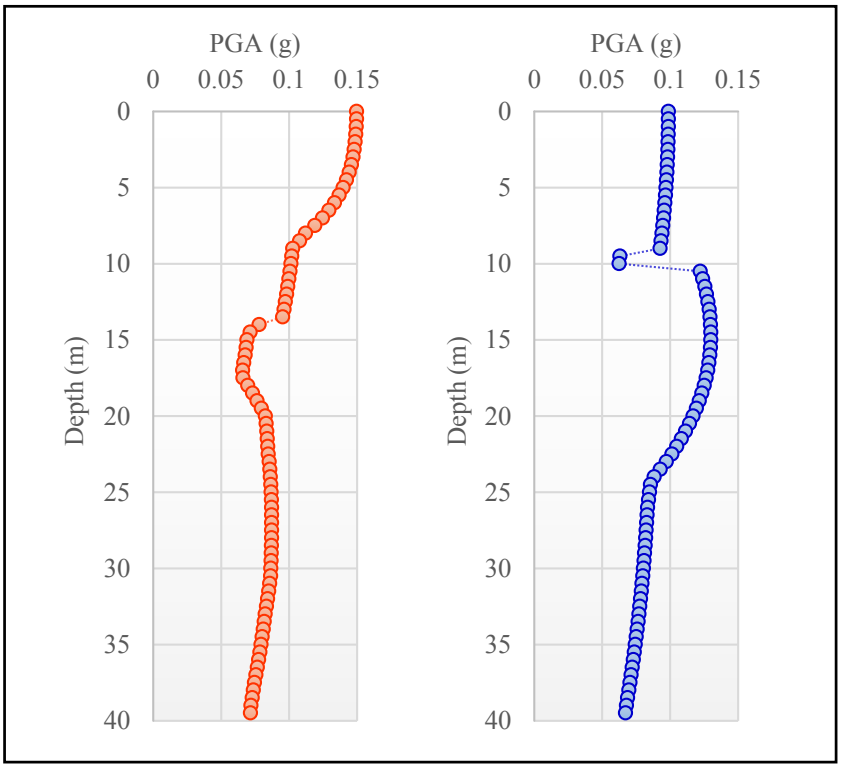

Figure 3.6 1D amplification profile of the study areas (BP: orange plots, BS: blue plots), responding from three different earthquake records which are (A) Mae Lao Earthquake, (B) Sangkhlaburi Earthquake, and (C) Thabeikkyin earthquake.

Table 3.6 Amplification factors of the study areas, responding from different earthquake records. Seismic waves were scaled to 0.1 g. Amplification factor is defined as PGA at the ground surface to PGA at the top of the bottommost layer.

	BP	**BS**
Mae Lao Earthquake (6.3 M_w) May 5, 2014	1.74	1.19
Sangkhlaburi Earthquake (4.8 M_w) July 14, 2015	1.73	1.36
Thabeikkyin Earthquake (6.8 M_w) November 11, 2012	2.09	1.47

CHAPTER IV
DISCUSSION

The results from our study includes the synchrotron x-ray diffraction analyses by the Rietveld method using MAUD software. The constituent minerals of the soil samples in our study areas imply their depositional environment and their degree of preferred orientation also varies with depth. Shear wave velocities obtained from the soil's mineral composition and stiffness tensors are compared with previous studies of shear wave velocities measured from field tests. Moreover, the response behaviors of the surface shown in values of peak ground acceleration (PGA) and amplification factor also vary with the three earthquake records. The earthquake characteristics are likely to influence the different patterns of amplification. The applications of this study towards seismic hazard and constructions are also discussed in this chapter.

4.1 MINERAL COMPOSITION

The soil samples are mainly composed of clay contents, i.e., illite-mica, montmorillonite, and dickite in total of 60-80 vol%. Our observations are consistent with previous studies of the characterization and properties of Bangkok soils by Tan (2003) which report kaolinite, illite, and montmorillonite as dominant minerals in the Bangkok Clay. Dickite ($Al_2Si_2O_5(OH)_4$) is a polymorph of kaolinite, as shown in Figure 4.1C, and has monoclinic crystal structure. Illite-mica ($(K,H_3O)(Al,Mg,Fe)_2(Si,Al)_4O_{10}[(OH)_2,(H_2O)]$) illustrated in Figure 4.1D is a phyllosilicate complex of illite interlayered with muscovite . Montmorillonite ($(Na,Ca)_{0.33}(Al,Mg)_2(Si_4O_{10})(OH)_2 \cdot nH2O$) in Bangkok clay is classified as a high-swelling type (Ohtsubo *et al.*, 2000), which contains a number of water molecules in its structure as shown in Figure 4.1E. A study by Cox (1968) suggests that the presence of montmorillonite in Bangkok clay would also characterize the high liquid limit which means that the soil acquires high water content to change the consistency of itself, from plastic to liquid. Montmorillonite is also a high activity layered silicate clay, having high cation exchange capacity due to their large surface area. They have a great capacity to retain and supply nutrients such as calcium, magnesium, potassium, and ammonium. As a result, these clays tend to produce highly fertile soils.

The occurrence of clay minerals can develop understandings of their depositional environments. Kaolinite and dickite is favored by acidic conditions such as freshwater environment or subaerial environment. Illite-mica may be deposited by marine deposits and may change to montmorillonite (smectite group) by means of the following reaction (Hower *et al*., 1976):

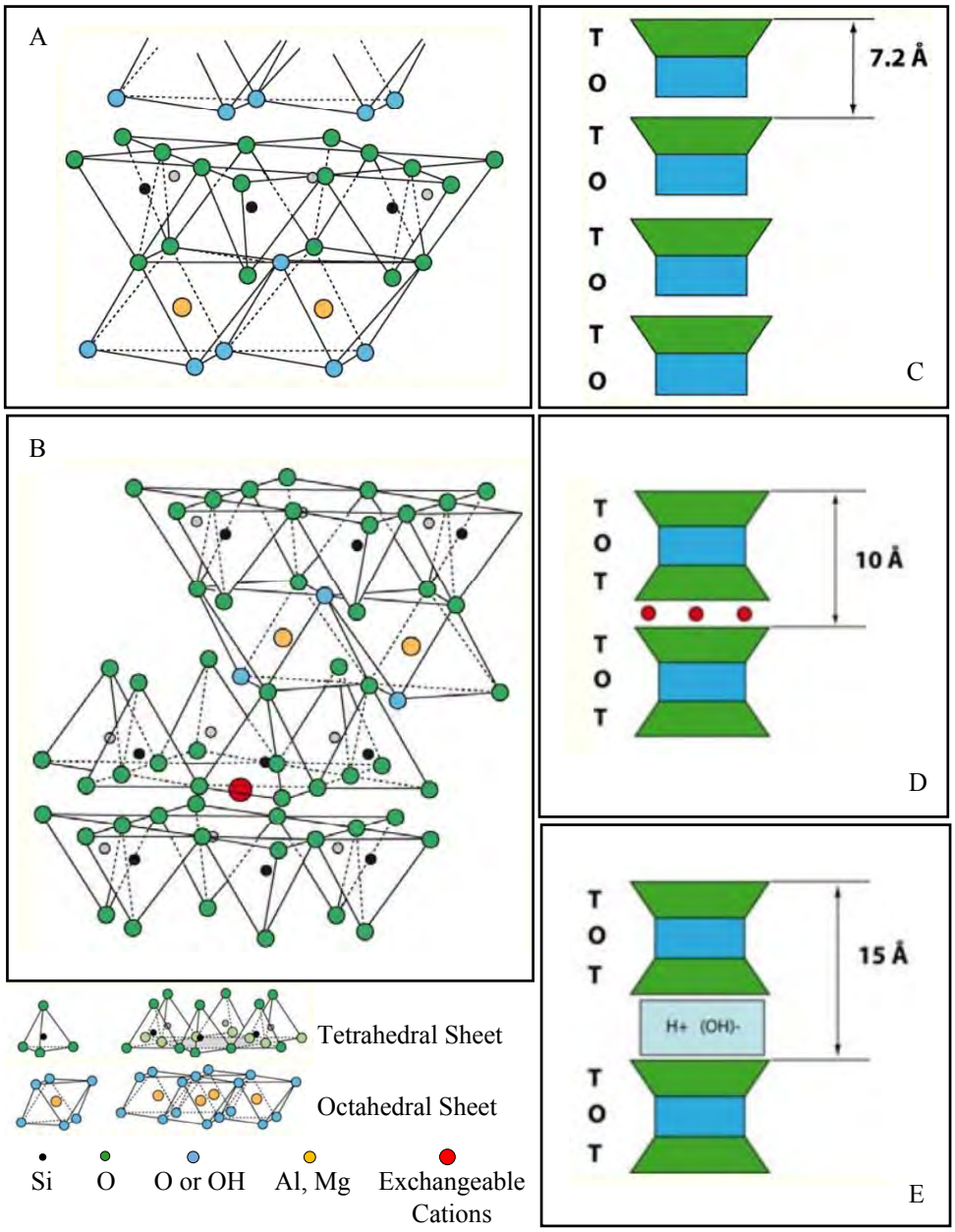

Figure 4.1 Clay minerals structure of dickite, illite-mica, and montmorillonite. Illustration of the bonding atoms forming different combinations of tetrahedral [T] and octahedral [O] sheets. (A) Dickite composing of 1 tetrahedral sheet and 1 octahedral sheet linked together; (B) Illite-mica composing of 2 tetrahedral sheets and 1 octahedral sheet linked together with large interlayer cations; (C) The structure of dickite in simple shapes representing T and O sheets; (D) Illite-mica with interlayer charges in between; (E) Montmorillonite with water molecules and cations. (Kündig R. (2015). *Clay and clay minerals* [PowerPoint slides]. Retrieved from http://www.sgtk.ch/rkuendig/dokumente/FS10_Clay_handout.pdf)

$$\text{Smectite} + Al^{3+} + K^{+} = \text{Illite} + Si^{4+}$$

which the simple reaction shown above predicts a gain of one aluminium atom and a loss of one silicon atom for a gain of one atom of potassium. The actual reaction is somewhat more complicated in that there is also a loss of iron and magnesium from the smectite layers. This transition of illite to smectite may occur by oxidation processes. The formation and occurrence of montmorillonite is favored by the alkaline conditions such as seawater. Moreover, it has been found that there is a variation of kaolinite and montmorillonite and also an alteration process of montmorillonite to kaolinite. This alteration can occur either during transportation or after deposition or during both stages. It is clear that Bangkok soils were deposited in a wide range of environmental conditions from acidic to alkaline, which favor the formation of kaolinite, illite, and montmorillonite. The depositional environment of Bangkok clay can be interpreted as deltaic region (Shibuya and Tamrakar, 2003). The deltaic region refers to the paleoenvironment of marine and brackish water deposit in the Lower Central Plain of Thailand during Holocene epoch. It accommodated a transgression and regression which causes river flow to interact with seawater (Choowong, 2011), resulting in rapid sediment accumulation of soft Bangkok clay sequence.

4.2 CRYSTALLOGRAPHIC PREFERRED ORIENTATION

Despite the abundance of clay volumes in soil samples, their magnitudes of crystallographic preferred orientation (CPO) are comparably low. All clay minerals, i.e., illite-mica, dickite, and montmorillonite at BP and BS have preferred orientation on (001) planes and their degrees of CPO range from 1.2 to 4.1 multiples of random distribution (m.r.d.). The CPO of our soil samples are relatively low comparing to other clay-rich materials such as fault gouges, shale, and schist. Our samples have weak textures similar to fault gouges from San Andreas Fault (Wenk *et al*., 2010). The fault gouges display textures of 1.1 to 2.0 m.r.d., which is attributed to heterogeneous deformation as well as dissolution-precipitation reactions. Compared to shale and schist, the CPO of the soil samples in this study are relatively low. Muderong Shale in Australia (Kanitpanyacharoen *et al*., 2015) have maximum values on pole figure (001) of 3.6 to 5.5 m.r.d. Kimmeridge Shale from the North Sea sedimentary basin (Wenk *et al*., 2010) suggests an (001) maximum for clay minerals of 1.7 to 5.6 m.r.d. and this is due to sedimentation and compaction. The strongest fabrics were observed in schists from metamorphic rocks in the Alps (Wenk *et al*., 2010) having 4.5 to 13.5 m.r.d. and developed by deformation as well as recrystallization in a stress field. The weak preferred orientation of the samples in BP and BS may be due to low compaction and sedimentation of unconsolidated soil, alteration, and less stress history.

Greater depth should have higher values of m.r.d. due to compaction. However, the CPO of our samples greatly varies with depth (Figure 3.4). Particularly BS soil sample at 9.00 m depth, the CPO increases significantly with maximum m.r.d. of 2.0 to 2.6 and are higher than the depth below. The increase of CPO is likely because of rapid increase of clay content, which implies heterogeneity of soil samples. Similar to BP soil

sample at 17.25 m depth, the CPO also increases consequent to the high clay content, having maximum m.r.d. of 2.2 to 4.1. The low amount of quartz (16-17 vol%) and high clay content (78-83 vol%) at these two depths result in the rise of CPO.

4.3 SHEAR WAVE VELOCITY

Shear wave velocities parallel to the horizontal plane (V_{Sh}) obtained in this study are 90-150 m/s and 70-130 m/s for BP and BS, respectively. The values follow trends of Bangkok soil shear wave velocity studied by Ashford *et al*. (1997) which the velocities are obtained from empirical correlations based on available field and laboratory measurements, and in situ tests (downhole method). Ashford *et al*. (1997) specify the shear wave velocity for Bangkok soft clay, approximately the thickness of 15 to 20 m, to be 60-100 m/s. Most of the V_{Sh} from our study (70-150 m/s) are consistent with the previous values. In addition, a study by Duangsano (2014) also suggest shear wave velocity of 100 m/s for the soft clay layer at Chulalongkorn University (CU), located approximately 10 km from BP and BS. The shear wave velocity were obtained from empirical equations, downhole method, and microtremor measurements. In general, V_{Sh} from our study are also consistent with shear wave velocities from Duangsano (2014) as compared in Figure 4.2.

Bangkok clay can also be classified as site E soil by the National Earthquake Hazard Reduction Program site classes (NEHRP). The maximum V_S of site E soil for the upper 30 m soil layer is 180 m/s. Therefore, velocities greater than 100 m/s in both BP and BS are possible. However, the top layer of Bangkok soil profiles consist of soft clay which has shear wave velocities less than 100 m/s and increases considerably with depth (Duangsano, 2014). In contrast, V_{Sh} near the surface of BP and BS are 150 m/s and 130 m/s, respectively. The increase in velocity may be overestimated during the calculations due to several reasons. First, the polycrystal tensor of the clay minerals were not straightforward measured, but calculated from the single-crystal stiffness tensors. Second, no confining pressure was considered in the calculations which may result in unrealistic shear wave velocity. Moreover, the averaging method in BEARTEX software does not take water content into account for the V_{Sh} calculations. The calculated V_{Sh} in this study are greater than the actual velocity of the intrinsic soil comprising of high porosity and water content.

Vasin *et al*. (2013) experimented and modeled various stiffness coefficients (C_{ij}) of Kimmeridge Shale. The experiment shows that if water-filled pores are added to the model of Kimmeridge Shale, elastic constants will significantly decrease, particulary C_{44} and C_{66}, compared to the model with no porosities. Porosities influence lower elastic constants which the decreased C_{44} and C_{66} consequently result in lesser V_{Sh} and V_{Sv}. For example, approximately 7.5% water-filled pores added to the no-pore model, decreases C_{66} and results in a V_{Sh} decrease of about 1.5 km/s. This means that if 1% water-filled pore is added into the material, its velocity will decrease 200 m/s. To satisfy the V_{Sh} calculations from BEARTEX, a 21.5% porosity is applied to the soil samples and velocities are reduced by 4.3 km/s. However, each depth may contain more or less

porosity and water content. Near surface soils may particularly have higher porosities than 21.5% and should have lower V_{Sh} values. For this reason, V_{Sh} of 130-150 m/s near the surface may be overestimated.

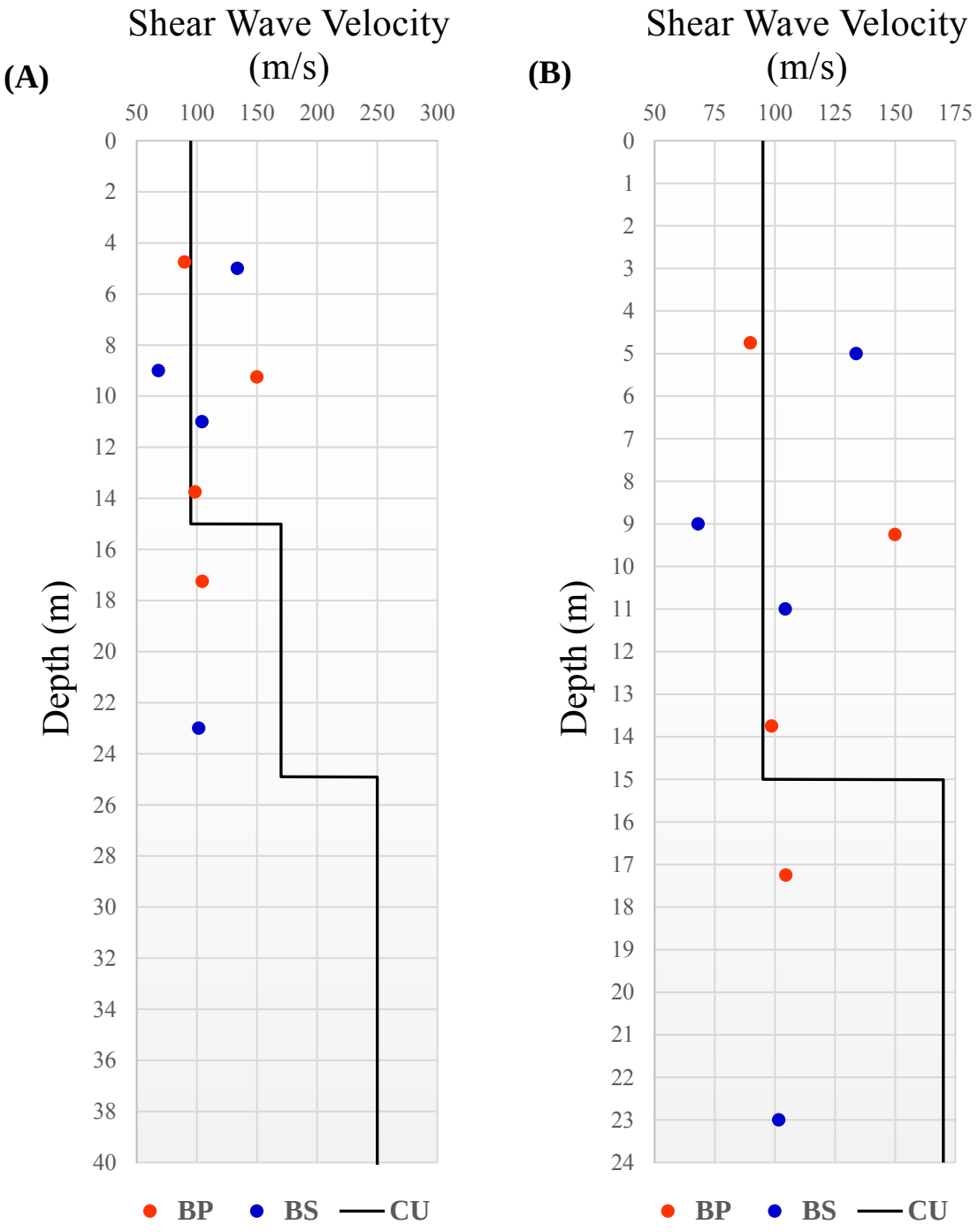

Figure 4.2 Comparison of shear wave velocities at BP and BS with shear wave velocities of Bangkok clay at Chulalongkorn University (CU) study site from the study by Duangsano (2014). (A) Shear wave velocity profile at 0-40 m and (B) 0-24 m. The shear wave velocities are approximately 100 m/s for the soft clay layer. Soft clay layer reach approximately 20 m at BP and BS, and approximately 15 m at CU. At greater depth is the 1st stiff clay layer with increasing velocity.

4.4 AMPLIFICATION MODELING

4.4.1 Ground Motion Response and Earthquake Characteristics

The study areas at BP and BS possess amplification factors from 1.7 to 2.1 and 1.2 to 1.5, respectively when responded from 0.1 g-scaled input motions. The results are consistent with the amplification modeling by Yanuviriyakul and Suttisak (2009) (Figure 4.3). They suggest that the amplification factors of Bangkok area are 1.5 to 2.0 when responded from significant earthquake events scaled to 0.1 g.

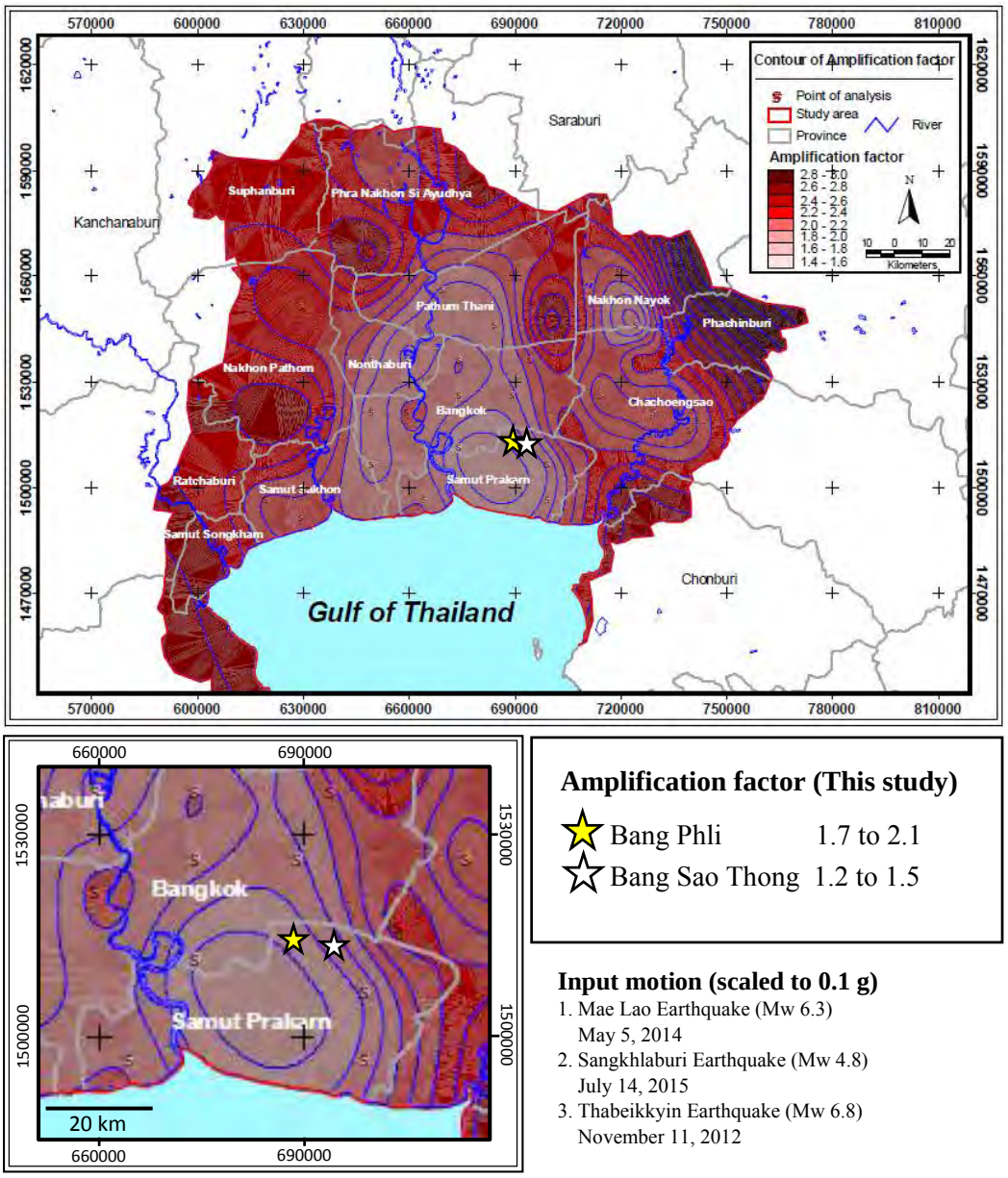

Figure 4.3 Amplification factor at the surface of soft Bangkok clay, including values at BP and BS in this study. (Modified from Yanuviriyakul and Soralump, 2009)

The amplification factors vary with different earthquake events due to the specific characteristics of each input waveforms. For example, the amplification factor at BS responded from Mae Lao Earthquake, Sangkhlaburi Earthquake, and Thabeikkyin Earthquake are 1.2, 1.4, and 1.5, respectively. The main factors influencing ground motion response are the frequency of seismic waves, frequency of sediments, and duration of shaking. Different shaking patterns are caused by the resonance of earthquake and soil frequencies which finally vary the amplification factors. Among the three input motions in this study shown in Figure 2.4, the earthquake characteristic and frequency of Thabeikkyin Earthquake resulted in the highest amplification factors which are 2.1 at BP and 1.5 at BS.

Each selected earthquake events in this study are particularly examples of ground motion response induced by earthquakes from different seismogenic zones. Sagaing Fault Zone and Phayao Fault are cases for teleseismic sources, located approximately 800-900 km and 600 km from the study areas, respectively. Three Pagoda Fault Zone, located about 200 km from the study areas, is an example for local seismic sources. For the reason that all input motions are scaled to 0.1 g, the source to site distance and the earthquake magnitude are not the controlling elements of amplification. The ground motion response are mainly characterized by the earthquake's frequency as explained earlier.

If the input motion were not normalized, the PGA measured at TMDA station in Bangkok would be 0.0006 g, 0.0005 g, and 0.0001 g for Mae Lao Earthquake, Thabeikkyin Earthquake, and Sangkhlaburi Earthquake, respectively. In this case, the source to site distance and the earthquake magnitude are considerable for amplification. Phayao Fault and Sagaing Fault Zone are capable of causing high magnitude earthquakes (Mw 6.0 to 8.0) than Three Pagoda Fault Zone (Mw 5.0). This means that although Three Pagoda Fault Zone is located near the study areas, the ground motion may be weaker than the response from distant faults because of its low magnitude. Another effect of low magnitude earthquakes from near earthquake sources is that the ground shaking at the surface can be lesser than the response from far sources although the amplification factor is greater. For instance at BP, the PGA at the surface responded from Sangkhlaburi Earthquake is 0.0002 g (amplification factor=2.7), and is lower than the response from Mae Lao Earthquake of 0.0009 g (amplification factor = 2.1) though having higher amplification factor.

4.4.2 Implications for Mae Chan Fault

Mae Chan Fault will also be discussed in this part. Mae Chan Fault is located approximately 70-80 km to the north of Phayao Fault (Figure 4.4) and has the possibility of generating earthquakes in the near future. The latest earthquake caused by this fault occurred on December 22, 1925 with an mb of 6.5. Its recurrence interval of great earthquakes is approximately 100 years (Pailoplee and Choowong, 2012), which means that Mae Chan Fault has the potential to generate significant earthquakes within decades. So it is considered as one of the most worrying faults in Thailand. To emphasize, although there are no amplification modeling from earthquake events

caused by Mae Chan Fault due to the lack of record, the response from Mae Lao Earthquake caused by Phayao Fault in this research intends to represent the response from Mae Chan Fault as well. The assumption is that the characteristics of the generated earthquakes from Phayao Fault and Mae Chan Fault are similar because they are both strike-slip active faults in the northern part of Thailand. The study areas will amplify the ground motion from these faults approximately 1.2 to 1.7 times.

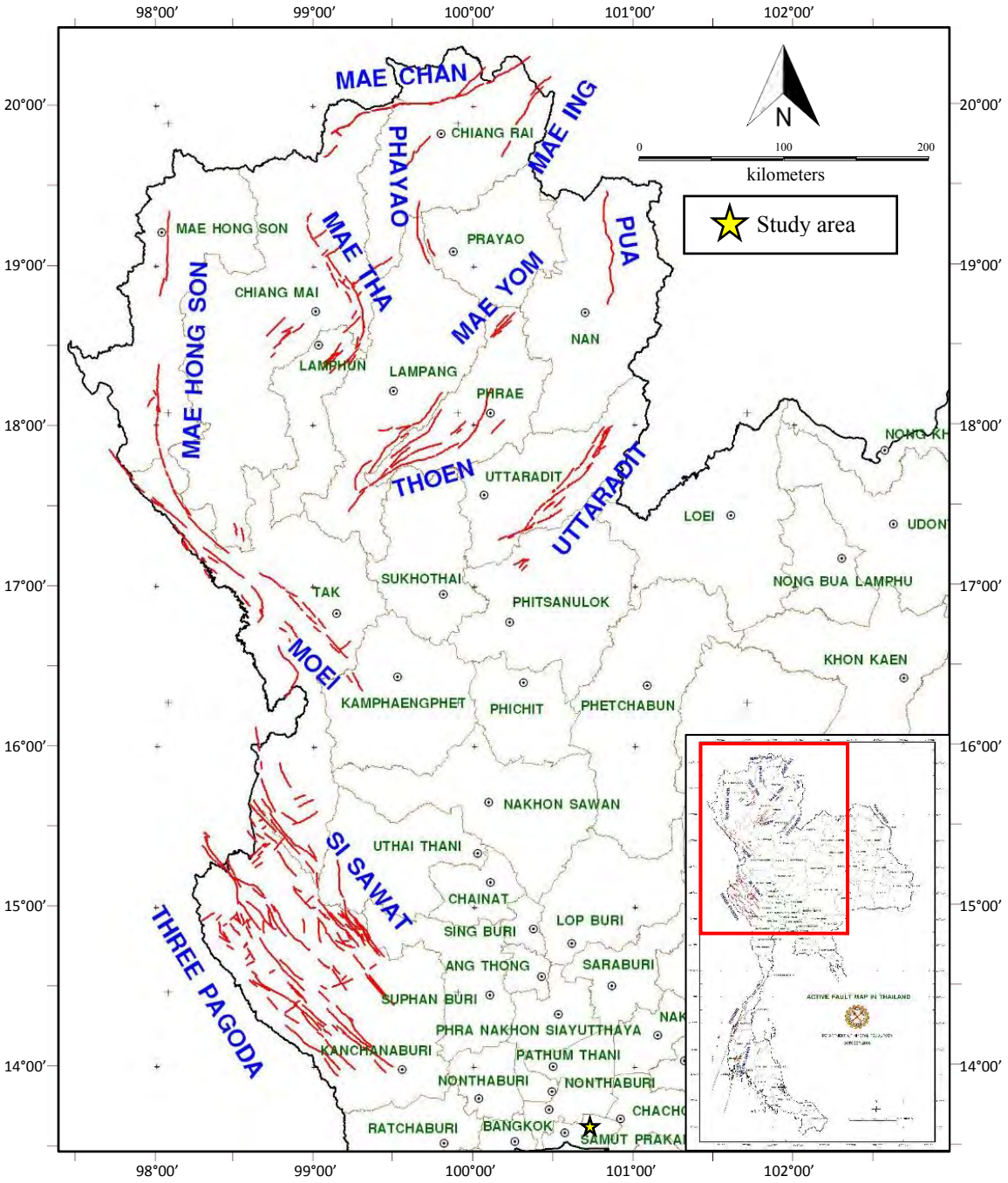

Figure 4.4 Location of Mae Chan Fault, approximately 70-80 km to the north of Phayao Fault. (Modified from Department of Mineral Resources, Thailand)

4.5 APPLICATIONS

4.5.1 Amplification Factor and Peak Ground Acceleration (PGA)

The amplification factor and PGA at the surface are used to evaluate ground motion response. The effect of the amplification factor is shown in terms of how much the soil amplifies the input acceleration. It is generally used for structure assessment especially when there is no chance for resonance, i.e., the more amplification factor the more shear force at the surface. Our study areas suggest amplification factors from 1.2 to 2.1 which means that the soil underlying Samut Prakan significantly amplifies the ground motion. PGA is also a natural simple design parameter since it can be related to a force. For simple design, one can design a building to resist a certain horizontal force. For example, the PGA at the surface of our study areas range from 0.09 to 0.15 g, so the buildings constructed in this area should be able to resist those PGA.

4.5.2 Earthquake Response Spectra

Damages from earthquakes are not only caused by ground motion amplification, but also resonance. This phenomenon occurs when the predominant period of the earthquake ground motion matches the natural period of structures, resulting in destructions due to the increase of acceleration. The ground shaking has different frequency content or period. The predominant period is defined as a period of the peak spectral amplitude of predominant component of motion (Dravinski *et al*., 1992). An example case of Michoacan earthquake in Mexico on September 19, 1985 by which the ground underwent predominant periods from 1.0 to 2.5 s (Dravinski *et al*., 1992). The period corresponded with the collapsed buildings in that region. The buildings between about 6 and 20 stories in height resonated at a similar period, which greatly increased the accelerations within them (Arnold, 2006). Warnitchai *et al*. (2000) and Yanuviriyakul and Soralump (2009) report the predominant period of Bangkok area to be 0.5-1.0 s and 0.6-0.8 s, respectively. This range in tune the period of a 5- to 10-story building and will be discussed further.

Another analysis to assess the peak response of buildings is called the “response spectrum” which is also obtained from DEEPSOIL modeling in this study. Response spectrum is simply a plot between spectral acceleration (SA) and period of the ground. SA describes the maximum acceleration in an earthquake on an object (while PGA describes the acceleration of ground particles). It is approximately what is experienced by a building, as modeled by a particle on a massless vertical rod having the same natural period of vibration as the building. SA would also be a good index to hazard to buildings, but ought to be more closely related to the building behavior than peak ground motion parameters. The response spectrum enables the engineer to identify the resonant frequencies at which the building will undergo peak spectral accelerations (PSA). Based on this knowledge, the building design can be adjusted to ensure that the building period does not coincide with the site period of maximum response (Arnold, 2006). The typical building periods are shown in Figure 4.5.

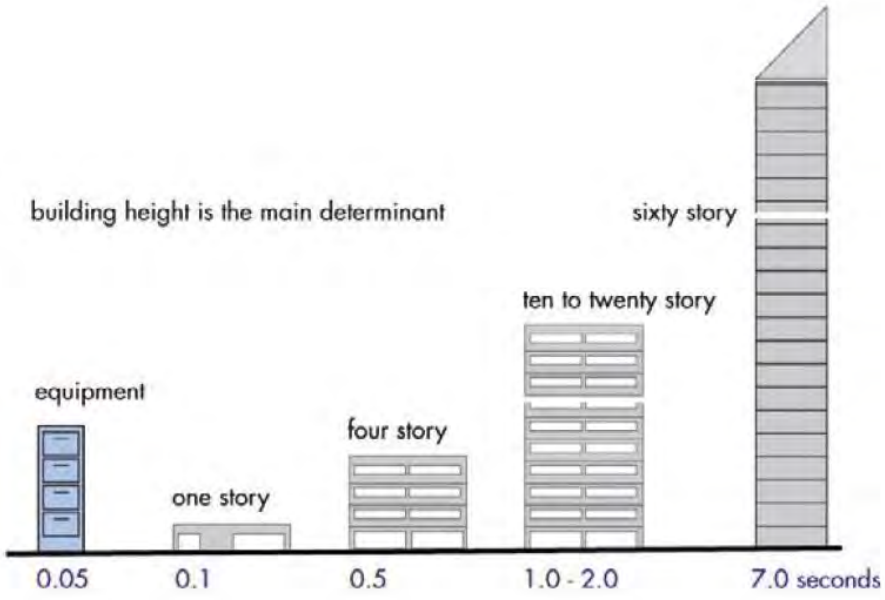

Figure 4.5 Comparative building periods, determined by height. These values are approximations: the structural system, materials, and geometric proportions will also affect the period (Arnold, 2006).

The possibility of earthquake hazard can be reduced by making sure that the building period will not concur with that of the ground. For example, the response spectrums at BP responded from Mae Lao Earthquake (Figure 4.6A) and Thabeikkyin Earthquake (Figure 4.6B) have the period of maximum SA at approximately 2-3 s. If the building's natural period encounters 2-3 s, and coincide with the predominant period of the ground motion, resonance will occur. The shaking will be increased to the possibility of SA up to about 0.7 g. This is considered as a strong ground motion. However, the predominant period of Bangkok area suggested by Yanuviriyakul and Soralump (2009) is 0.6-0.8 s, which does not coincide with 2-3 s as argued. Therefore, the buildings in the city will not face high SA when responded from these two events. The two earthquakes in the examples are caused by teleseismic earthquake sources, i.e., Phayao Fault and Sagaing Fault Zone. Distant earthquakes are generally characterized by long period seismic waves which usually match the natural vibration period of tall buildings. In contrast, local earthquakes with short periods resonate with the frequency of one or two stories of buildings. Based on this example, constructions in Samut Prakan especially high buildings should be designed to cope with long period earthquakes from distant sources. To prevent strong ground motion, the designed structures should avoid natural periods of 2-3 s.

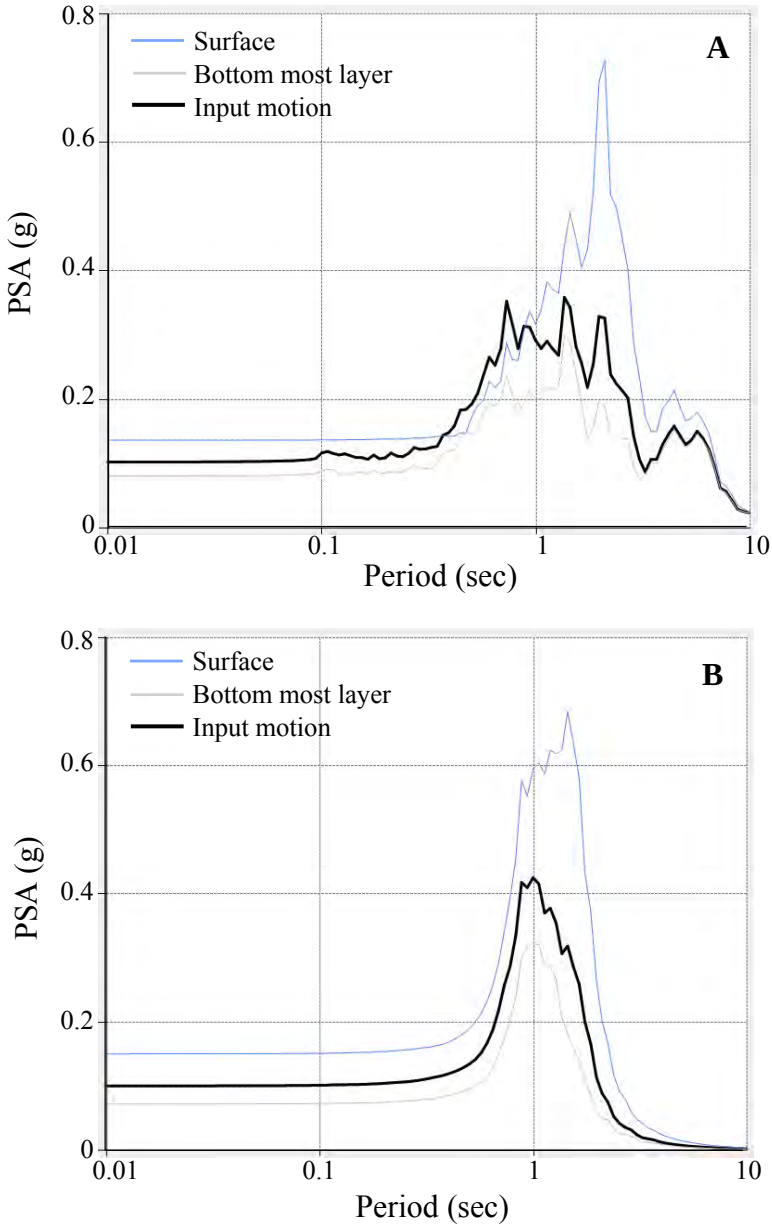

Figure 4.6 Response spectrum of (A) Mae Lao Earthquake and (B) Thabeikkyin Earthquake at BP, modeled from DEEPSOIL in this study. The figures are plotted between peak spectral acceleration (PSA) and period of the ground.

4.6 FUTURE WORK

The earthquake waveforms in the input motions are caused from strike-slip faults. Among the earthquake sources in the modeling, Phayao Fault, Three Pagoda Fault Zone, and Sagaing Fault Zone are all dextral strike slip faults, but Mae Chan Fault occupy a sinistral strike slip motion. To encompass the ground motion behavior caused by different fault movements, it is suggested for future works to apply the method in this study to model amplification factors caused by dip-slip faults. The intriguing events for the modeling are the Mw 9.1 Indian Ocean earthquake on December 26, 2004 or the Mw 8.6 Northern Sumatra (Nias) earthquake on March 25, 2005, both caused by

the Sumatra-Andaman subduction zone. These events have records of the III-V on the Mercalli Intensity scale which were also felt in Bangkok and parts of Thailand.

More shear wave velocities at different depths should be provided for the DEEPSOIL modeling. In this software, the ground motion response are modeled layer by layer. Each single thickness has a specific shear wave velocity, dynamic soil properties, and damping ratio, which have an effect on the amplification (Figure 2.2). The less thickness of one layer, the better accuracy of the ground motion response. Our study uses thickness of 0.5 m (total of 80 layers) for the modeling. However, this study has only four V_S data per study area, so the velocity at other depths are extrapolated from the known values. If each of the 0.5 m thickness has a specific velocity, the amplification modeling will be more realistic. More soil samples should be analyzed to provide shear wave velocities at other depths. Also, the soil log data from the drilling are also recommended, to input the correct soil type in the soil profile for the amplification modeling.

Shear wave velocity for seismic response studies can be obtained by various approaches. For instance, Ashford et al. (1997) measured V_S from downhole method and from empirical equations. Duangsano (2014) also used microtremor surveys. This study obtained V_S from mathematical averaging methods in BEARTEX software, based on mineral composition and elastic properties of soil samples. If the approach of this study do consist with the in situ-measured shear wave velocities by engineering methods, our research takes some advantages by means of the following reasons. First, this method requires less amount of samples. Only about 1 cm^3 is needed for synchrotron x-ray diffraction. The synchrotron experiment also takes less time, approximately 10-15 minutes per sample. Second, our study takes mineralogy into account including the minerals preferred orientation. Without considering the minerals orientation distributions in the soil samples, the calculated shear wave velocity will significantly decrease about 20-30%. Thus, this technique precisely specifics the geology and velocity of the study areas compared to values derived from empirical equations. The effects of shear wave velocity calculated from mineral composition and elastic properties in this study should be further compared with values from seismic surveys and soil mechanics experiments. If these different approaches of obtaining shear wave velocity are alike, the method conducted in this research is another alternative way to understand ground motion response from earthquakes.

The software, BEARTEX, used for the velocity calculations does not consider the soil's porosity, which should be measured and considered in the calculations. The program still lack many factors to take into consideration such as porosity, pore shape, or water content. This should be further improved by the differential effective medium (DEM) approach and self-consistent averaging method. The shape of crystallites and pores, their volume fractions, and their orientation distributions play important roles in this method. The main idea is that properties of multiphase material (effective medium) can be numerically calculated with a stepwise procedure, by incrementally adding inclusions of one phase into the host material. Such an approach has been applied to

calculate properties of mineral aggregates, including sedimentary rocks and shales (Vasin *et al*., 2013). By considering various essential parameters, this method will give more realistic velocity values of the study areas.

CHAPTER V
CONCLUSIONS

Ground motion amplification can raise the level of ground shaking especially in regions underlain by soft sediments. The effect increases damages from earthquakes. To assess the response behaviors of ground motion, the amplification factor in Samut Prakan is observed by shear wave velocities derived from mineral composition and elastic properties of soil samples. Synchrotron x-ray diffraction was applied to the soil samples from Bang Phli (BP) and Bang Sao Thong (BS) districts. The mineral composition, their volume fraction, and their crystallographic preferred orientation were analyzed using the Rietveld refinements in MAUD software. Results show that the study areas composed of approximately 60-80 vol% of clay minerals which are illite-mica, montmorillonite, and dickite. The clay minerals display maximum preferred orientation of 1.2 to 4.1 m.r.d. Quartz is also dominant and other minor minerals include calcite, pyrite, halite, gypsum, and magnesite. Elastic properties of the soil was calculated by mathematical averaging method in BEARTEX software, which was further incorporated with the composing mineral and their amount to obtain shear wave velocity in the horizontal plane (V_{Sh}). A 21.5% porosity estimation was applied to the velocity to reduce the overestimated value. The estimated V_{Sh} of BP and BS are approximately 90-150 m/s and 70-130 m/s, respectively.

Shear wave velocities were taken into account to model the 1D amplification profile in DEEPSOIL program. Shear wave velocity, soil data, and input motion are the main contributing factors for the modeling. The amplification profile was modeled to 40 m deep. For the first 20 m, the soil data and V_{Sh} use values from soil logs and the previously calculated V_{Sh}. The input motion or earthquake waveforms are selected from three different earthquake sources which are Phayao Fault (Mao Lao Earthquake), Three Pagoda Fault Zone (Sangkhlaburi Earthquake), and Sagaing Fault Zone (Thabeikkyin Earthquake). These earthquake events are scaled to peak ground acceleration (PGA) of 0.1 g. The amplification profiles display the different PGA at each soil layer when responded from the three seismic records. Then, the amplification factor was calculated from the PGA at the surface by the PGA at the top of the bottom most layer. Results show that BP and BS can amplify the ground shaking 1.7 to 2.1 and 1.2 to 1.5 times, respectively. It is suggested that the soil underlying Samut Prakan have the ability to increase the ground motion when the soil particles are induced by earthquake forces of 0.1 g.

Our study introduces an alternative approach to understand response behaviors of ground motion triggered by earthquakes. However, the shear wave velocities should be refined. The calculations should necessarily consider significant factors such as porosity, pore shape, and water content of the soil samples. Differential effective

medium (DEM) approach and self-consistent averaging method are suggested to further improve the shear wave velocities, and comparison to in situ testing should be made.

REFERENCES

Arnold, C. (2006). Earthquake effects on Buildings. *In:* FEMA (ed.) *Desiging for earthquakes: A manual for architects.* California: the Earthquake Engineering Research Institute (EERI).

Ashford, S. A., Jakrapiyanun, W. & Lukkunaprasit, P. (1997). Amplification of earthquake ground motions in Bangkok. Bangkok, Thailand: Chulalongkorn University.

Bass, J. D. (1995). Elasticity of Minerals, Glasses, and Melts. *In:* Ahrens, T. J. (ed.) *Mineral Physics & Crystallography: A Handbook of Physical Constants.* Washington, DC: American Geophysical Union.

Boore, D. M. (2004). Estimating $\bar{V}s(30)$ (or NEHRP site classes) from shallow velocity models (depths < 30 m). *Bulletin of the Seismological Society of America,* 94**,** 591-597.

Choowong, M. (2011). Quaternary. *In:* Ridd, M. F., Barber, A. J. & Crow, M. J. (eds.) *The Geology of Thailand.* Geological Society of London.

Cox, J. B. (1968). A Review of the Geotechnical Characteristics of the Recent Marine Clay in Southeast Asia. Asian Institute of Technology Research Report.

Dewhurst, D. N. & Siggins, A. F. (2006). Impact of fabric, microcracks and stress field on shale anisotropy. *Geophysical Journal International,* 165**,** 135-148.

Dravinski, M., Yamanaka, H. & Kagami, H. (1992). Site amplification through measurement of long period microtremors: Predominant period of motion. *10th World Conference on Earthquake Engineering.* Balkema, Rotterdam.

Duangsano, O. (2014). *Nonlinear site response analysis and ground motion amplification in Bangkok subsoil.* Master, King Mongkut's University of Technology Thonburi.

Fenton, C. H., Charusiri, P. & Wood, S. C. (2003). Recent paleoseismic investigations in Northern and Western Thailand. *Annals of Geophysics,* 46**,** 957-981.

Grim, R. E. & Bradley, W. F. (1940). *Investigation of the effect of heat on the clay minerals illite and montmorillonite,* Urbana, Authority of the State of Illinois.

Hashash, Y. M. A., Musgrove, M. I., Harmon, J. A., Groholski, D., Phillips, C. A. & Park, D. (2015). DEEPSOIL V6.1, User Manual. Urbana, IL: Board of Trustees of University of Illinois at Urbana-Champaign.

Hearmon, R. F. S. (1979). The elastic constants of anisotropic materials and other anisotropic materials. *In:* Hellwege, K. H. & Hellwege, A. M. (eds.) *Landolt-Börnstein Tables.* Berlin: Springer-Verlag.

Heyliger, P., Ledbetter, H. & Kim, S. (2003). Elastic constants of natural quartz. *The Journal of the Acoustical Society of America,* 114**,** 644-650.

Holmberg, S. (1977). Some engineering properties of soft Bangkok clay. *Geotechnical Engineering,* 8**,** 1-19.

Hough, B. (1969). *Basic Soil Engineering,* Newyork, Ronald Press Company.

Hower, J., Eslinger, E. V., Hower, M. E. & Perry, E. A. (1976). Mechanism of burial metamorphism of argillaceous sediment: 1. Mineralogical and chemical evidence. *Geological Society of America Bulletin,* 87.

Kanitpanyacharoen, W., Vasin, R., Wenk, H.-R. & Dewhurst, D. N. (2015). Linking preferred orientations to elastic anisotropy in Muderong Shale, Australia. *Geophysics,* 80**,** C9-C19.

Lysmer, J., Seed, H. B. & Schnabel, P. B. (1970). *Influence of base rock characteristics on ground response,* Berkeley, College of Engineering, University of California.

Mavko, G., Tapan Mukerji, & Dvorkin., J. (2009). *The Rock Physics Handbook*, Cambridge University Press.

Militzer, B., Wenk, H.-R., Stackhouse, S. & Stixrude, L. (2011). First-principles calculation of the elastic moduli of sheet silicates and their application to shale anisotropy. *American Mineralogist,* 96**,** 125-137.

Ohtsubo, M., Egashira, K., Koumoto, T. & Bergado, D. (2000). Mineralogy and chemistry, and their correlation with the geotechnical index properties of Bangkok clay: comparison with Ariake clay. *Soils and FoundationS,* 40**,** 11-21.

Ornthammarath, T., Warnitchai, P., Worakanchana, K., Zaman, S., Sigbjörnsson, R. & Lai, C. G. (2011). Probabilistic seismic hazard assessment for Thailand. *Bulletin of Earthquake Engineering,* 9**,** 367-394.

Pailoplee, S. (2013). Mapping asperities along the Sagaing Fault Zone, Myanmar using b-value anomalies. *Journal of Earthquake and Tsunami,* 07**,** 1371001.

Pailoplee, S. & Choowong, M. (2013). Probabilities of earthquake occurrences in Mainland Southeast Asia. *Arabian Journal of Geosciences,* 6**,** 4993-5006.

Shibuya, S. & Tamrakar, S. B. (2003). Engineering properties of Bangkok clay. *In:* Tan, T. S. (ed.) *Characterisation and Engineering Properties of Natural Soils.* CRC Press.

Simmons, G. & Birch, F. (1963). Elastic Constants of Pyrite. *Journal of Applied Physics,* 34**,** 2736-2738.

Somboon, J. R. P. (1988). Paleontological study of the recent marine sediments in the lower central plain, Thailand. *Journal of Southeast Asian Earth Sciences,* 2**,** 201-210.

Tanabe, S., Saito, Y., Sato, Y., Suzuki, Y., Sinsakul, S., Tiyapairach, S. & Chaimanee, N. (2003). Stratigraphy and Holocene evolution of the mud-dominated Chao Phraya delta, Thailand. *Quaternary Science Reviews,* 22**,** 789-807.

Vasin, R. N., Wenk, H.-R., Kanitpanyacharoen, W., Matthies, S. & Wirth, R. (2013). Elastic anisotropy modeling of Kimmeridge shale. *Journal of Geophysical Research: Solid Earth,* 118**,** 3931-3956.

Warnitchai, P., Sangarayakul, C. & Ashford, S. A. (2000). Seismic hazard in Bangkok due to long-distance earthquakes. *12th World Conference on Earthquake Engineering.* New Zealand.

Wenk, H.-R., Kanitpanyacharoen, W. & Voltolini, M. (2010). Preferred orientation of phyllosilicates: Comparison of fault gouge, shale and schist. *Journal of Structural Geology,* 32**,** 478-489.

Wenk, H.-R., Matthies, S., Donovan, J. & Chateigner, D. (1998). BEARTEX: a Windows-based program system for quantitative texture analysis. *Journal of Applied Crystallography,* 31**,** 262-269.

Yanuviriyakul, A. & Soralump, S. (2009). Response behaviors of soft Bangkok clay induce by earthquake forces. *The 14th National Conventionon Civil Engineering.* Suranaree University of Technology.

APPENDIX A

SYNCHROTRON X-RAY DIFFRACTION PATTERNS

A.1 1D X-ray Diffraction Patterns

The soil samples were quantified by synchrotron x-ray diffraction and analyzed by the Rietveld refinements in MAUD software. The analyses provide data of composition and amount of minerals in the soil, and their crystallographic preferred orientation. The diffraction patterns in MAUD show the experimented and calculated diffraction peaks of the mineral phases. The height of each peak indicates its intensity. Their volume fraction are determined by the area below the calculated line. The constituent minerals in the soil samples are quartz, illite-mica, montmorillonite, and dickite. Other minor minerals include calcite, pyrite, halite, gypsum, and magnesite. The following figures show the diffraction patterns and mineral composition of the eight samples from BP and BS.

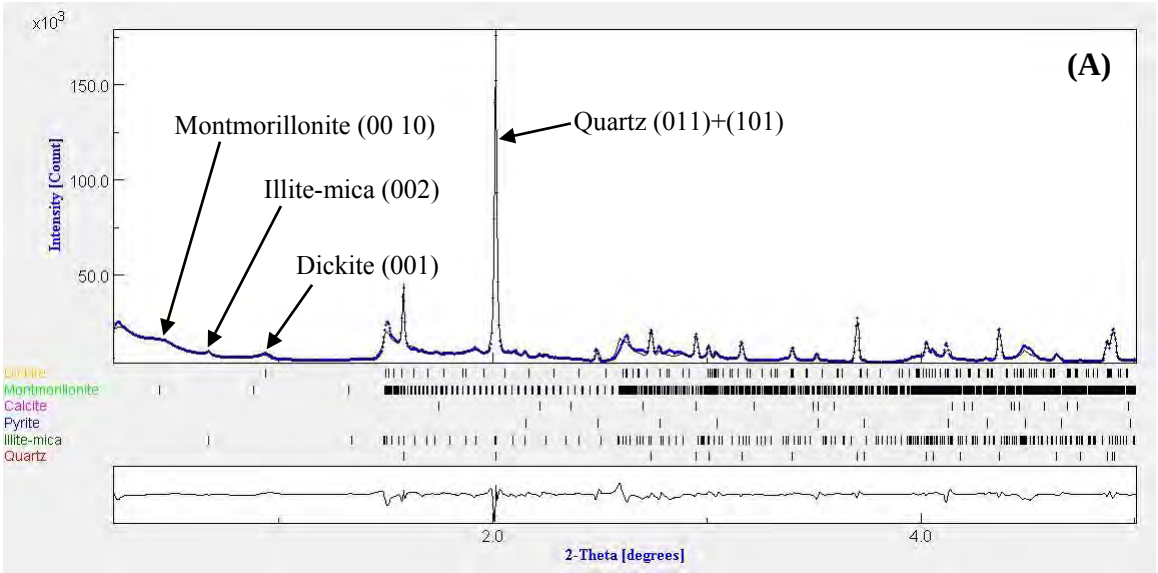

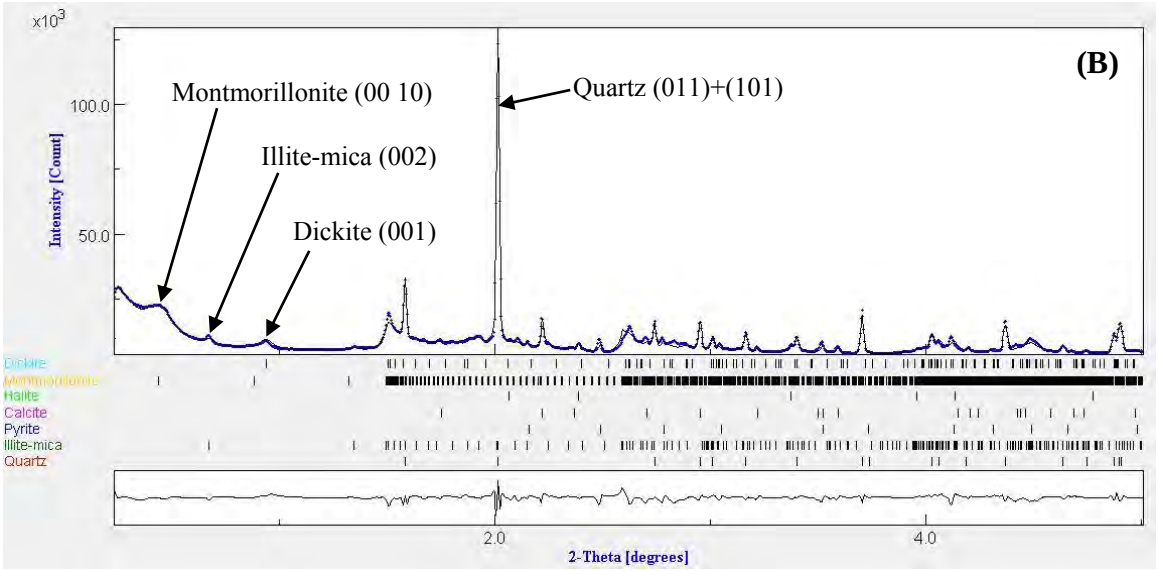
(B)
x10^3
Montmorillonite (00 10)
Illite-mica (002)
Dickite (001)
Quartz (011)+(101)
Intensity [Count]
100.0
50.0
Dickite
Montmorillonite
Halite
Calcite
Pyrite
Illite-mica
Quartz
2.0
4.0
2-Theta [degrees]

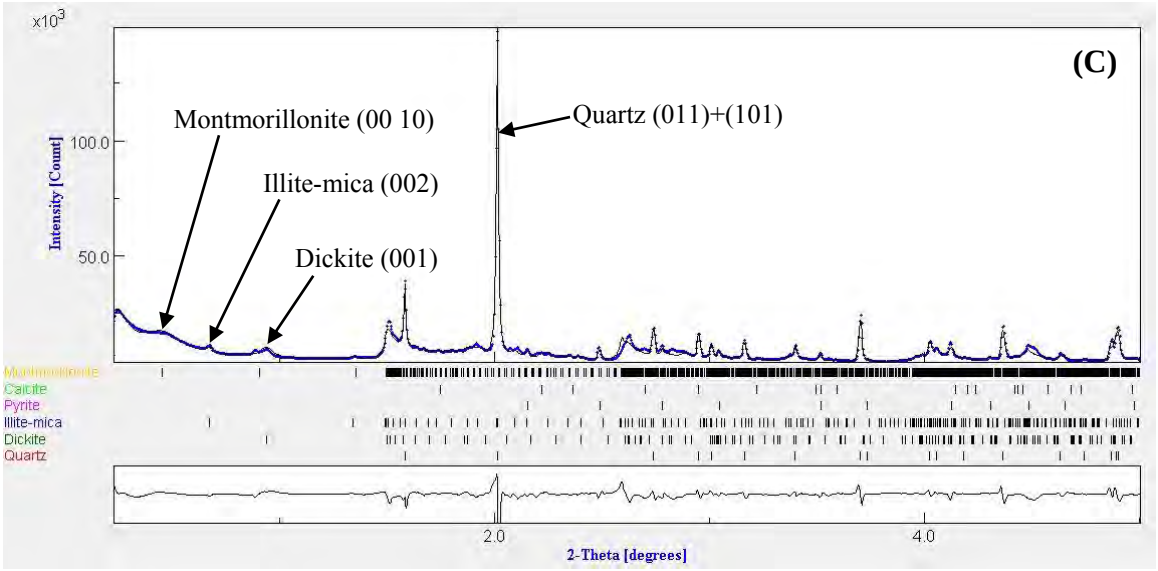
(C)
x10^3
Montmorillonite (00 10)
Illite-mica (002)
Dickite (001)
Quartz (011)+(101)
Intensity [Count]
100.0
50.0
Montmorillonite
Calcite
Pyrite
Illite-mica
Dickite
Quartz
2.0
4.0
2-Theta [degrees]

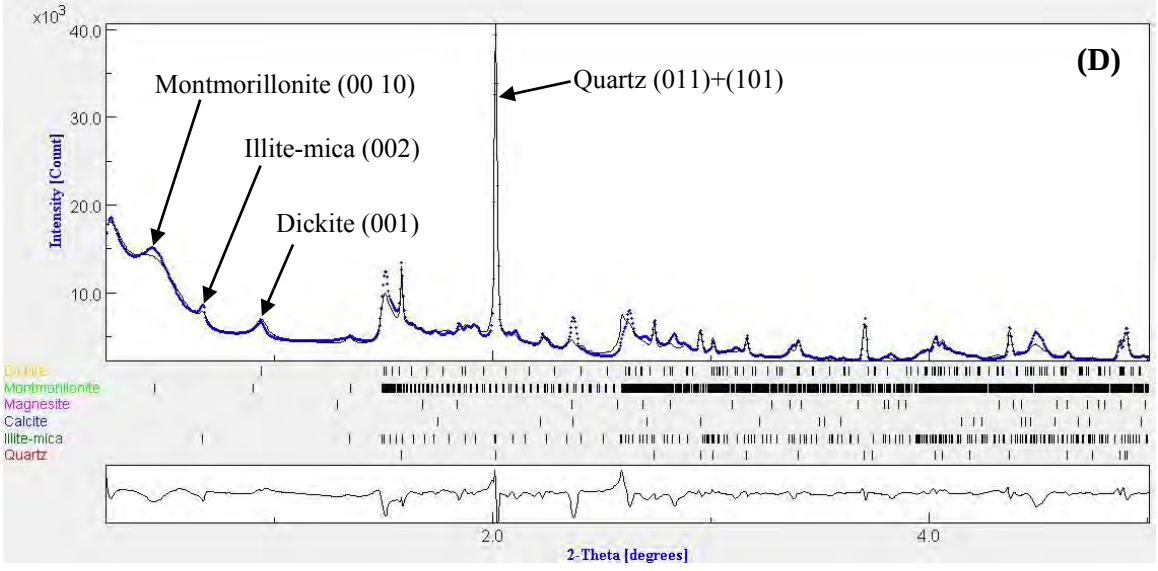
(D)
x10^3
Montmorillonite (00 10)
Illite-mica (002)
Dickite (001)
Quartz (011)+(101)
Intensity [Count]
40.0
30.0
20.0
10.0
Dickite
Montmorillonite
Magnesite
Calcite
Illite-mica
Quartz
2.0
4.0
2-Theta [degrees]

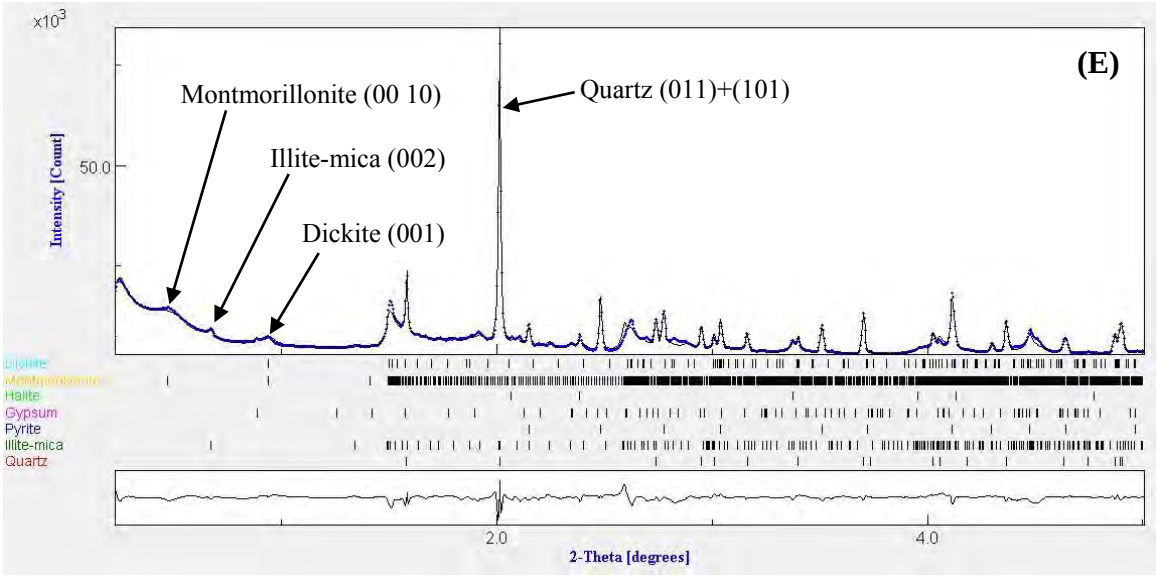
(E)
x10^3
Intensity [Count]
50.0
Montmorillonite (00 10)
Quartz (011)+(101)
Illite-mica (002)
Dickite (001)
Halite
Gypsum
Pyrite
Illite-mica
Quartz
2.0
4.0
2-Theta [degrees]

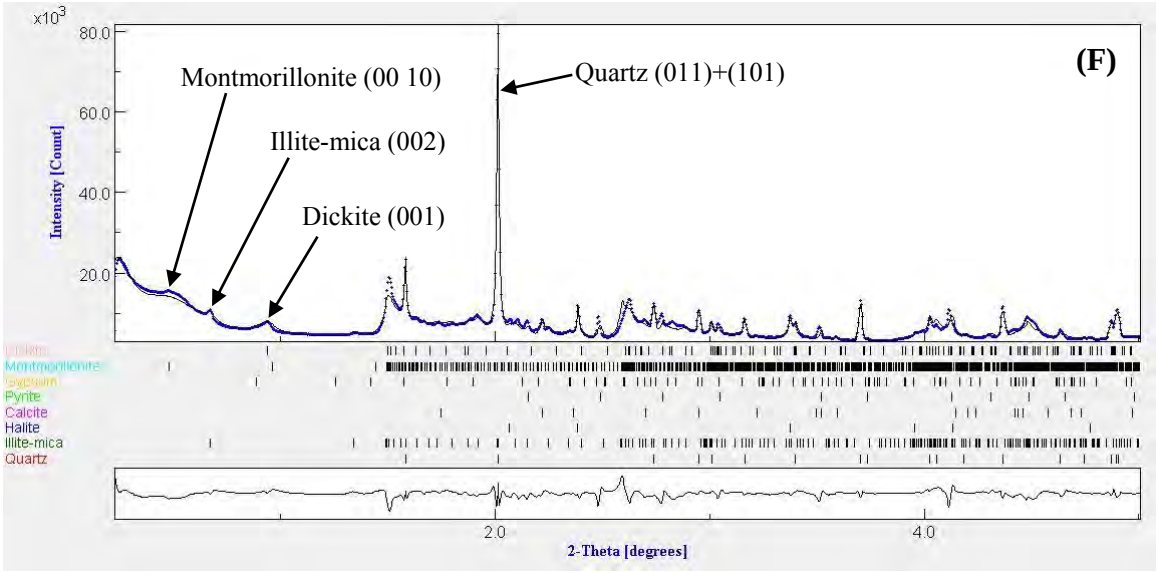
(F)
x10^3
80.0
60.0
40.0
20.0
Intensity [Count]
Montmorillonite (00 10)
Quartz (011)+(101)
Illite-mica (002)
Dickite (001)
Montmorillonite
Gypsum
Pyrite
Calcite
Halite
Illite-mica
Quartz
2.0
4.0
2-Theta [degrees]

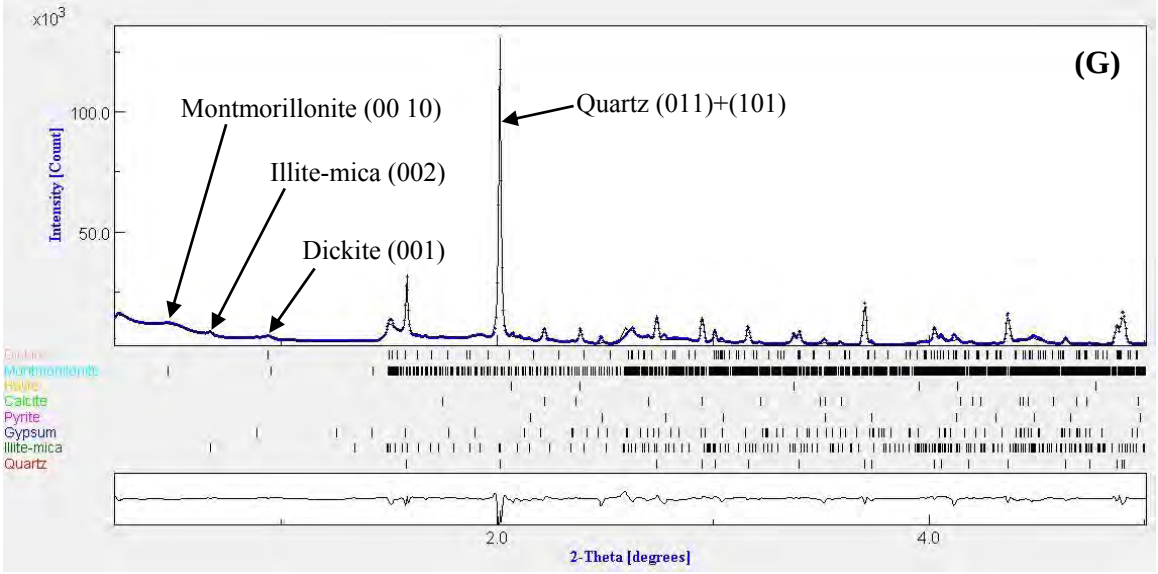
(G)
x10^3
100.0
50.0
Intensity [Count]
Montmorillonite (00 10)
Quartz (011)+(101)
Illite-mica (002)
Dickite (001)
Montmorillonite
Calcite
Pyrite
Gypsum
Illite-mica
Quartz
2.0
4.0
2-Theta [degrees]

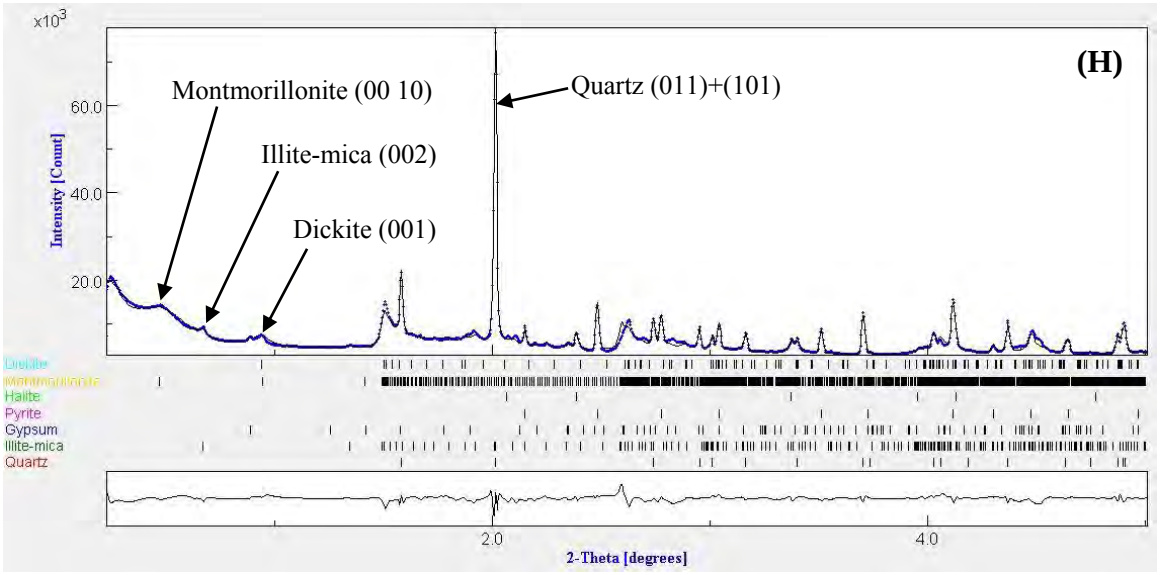

Figure A.1 Diffraction patterns of (A) BP 475, (B) BP 925, (C) BP 1375, (D) BP 1725, (E) BS 500, (F) BS 900, (G) BS 1100, and (H) BS 2300 soil samples. Dots are experimental data and solid lines indicate the Rietveld fit. Scale is 2-Theta (degrees) and the location of diffraction peaks for individual phases are indicated at the bottom.

A.2 2D Map Plots

The 2D map plots are stacks of 36 diffraction images of the samples. The observations are at the bottom while the calculated refinements are at the top. The clay minerals in some samples display high degree of preferred orientation such as BP 1725 and BS 900. In synchrotron x-ray diffraction, the samples were rotated around the horizontal axis from -45° to 45° in 15° increments to improve the pole figure coverage for texture analysis. For the other soil samples, the 2D map plots shown in Figure A.2 are also at the rotated angle with the strongest texture from the experiment, but the sheet silicates in these samples display weak preferred orientation.

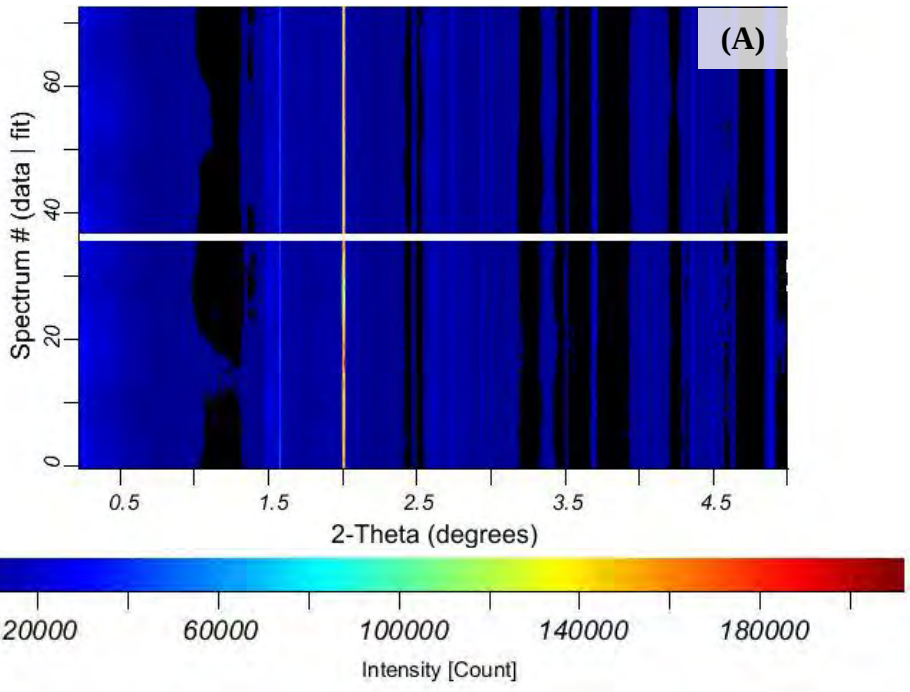

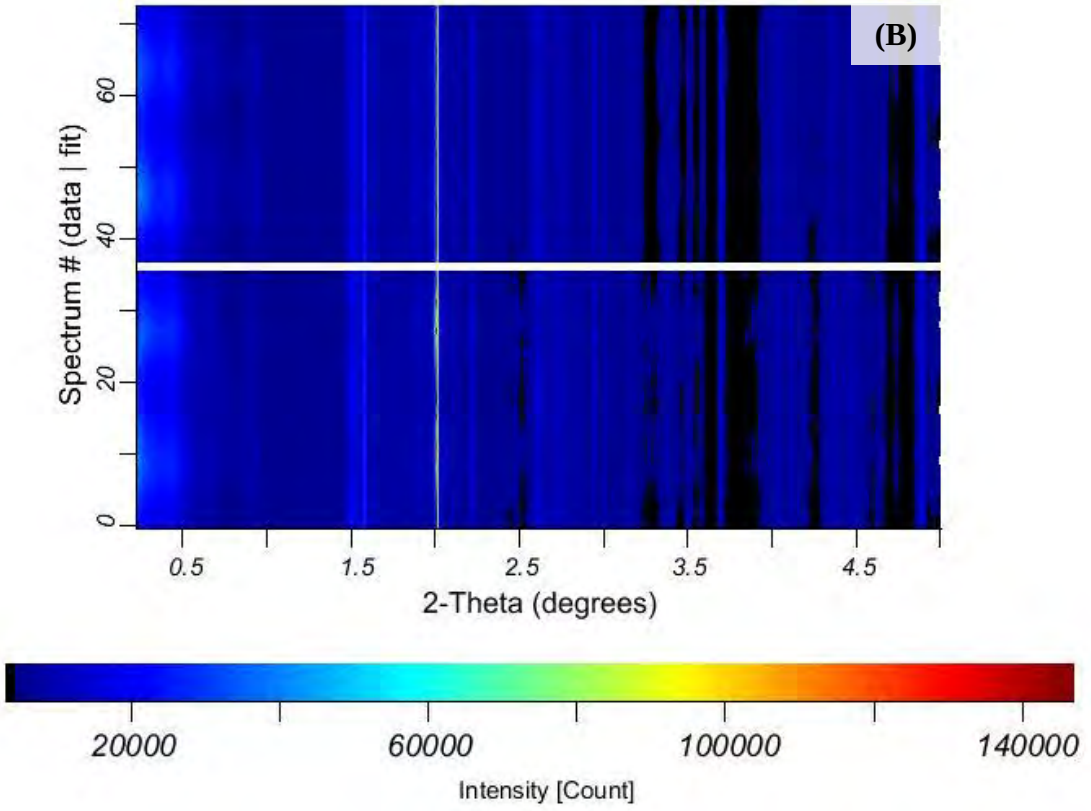
(B)
Spectrum # (data | fit)
0
20
40
60
0.5
1.5
2.5
3.5
4.5
2-Theta (degrees)
20000
60000
100000
140000
Intensity [Count]

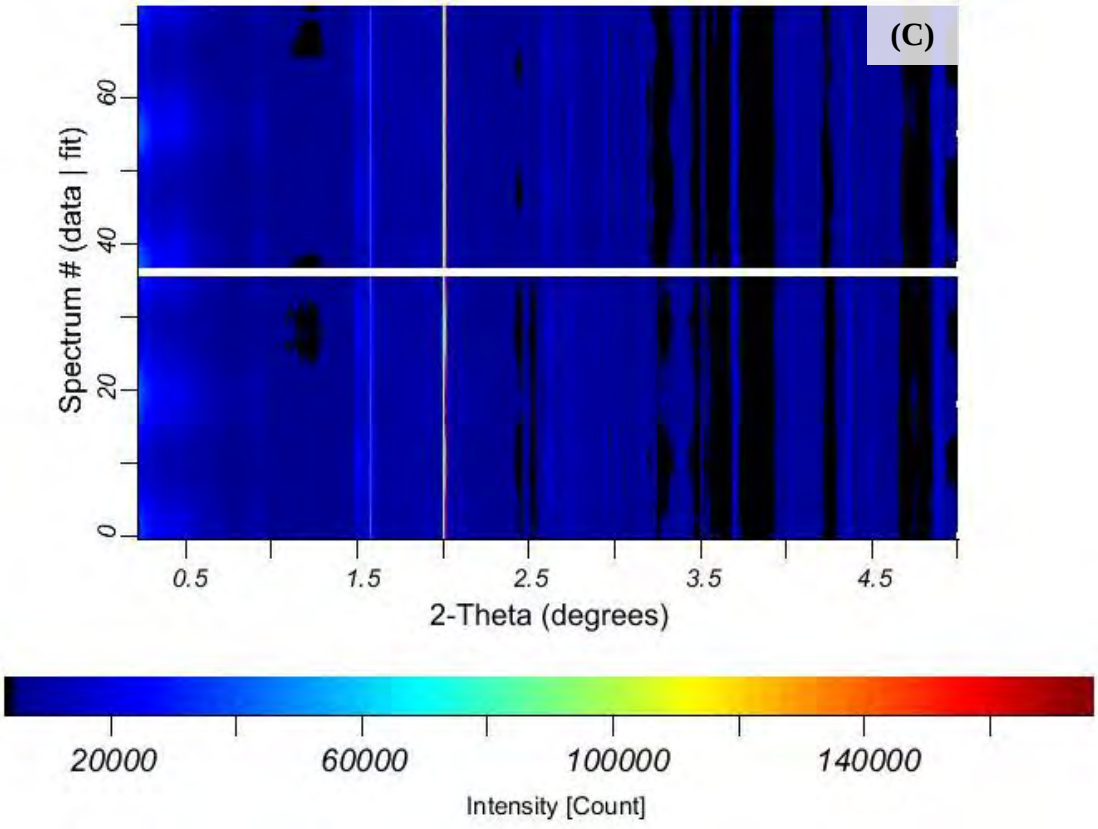
(C)
Spectrum # (data | fit)
0
20
40
60
0.5
1.5
2.5
3.5
4.5
2-Theta (degrees)
20000
60000
100000
140000
Intensity [Count]

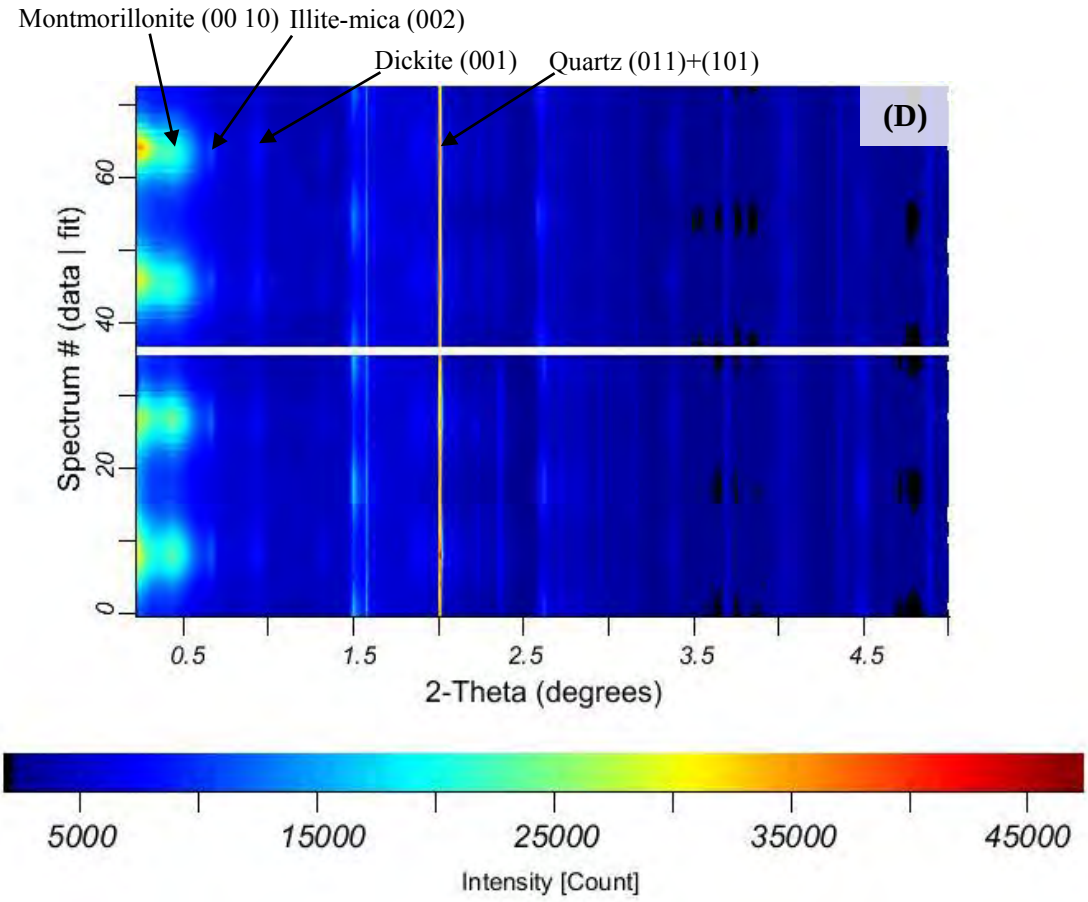
Montmorillonite (00 10)
Illite-mica (002)
Dickite (001)
Quartz (011)+(101)
(D)
Spectrum # (data | fit)
0
20
40
60
0.5
1.5
2.5
3.5
4.5
2-Theta (degrees)
5000
15000
25000
35000
45000
Intensity [Count]

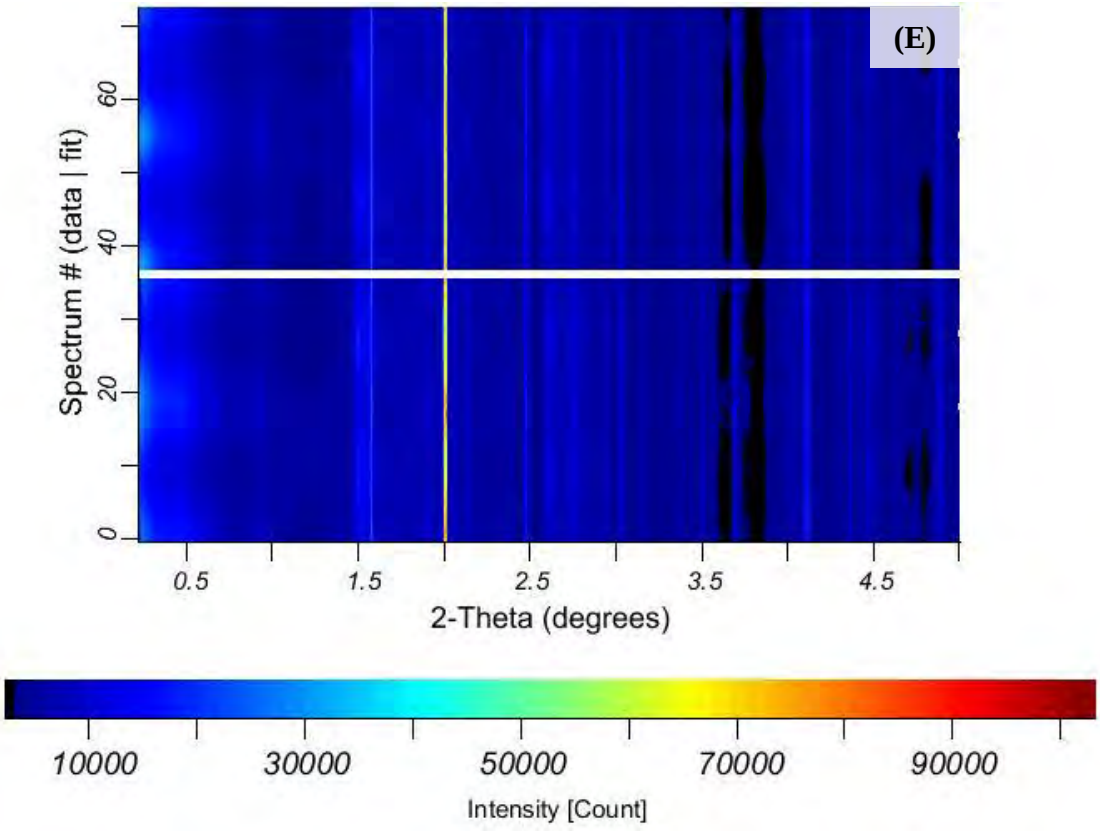
(E)
Spectrum # (data | fit)
0
20
40
60
0.5
1.5
2.5
3.5
4.5
2-Theta (degrees)
10000
30000
50000
70000
90000
Intensity [Count]

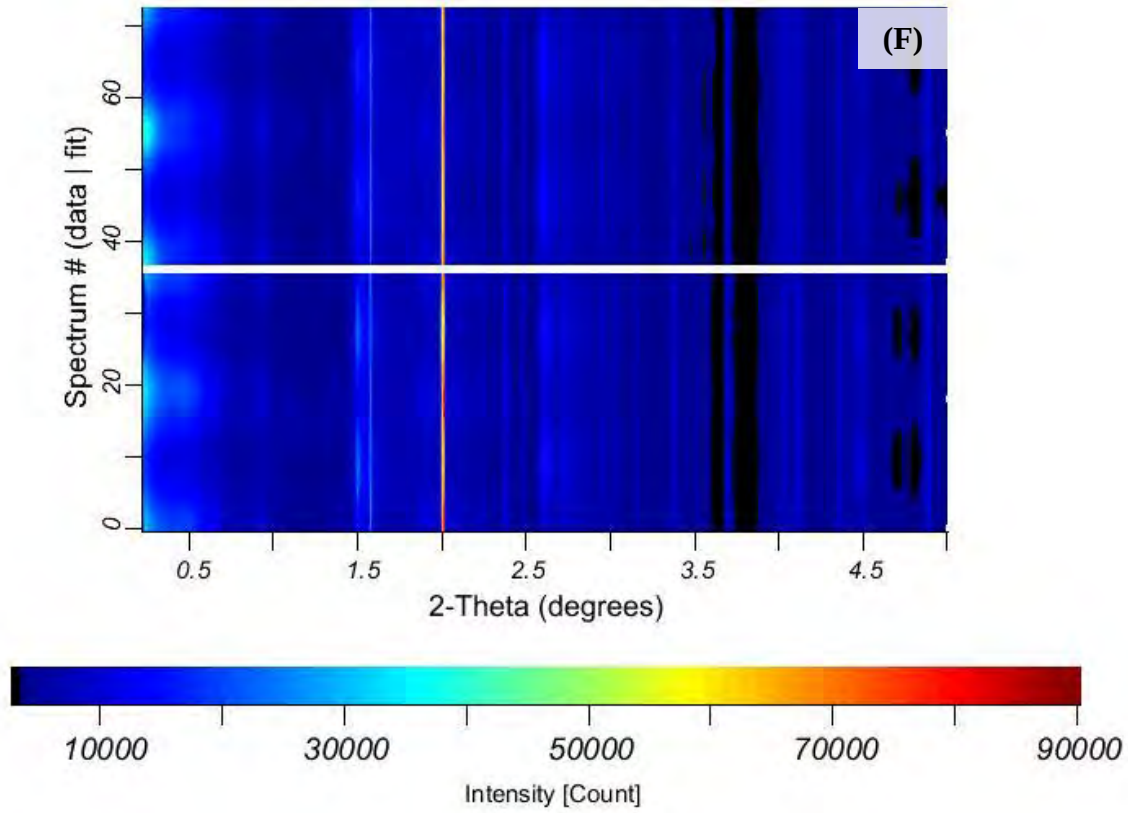
(F)
Spectrum # (data | fit)
0
20
40
60
0.5
1.5
2.5
3.5
4.5
2-Theta (degrees)
10000
30000
50000
70000
90000
Intensity [Count]

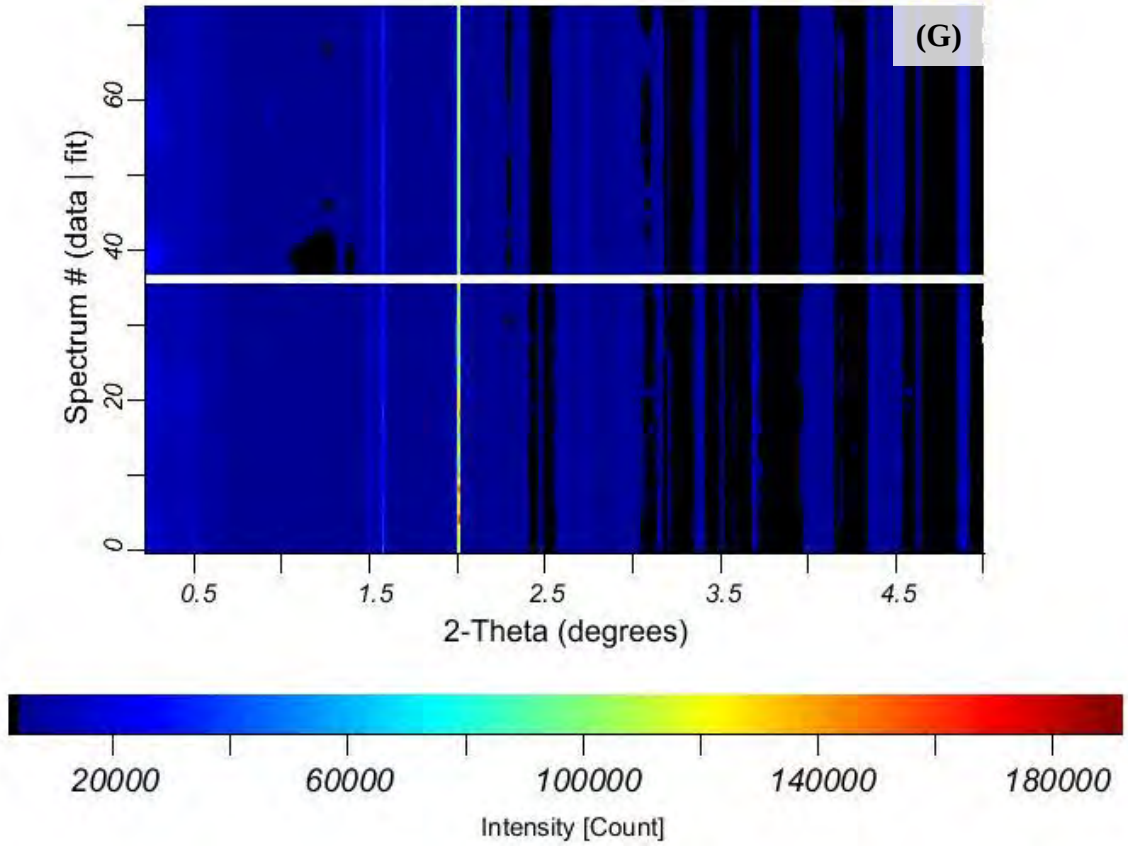
(G)
Spectrum # (data | fit)
0
20
40
60
0.5
1.5
2.5
3.5
4.5
2-Theta (degrees)
20000
60000
100000
140000
180000
Intensity [Count]

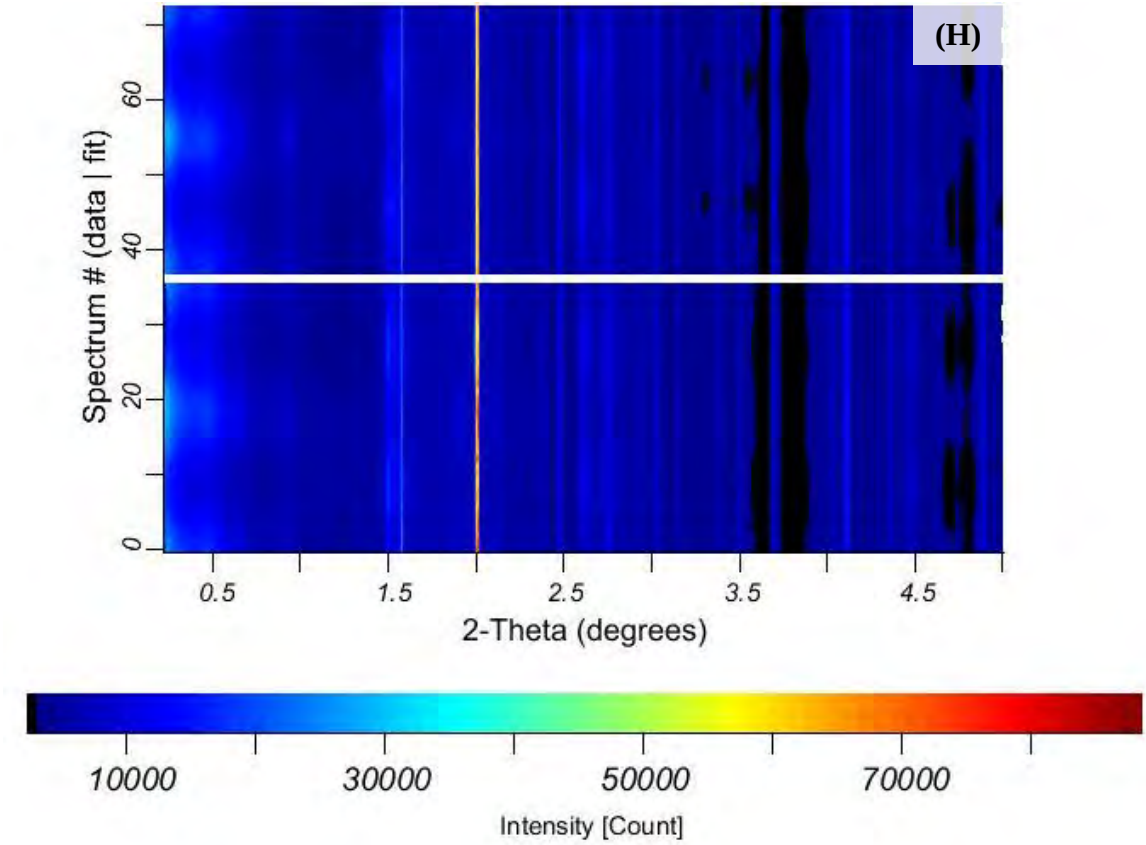

Figure A.2 Two dimensional map plots of (A) BP 475, (B) BP 925, (C) BP 1375, (D) BP 1725, (E) BS 500, (F) BS 900, (G) BS 1100, and (H) BS 2300 soil samples. The plots show the stacking of diffraction patterns, comparing experimental data (bottom) with calculated spectra (top), and display the strongest texture among images of seven tilting angles which the degree of tilting are labelled at each samples. Scale is 2-Theta (degrees). An example of the clay mineral peak positions are labeled at sample (D).

APPENDIX B

STIFFNESS TENSORS

For the shear wave velocity calculation, the single-crystal stiffness tensors of minerals at 0 K (Table 3.3) are incorporated with orientation distribution functions (ODFs) exported from MAUD, to determine the polycrystal stiffness tensors using TENS function in BEARTEX software. This section presents the geometric mean stiffness tensors incorporated with ODFs of minerals containing textures, which are illite-mica, montmorillonite, and dickite. Then, TENX function is used to calculate the multiphase stiffness tensors of the soil, by incorporating geometric mean stiffness tensors of the minerals with their volume fraction. The elastic constants of the soil, C_{44} and C_{66}, are determined which are used for the shear wave velocity calculation of the soil samples.

Table B.1 The geometric mean stiffness tensors of illite-mica, montmorillonite, and dickite of BP and BS soil samples at each depth. The tensors were incorporated with the mineral's ODFs by TENS function in BEARTEX software.

(A)

BP 4.75 m	C_{11}	C_{12}	C_{13}	C_{22}	C_{23}	C_{33}	C_{44}	C_{55}	C_{66}
Illite-mica	115.695	38.299	37.059	115.694	37.059	100.378	35.168	35.168	38.697
Montmorillonite	69.427	26.020	25.850	69.427	25.850	54.531	18.084	18.084	21.704
Dickite	110.197	37.117	37.481	110.197	37.481	115.749	37.637	37.637	36.540

(B)

BP 9.25 m	C_{11}	C_{12}	C_{13}	C_{22}	C_{23}	C_{33}	C_{44}	C_{55}	C_{66}
Illite-mica	113.894	38.006	37.371	113.894	37.371	103.068	35.690	35.690	37.944
Montmorillonite	67.704	26.101	25.740	67.704	25.740	57.542	18.390	18.390	20.802
Dickite	112.776	37.871	37.159	112.776	37.159	110.594	37.222	37.222	37.453

(C)

BP 13.75 m	C_{11}	C_{12}	C_{13}	C_{22}	C_{23}	C_{33}	C_{44}	C_{55}	C_{66}
Illite-mica	115.332	38.245	37.068	115.332	37.068	100.977	35.227	35.227	38.543
Montmorillonite	69.702	26.217	25.559	69.702	25.559	54.849	17.858	17.858	21.743
Dickite	110.096	37.114	37.538	110.096	37.538	115.794	37.716	37.716	36.491

(D)

BP 17.25 m	C_{11}	C_{12}	C_{13}	C_{22}	C_{23}	C_{33}	C_{44}	C_{55}	C_{66}
Illite-mica	123.637	39.396	36.146	123.637	36.146	89.732	33.233	33.233	42.120
Montmorillonite	73.903	26.368	25.568	73.903	25.568	48.764	17.152	17.152	23.768
Dickite	113.272	38.277	36.698	113.272	36.698	110.555	36.944	36.944	37.497

(E)

BS 5.00 m	C_{11}	C_{12}	C_{13}	C_{22}	C_{23}	C_{33}	C_{44}	C_{55}	C_{66}
Illite-mica	115.306	38.264	36.957	115.306	36.957	101.482	35.133	35.133	38.521
Montmorillonite	67.595	26.130	25.704	67.595	25.704	57.699	18.404	18.404	20.732
Dickite	110.455	37.080	37.514	110.455	37.514	115.312	37.570	37.570	36.688

(F)

BS 9.00 m	C_{11}	C_{12}	C_{13}	C_{22}	C_{23}	C_{33}	C_{44}	C_{55}	C_{66}
Illite-mica	115.186	38.241	36.840	115.186	36.840	101.898	35.039	35.039	38.473
Montmorillonite	67.794	26.219	25.365	67.794	25.365	58.541	18.082	18.082	20.788
Dickite	110.086	110.085	37.383	110.086	37.383	116.394	37.559	37.559	36.490

(G)

BS 11.00 m	C_{11}	C_{12}	C_{13}	C_{22}	C_{23}	C_{33}	C_{44}	C_{55}	C_{66}
Illite-mica	111.250	37.646	37.396	111.250	37.396	108.235	36.105	36.105	36.802
Montmorillonite	63.875	25.920	25.722	63.875	25.722	64.990	19.150	19.150	18.977
Dickite	111.383	37.312	37.399	111.383	37.399	113.155	37.404	37.404	37.035

(H)

BS 23.00 m	C_{11}	C_{12}	C_{13}	C_{22}	C_{23}	C_{33}	C_{44}	C_{55}	C_{66}
Illite-mica	116.358	38.399	36.887	116.358	36.887	99.736	34.912	34.912	38.980
Montmorillonite	67.313	26.219	25.657	67.313	25.657	58.302	18.473	18.473	20.547
Dickite	109.860	37.171	37.540	109.860	37.540	116.388	37.817	37.817	36.344

APPENDIX C
DEEPSOIL MODELING

C.1 Input Parameters for DEEPSOIL

The main input parameters for DEEPSOIL modeling are soil profile, soil dynamic properties, shear wave velocity, and input motion. The amplification profile are modeled to 40 m deep. However, BP and BS soil samples are limited to approximately 20 m deep. Therefore, the missing soil profile from 20-40 m are based on soil data of Chulalongkorn University (CU) derived from the study by Duangsano (2014) (Figure 2.4). BP, BS, and CU are located on the same sediment distribution, i.e., delta plain in the Lower Central Plain of Thailand. Our study assumes that the soil type of BP, BS, and CU are likely the same. Soil types (soft clay, stiff clay, sand) are defined from soil log data. Moreover, BP and BS also lack data of dynamic soil properties. So, the dynamic soil properties in our study are based on CU site as well. The values are extracted from shear modulus reduction curve and material damping curve of tested soil samples from CU.

Table C.1 Input soil profile in DEEPSOIL. BP and BS soil data include soil type and dynamic soil properties for the amplification modeling.

Layer Name	Unit weight	Vs (m/s)	Damping ratio	Ref strain	Ref stress	Beta	S	b	d	P1	P2	P3
Soft clay (C1)	16	95	2	0.12	0.18	1	1	0	0	0.58	0.264	0.45
Soft clay (C1*)	16	95	2	0.1982	0.18	1.515	0.915	0	0	0.58	0.2	0.45
1st Stiff clay (C2)	18	170	1.218	0.0636	0.18	1	0.919	0	0	0.628	0.206	3.25
1st Stiff clay (C3)	18	170	1.1207	0.07	0.18	1	0.919	0	0	0.628	0.204	3.25
1st Sand (C4)	20	250	0.7093	0.0395	0.18	1	0.919	0	0	0.642	0.230	3.2
1st Sand (C5)	20	250	0.6544	0.0439	0.18	1	0.919	0	0	0.638	0.224	3.25

Note: C1, C1*, C2, C3, C4, and C5 refers to the material curve used for the dynamic soil properties extraction. (Duangsano, 2014)

C.2 Peak Ground Acceleration of Soil Layers

The output from DEEPSOIL modeling display peak ground acceleration (PGA) of the soil layer at each depth. Each layer is 0.5 m thick, so there are 80 soil layers in total to sum up 40 m of the soil profile. The amplification factor calculation requires PGA from the first 0.5 m layer at the bottom most of the soil profile, and PGA at the surface. Besides calculating the amplification factor, PGA at the surface is also advantageous for ground motion assessment. Table C.2 presents the PGA at the bottom most layer and at the surface, responded at BP and BS from the three earthquake events scaled to 0.1 g.

Table C.2 PGA at BP and BS responded from Mae Lao Earthquake, Sangkhlaburi Earthquake, and Thabeikkyin Earthquake. All input motions are scaled to 0.1 g. PGA at the bottom most layer (layer 80) are below and PGA at the surface (layer 1) are on top.

	BP	**BS**
Mae Lao Earthquake	0.136 0.078	0.095 0.080
Sangkhlaburi Earthquake	0.127 0.074	0.087 0.064
Thabeikkyin Earthquake	0.150 0.072	0.099 0.067

APPENDIX D

RESPONSE SPECTRA

Apart from seismic hazard assessment from peak ground accelerations (PGA), response spectrum is also another application to determine the construction designs. Response spectrum is plotted between spectral acceleration (SA) and period of the ground. SA describes the maximum acceleration in an earthquake on an object, particularly buildings. Resonance between the ground and building period can cause buildings to sway in a strong motion, but it can be prevented by the use of this analysis. The response spectrum identifies the resonant period at which the building will undergo peak spectral accelerations (PSA). The possibility of earthquake hazard can be reduced by designing structures avoiding those resonant periods. This part presents the response spectra at BP and BS from the modeling in DEEPSOIL, responded from the three earthquake events in this study: Mae Lao Earthquake, Sangkhlaburi Earthquake, and Thabeikkyin Earthquake.

(A) Mae Lao Earthquake

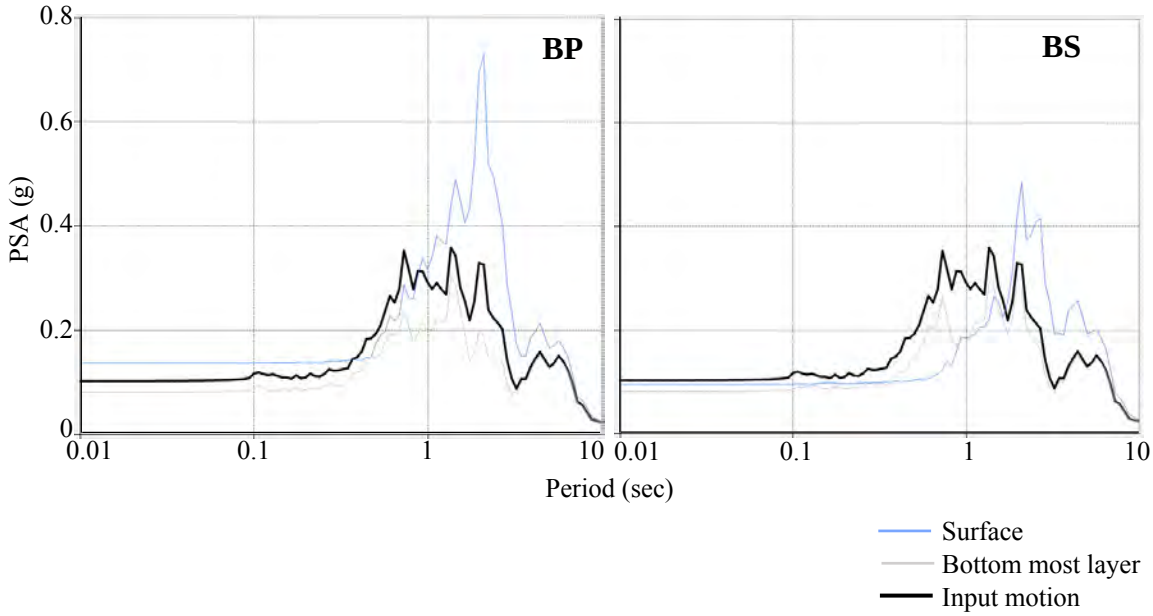

(B) Sangkhlaburi Earthquake

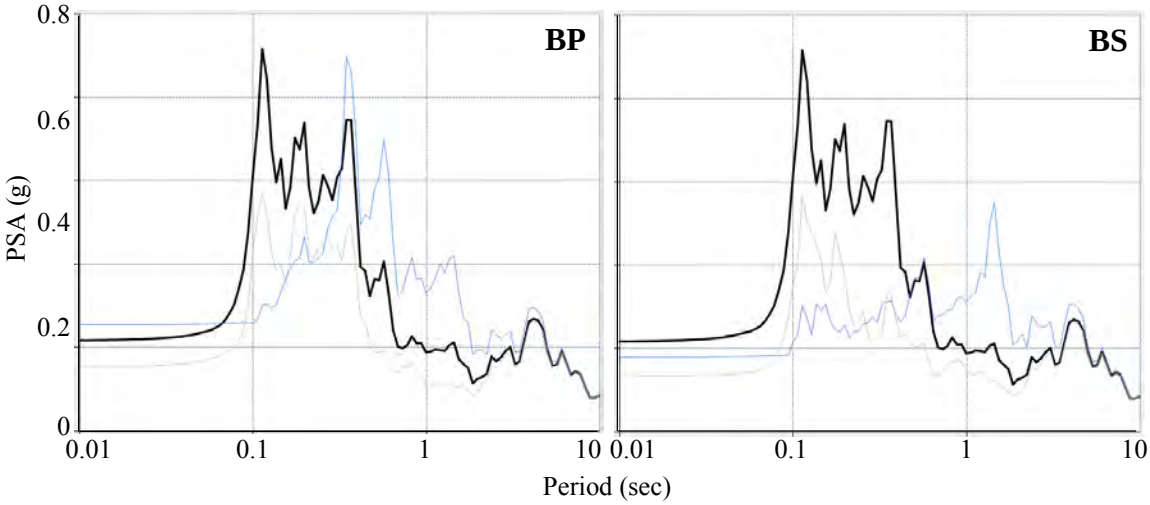

(C) Thabeikkyin Earthquake

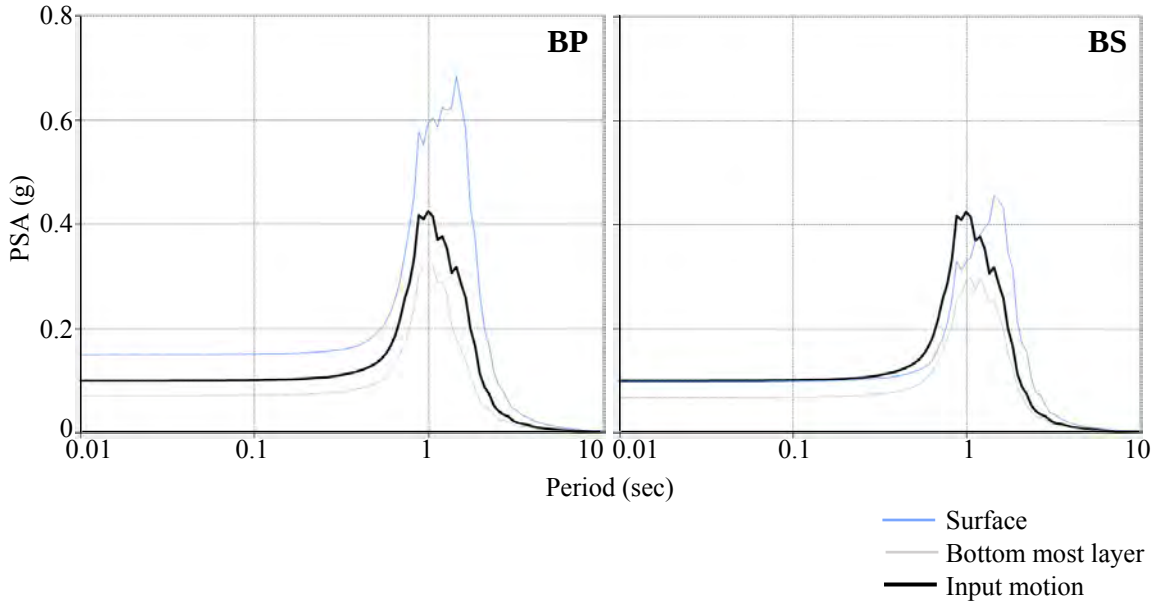

Figure D.1 Response spectra of BP and BS responded from (A) Mae Lao Earthquake, (B) Sangkhlaburi Earthquake, and (C) Thabeikkyin Earthquake. The plots are between peak spectral acceleration (PSA) and period of the ground.